Development of a method for bioanalysis of a nanomaterial in biological matrices

GEMA FERNÁNDEZ

MASTER´S DEGREE PROJECT, 45 ECTS
MOLECULAR BIOLOGY
DEPARTMENT OF BIOLOGY | LUND UNIVERSITY

LUND
UNIVERSITY

Supervisor:

Dr. Sania Bäckström

Spago Nanomedical AB

Medicon Village

June 2015

Table of contents

Abstract

Molecular imaging techniques have become an essential tool for cancer diagnosis. They have the potential to detect cancer at early stages and thus, they can change the outcome of the disease and patient prognosis. Magnetic resonance imaging (MRI) has arisen as one of the most promising imaging methods used for the screening of soft tumor tissues such as breast cancer. However, the specificity of MRI remains poor leading to misdiagnosis and many false positive findings. Thus, a wide range of new contrast agents (CAs) are being developed in order to enhance image resolution and safety in cancer diagnosis. For new drugs with an intended clinical use, it is necessary a deep insight into the viability of the molecule prior to clinical trials. Some *in vitro* analysis and *in vivo* animal studies are carried out in order to characterize the physicochemical properties of the compound and its toxicity. Problems to find the right methodology to detect and assess identity of nanoparticles after being injected into the blood have been previously found. In this project, a combined method to extract and characterize dummy particles, mimicking nanoparticles to be used as CAs, was developed. These particles consist of a polymeric core, which contains a metal ion inside, together with a coating attached to the surface. A new approach for characterization was investigated by using three analytical techniques: gel permeation chromatography (GPC) to extract and separate the nanoparticles by size, enzyme-linked immunosorbent assay (ELISA) to analyze the coating and inductively coupled plasma optical emission spectroscopy (ICP-OES) to analyze the core and metal ion. Different biological matrices, mainly serum and urine, were tested to prove identity. Results showed an efficient extraction of the material with a high rate of recovery by GPC. Moreover, the accuracy and sensitivity of ELISA and ICP-OES in detecting the coating and composition of nanoparticles respectively was proved. More importantly, identity of the extracted material in the biological matrices was demonstrated. Future studies are required to scale up the method and further test blood samples from *in vivo* trials to completely implement the method. However, here the first steps towards the validation of the method were performed which can help to understand changes in nanoparticles upon exposure to biological fluids in the body.

List of Abbreviations

BSA	Bovine serum albumin
CA	Contrast agent
CT	X-ray computed tomography
D	Translational diffusion coefficient
DLS	Dynamic light scattering
DTPA	Diethylene triamine penta-acetic acid
EDTA	Ethylenediaminetetraacetic acid
EDX	Energy dispersive X-ray
ELISA	Enzyme-linked immunosorbent assay
ELSD	Evaporating light scattering detector
EM	Electron microscopy
F	Fraction
FDA	Food and drug administration
FFF	Field flow fractionation
Gd	Gadolinium
GPC	Gel permeation chromatography
HPLC	High performance liquid chromatography
HRP	Horseradish peroxidase
HS	Human serum
ICH	International conference on harmonisation
ICP-OES	Inductively coupled plasma optical emission spectroscopy
LOD	Limit of detection

LOQ	Limit of quantitation
Mn	Manganese
MQ	Milli-Q
MRI	Magnetic resonance imaging
NPs	Nanoparticles
NSF	Nephrogenic systemic fibrosis
P	Phosphorus
PEG	Polyethylene glycol
PET	Positron emission tomography
RES	Reticuloendothelial system
RF	Radio frequency
R_H	Hydrodynamic radius
RI	Refractive index
SBF	Simulated body fluid
SDS-PAGE	Sodium Dodecyl Sulphate Polyacrylamide Gel Electrophoresis
SEC	Size exclusion chromatography
SEM	Scanning electron microscopy
SEM	Standard error of the mean
Si	Silicon
SOP	Standard operation procedure
SPECT	Single-photon emission computed tomography
TEM	Transmission electron microscopy
TMB	3, 3’, 5,5’-Tetramethylbenzidine

1. Introduction

Cancer is one of the leading causes of disease worldwide today. According to the World Health Organization, 14.1 million adults were diagnosed with cancer worldwide in 2012 and in the same year, it was responsible for 8.2 million deaths (1) (Figure 1). This number is expected to increase to 24 million cases by 2035 (2).

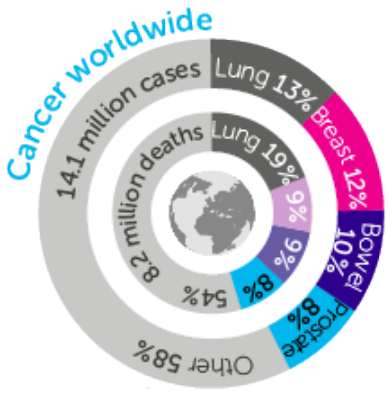

Figure 1. Estimation of cancer deaths and new cases worldwide in 2012 (Image modified from http://www.cancerresearchuk.org/cancer-info/cancerstats/world/cancer-worldwide-the-global-picture) (3).

Lung cancer is the most common type of cancer, accounting for 13 % of the total number of new diagnosed cases in 2012 followed by female breast cancer with 1.7 million new cases in the same year. Colorectal and prostate cancers are the next most abundant types of cancer on the list with 1.4 and 1.1 million new cases respectively (3). Breast cancer is the most common cancer type in women worldwide and represents one in four of all cancers among females (2). In fact, the incidence of this cancer is increasing in developed and developing countries due to an increment in the life span, urbanization and changes in the diet and lifestyle. Thus, there is an urgent need to implement more reliable early detection methods that can reduce these numbers and improve the prognosis of patients. Efforts should be focused not only on new treatments but also on early prevention and detection.

An accurate cancer screening requires high specificity and sensitivity. Some of the molecular imaging techniques available today are X-ray computed tomography (CT), optical imaging (OI), ultrasound (US), magnetic resonance imaging (MRI) and radionuclide imaging including single-photon emission computed tomography (SPECT) and positron emission tomography (PET) (4).

Molecular imaging is an emerging and potential tool used in cancer diagnosis, treatment and monitoring of tumor status (5). In the case of breast cancer, one of the most common screening methods used is mammography that provides an early detection and allows the treatment to be started before the cancer has spread. Some studies has shown that screening mammography helps to reduce the number of deaths in women over the age of 50 but women under that age do not benefit from this method (6). Moreover, mammography as well as CT and radionuclide methods (PET and SPECT), uses ionizing radiation that has the potential to cause cancer in repeated exposures. Another drawback of the mammography is its low sensitivity, missing a considerable number of tumors that require additional testing such as biopsy or ultrasound.

Thereby, these traditional screening technologies together with some of the most relevant treatments, such as surgery, radiation therapy and chemotherapy cause damage of healthy tissue and recurrence in cancer patients (7).

Altogether, there is a need for more reliable, safe, non-invasive and sensitive screening methods for early detection of cancer.

1.1 Magnetic resonance imaging

MRI has arisen, above other imaging modalities, as the most promising imaging technique available today for the detection of soft tissue cancer, such as solid tumors. It is a non-invasive method with high temporal and spatial resolution and absence of ionizing radiation (8). Instead of hazard-related radiation, it uses radio frequency (RF) radiation together with a magnetic field to produce three dimensional acquisitions of images *in vivo* of organs and tissues in a very short period of time. It is based on the interaction between atomic nuclei and their movement in a magnetic field. The atomic structure is composed of a nucleus (protons, neutrons) and electrons orbiting around the nucleus. One important property of the atomic nuclei used in MRI is the tendency of the particles to rotate around an axis at a constant rate. Adequate atomic nuclei for MRI are those that have an unpaired proton or neutron. These charged nuclei that are spinning, induce a magnetic field and act as tiny magnets with a magnetic dipole (9).

An MRI system relies on the signals from the hydrogen atoms (H), because they are highly abundant in the form of water within the body and have a large magnetic moment. The nucleus of an H atom contains an unpaired charged proton that in the absence of a magnetic field is spinning in a random orientation with zero magnetization. However, when an external magnetic field (B_o) is applied, the nuclear axes will align in the same direction as the B_o field (longitudinal direction) creating a net magnetization vector (NMV). These spins rotate around B_o at a specific frequency (ω) which is part of the RF range. If short RF pulses (excitation) are given at 90º to the NMV, the spins will absorb energy and change direction to the transversal plane. Once the pulse is switched off, the nucleus will return to its original spin state of lower energy in the longitudinal direction. The recovery step to the longitudinal plane is called spin-lattice relaxation (T_1) whereas the decline along the transverse plane is called spin-spin relaxation (T_2) (Figure 2A). During the T_1 recovery energy is released from the nuclei while in the T_2 process the energy is exchanged between the nuclei (10). A radio wave signal is emitted at a certain frequency and detected by the voltage induced in a receiving coil after the end of the pulse. This voltage is registered on a computer that analyzes and converts it into an image.

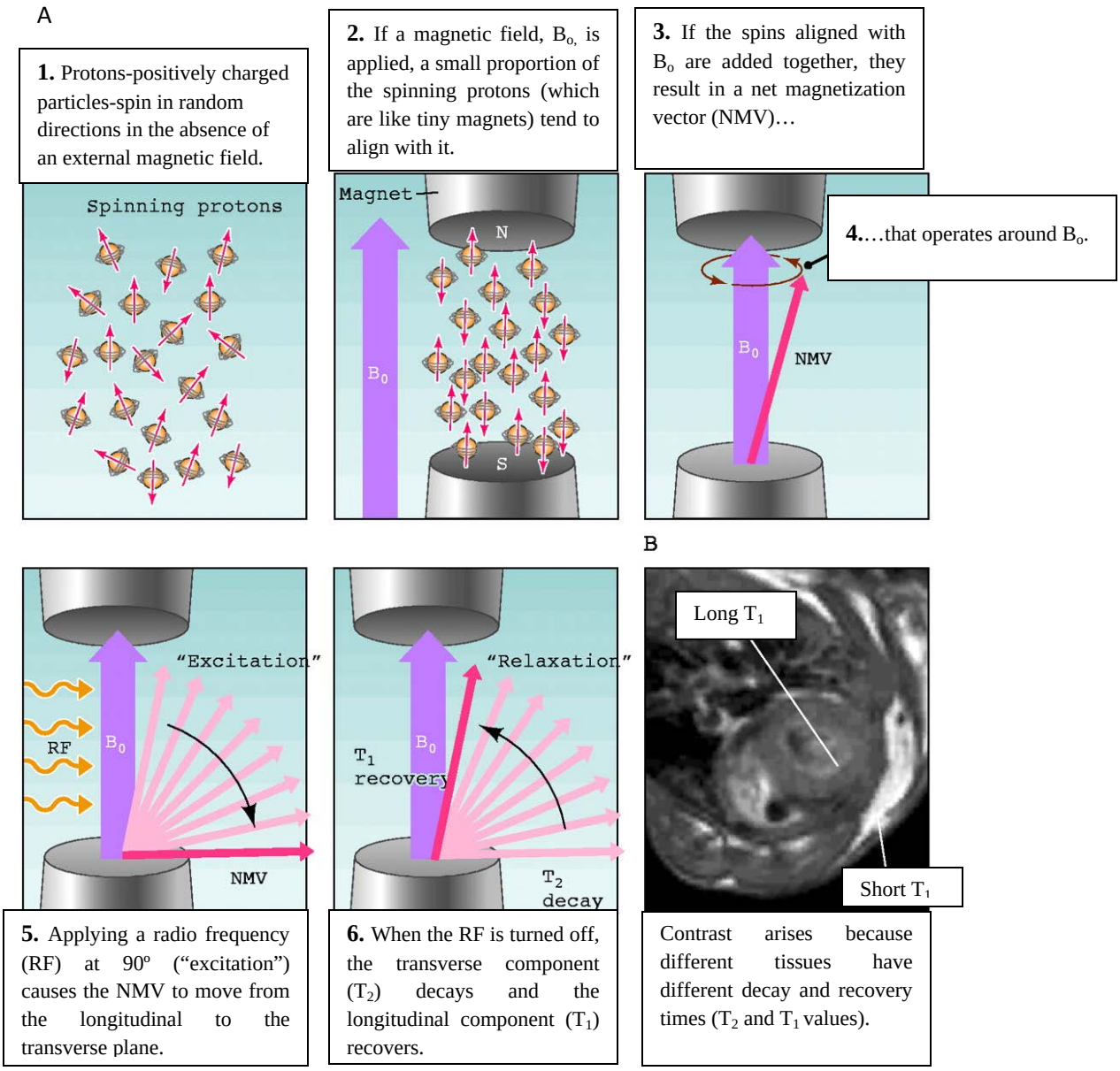

Figure 2. Schematic description of how MRI works. A) Steps taking place during the MRI process with the excitation and relaxation events **B)** Contrast in tissues is created due to a different T_1 and T_2 relaxation times that produces different intensity signals (Image modified from Pautler, 2004) (10).

Contrast in MRI images results from variations in water proton density and relaxation rates (T_1 and T_2) in different tissue types causing a difference in signal strength based on changes in tissue water structure (Figure 2B). Normally, T_1-related images are used to discriminate the anatomy of the body whereas T_2-weighted images are used to detect abnormal tissues. In T_1-based images, a tissue with a short T_1 will produce a higher intensity signal compared to tissues with longer T_1, appearing as bright white and dark respectively (9). Since inherent tissue contrast is not always enough to provide high resolution, MRI contrast agents (CAs) are injected intravenously to increase image contrast by changing the T_1 and/or T_2 of water molecules altering the local magnetic field. Traditionally, the CAs used have been based on iron oxide particles and chelates of the gadolinium ion (Fe_2O_3 and Gd^{3+} respectively).

1.1.1 Contrast agents in MRI

The main advantage of MRI is its high resolution although the main drawback is its low specificity giving false positive results. The innate differences in water content and in the water relaxation times T_1 and T_2 in the abnormal tissue are not usually high enough to produce a sensitive diagnosis. Therefore, there has been an increasing attempt to enhance image resolution by using CAs. CAs are chemical compounds that, after intravenous injection, increase the image contrast by enhancing the relaxation process (11). The design of these agents depends on physicochemical properties of these particles such as chemical composition, size and surface. Their ability to produce changes in the relaxation times depends on the intensity of the effect that they produce compared to the intrinsic relaxation times of the tissues (8).

Certain CAs consist of super-paramagnetic particles, such as iron oxide particles, which reduce the T_2-transversal relaxation, resulting in a darker image. The most common agents are based on iron oxide (Fe_2O_3) particles (12). Although super-paramagnetic iron oxide nanoparticles have been approved by the Food and Drug Administration (FDA) for human uses, these agents are not used any more due to negative contrast enhancement and their prolonged *in vivo* contrast enhancement, up to several months (13).

The most widely used CAs include paramagnetic molecules that shorten T_1 relaxation time giving a brighter image. Some of these molecules are chelates of the gadolinium ion (Gd^{3+}) and the manganese ion (Mn^{2+}). They contain a metal ion and a chelating ligand. The chelating ligand binds to the metal ion and forms a chelate complex that is excreted from the body without causing toxicity. Paramagnetic atoms such as Gd have one or more unpaired electrons with a high magnetic moment that will change the magnetic state in the H atoms. In almost half of the MRI diagnostic investigations, chelates of Gd ions such as Gd-diethylene triamine penta-acetic acid (DTPA) are used to create contrast by reducing the T_1 relaxation time of protons in the surrounding water and thereby increasing the intensity in T_1-weighted images. Gd ions bind to a chelate, such as DTPA, that decreases the toxicity of free Gd ions (14). The majority of these agents are low molecular weight compounds that diffuse into the extracellular space without any targeting effect. Gd CAs are efficient for the diagnosis of brain tumors by making possible to detect damage to the blood-brain barrier and for detection in breast cancer by measuring the increased uptake of agent by the tumor tissue (14). The latter exploits the fact that the tumors have an enhanced permeable vasculature from where the agent can leak into the extracellular space and the rate of this event depends on the properties of the neovasculature of the tumor. When the agent is delivered at high concentration rates in the blood, it creates a large magnetic field there compared to the surrounding tissues and causes a signal loss in T_2 weighted images (15).

However, the use of Gd-based CAs is known to give toxic side-effects, especially the occurrence of nephrogenic systemic fibrosis (NSF) in patients with renal failure. NSF is an acquired fibrosis disease that produces swelling of extremities and hardening of the skin and trunk that is gradually spread to other organs such as lung, heart, liver and muscles causing sclerosis (16). Gd-chelates might cause an iron-liberating effect with an increased concentration of this free metal ion in serum which is highly toxic, leading to metabolic acidosis and fibrosis (17). Moreover, patient-related factors also have an influence in the

development of this disease when being exposed to Gd ions. In fact, the half-life of Gd-based CAs in patients with normal renal function is around 1.3 hours whereas the clearance rate is slower in those that have an impaired renal function with an increasing half-life and more probability of toxic ion release (18).

Therefore, new contrast agents are needed in order to increase safety and resolution in cancer diagnosis.

1.2 Nanoparticles for cancer diagnosis and therapy

Nanotechnology in cancer has emerged as a new potential field which includes the design of material in a scale range from 1-100 nanometers with clinical use for cancer therapy and diagnosis. These nanoparticles (NPs) are versatile molecular devices with diverse applications in clinical medicine as drug-delivery carriers through passive or active targeting and as diagnostic tools. The advantage of using nanotechnology is the wide range of functionalities that can be introduced in the nanoparticle structure. These modifications include the addition of ligands to the surface, modification of the surface with coatings that increase circulation times and loading of a therapeutic drug among others (19). Although there is an increasing number and variety of nanoparticles, the majority of them can be classified into two main types: particles made of organic molecules as the main component and inorganic particles usually containing metals as a core (Figures 3A and B).

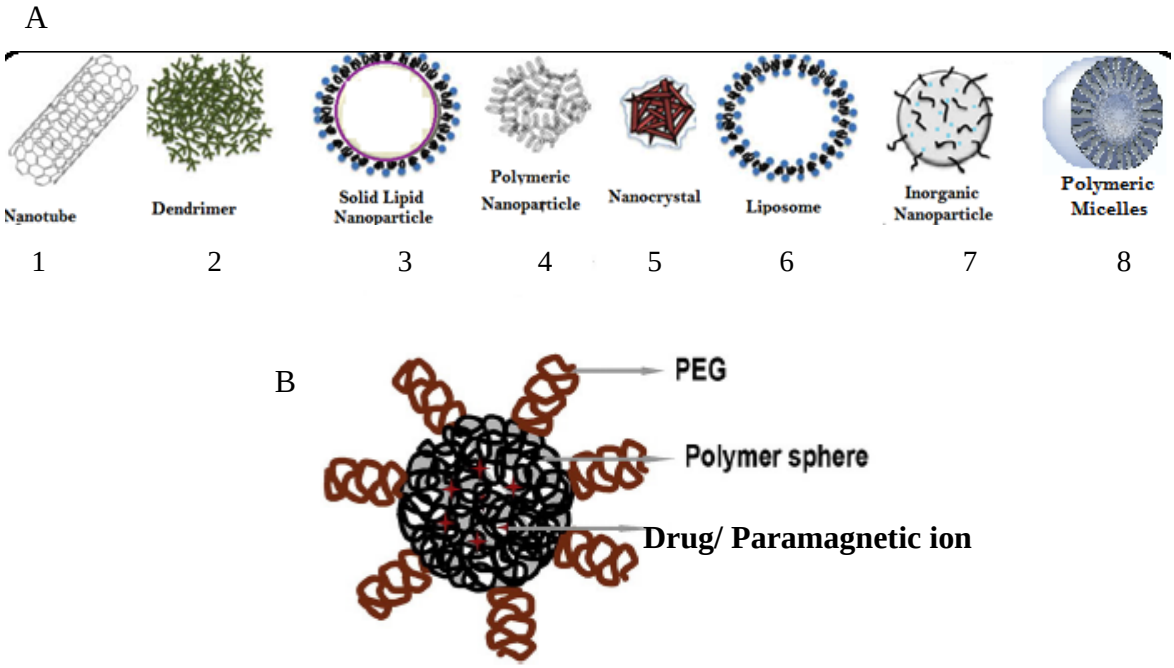

Figure 3. Most important types of nanoparticles for imaging diagnosis and therapy **A)** Different types of organic and inorganic particles **1**. Nanotubes, composed of rings, can carry a drug inside or attached to the sides **2.** Dendrimers, globular macromolecules with branching ends **3.** Solid lipid nanoparticle **4.** Polymeric nanoparticles, made of cross-linked polymers **5.** Nanocrystals **6.** Liposomes, colloid structure with a lipid bilayer **7**. Inorganic nanoparticle **8.** Polymeric micelles with an aqueous core and polymer shell (Image modified from Athar and Jyoti Das, 2013) (66) **B)** Detailed description of a polymeric nanosphere composed of a central core and a coating attached to the surface (Image modified from Nazir et al., 2013) (20).

Carbon nanotubes, liposomes, dendrimers and micelles have been used for clinical applications since they can be conjugated with therapeutic agents and targeting ligands. Liposomes have been used as vectors for drug-delivery in breast cancer and dendrimers have the potential to visualize abnormal tissues through MRI (21). The majority of inorganic nanoparticles have a common structure that contains a central core which defines the magnetic, optical or fluorescent properties and an external coating on the surface that isolates and protects the core from degradation. Within this group, paramagnetic and super-paramagnetic particles are used for MRI diagnosis. Recently, Mn-based contrast agents have gained attention as a potential alternative. This new approach is based on the fact, that unlike lanthanides such as Gd, Mn is native to the body as a cofactor for enzymes (22).

In this context, the company Spago Nanomedical AB is currently involved in the development of an innovative nanomaterial, called IonXgel, with an intended clinical use. IonXgel is used together with Mn to create a nanoparticle-based contrast agent that can improve early diagnosis in cancer through MRI. It has been demonstrated that this nanomaterial enables a better detection of small tumors in soft tissues such as in breast cancer and thus, it will be able to decrease the number of false positives (23). The main component is a nanomaterial made of organosilicophosphonate polymers coated with polyethylene glycol (PEG) where either a paramagnetic ion such Mn or Gd can be loaded. These nanoparticles have medical applications as MRI contrast agents.

These particles will accumulate selectively in the tumor tissue through passive targeting caused by physiological differences between the normal and the tumor tissue due to the so called enhanced permeability and retention (EPR) effect.

1.3 Passive targeting: the enhanced permeability and retention effect

The advantage of designing particles in the nanometer scale is that they can leak out to specific sites in the tumor thanks to an enhanced permeability in the tumor vasculature (Figure 4). In fact, passive targeting is achieved because of the distinctive anatomical and physiological characteristics of the tumor microenvironment. Some of the main features in the development of cancer are an acidic pH, hypoxia, hypoglycemia, inflammation and genetic mutations (20).

When cancer cells start to grow in a fast and uncontrolled manner, they begin to create new blood vessels to supply their oxygen and nutrition demands, during the so called angiogenesis (24). However, these blood vessels are defective and present fenestrations between the endothelial cells as well as an elevated production of vascular permeability mediators such as nitric oxide. They are characterized by a disorganized structure lacking a functional lymphatic drainage system which gives retention of the particles in the tumor tissue for a longer time. Consequently, the delivery of a certain size particle through passive targeting causes the extravasation of this particle through the abnormal blood vessels and its accumulation in the tumor tissue at a higher concentration than in normal tissues (Figure 4) (25). The low pH in tumor tissues has also been exploited to deliver drug-carriers such as micelles and drug-conjugates that lose their structure and release the therapeutic component at an acidic pH (20). The heterogeneous nature of tumors makes ligand-mediated targeting difficult. However, the EPR effect uses the unique characteristic of leaky tumor vasculature which is common for

almost all solid tumors regardless of other specific features (25). Thus, the importance of the EPR effects resides in the ability to target a wide variety of tumors.

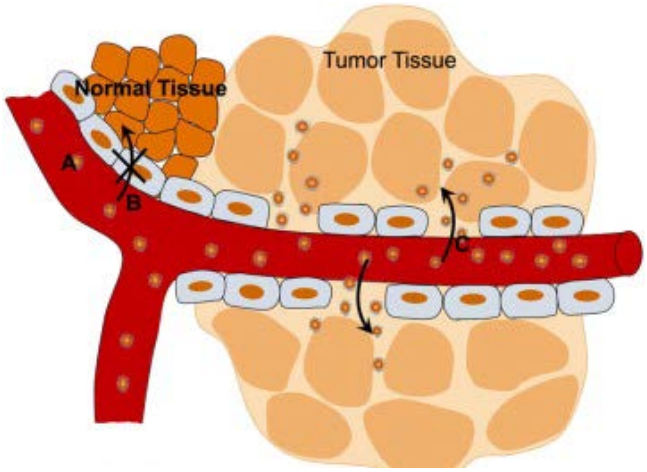

A=Drug

B=Tight packing of normal vasculature preventing drug uptake by normal body tissue

C=Permeation of drug to tumors through leaky blood vasculature (EPR effect)

Figure 4. Nanoparticles are delivered to the tumor using a passive targeting strategy in which the molecules accumulate at the tumor spots leaking from the abnormal vasculature and will remain longer there. The EPR effect allows these events due to the differences in the design of the blood vessels between tumor and normal tissues: enhanced permeability, fenestrations and chaotic architecture (Image modified from Nazir et al., 2014) (20).

1.4 PEGylation of nanoparticles

The surface of nanoparticles can be coated with either biodegradable or non-biodegradable polymers to avoid undesired interactions once they are delivered into the blood circulation. PEG is the most commonly used non-ionic and hydrophilic polymer to coat the surface of particles intended for medical use. It consists of a combination of different numbers of ethylene glycol monomers that modify the interface layer between the nanoparticle core and the surrounding environment (26). It is inexpensive and it has been approved by the FDA for more than 20 years.

PEG reduces aggregation events that otherwise can cause molecular trapping in the liver or lungs by capillary occlusion. It also decreases the uptake by the organs of the reticuloendothelial system (RES) (liver and spleen) increasing the circulation time in the blood of the nanoparticles, and thus, their half-life and biodistribution (27). In consonance, PEGylated molecules show a decreased interaction with proteins or other blood components as well as lower accessibility to enzyme degradation and immune recognition (Figure 5). Thanks to the hydrophilic properties, it provides the PEGylated molecule with high solubility that increases its stability in aqueous matrices such as water, serum and urine. However, some adverse effects arise from the metabolism of PEG caused by secondary products. Moreover, it is non-biodegradable and it might cause some hypersensitivity reactions (28).

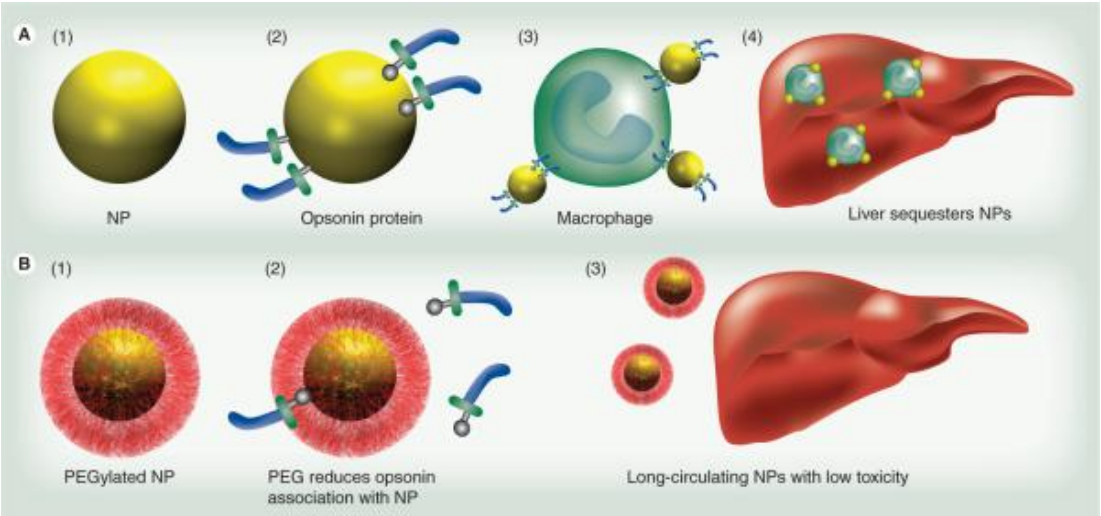

Figure 5. PEG decreases the uptake from the RES as well as the interaction with blood proteins and molecules from the immune system such as opsonins. **(A)** When a naked particle enters the body, it is covered by opsonins that trigger the action of macrophages and liver uptake **(B)** When a particle coated with PEG enters the body, it remains hidden from the opsonins, increasing its bioavailability for the intended purpose (Image reproduced from Jokerst et al., 2011) (26).

1.5 Protein-nanoparticle interaction: the protein corona

Upon exposure to a biological fluid, nanoparticles interact with proteins that may adsorb to their surface forming the so called nanoparticle-protein corona. This protein corona can affect the biodistribution and cellular uptake of the nanoparticles *in vivo*. The process is a dynamic event where the interactions are constantly changing due to different affinities of the proteins for the nanoparticles. Long-lasting binding of proteins will form a “hard” corona whereas a more rapid and weak adsorption will create a “soft” corona (29). The composition of this corona is variable and depends on the amount of available proteins, the surface properties of nanoparticles and the surrounding environment. In human plasma, the highest abundant proteins such as serum albumin, immunoglobulins and apolipoproteins might be the first ones binding to the surface of nanoparticles. Other proteins, such as opsonins, can also coat the nanoparticles creating a hallmark that is recognized by the immune system leading to a phagocytosis event that increases liver uptake. The result is a decreased circulation time and an increased clearance rate (30). Moreover, binding of proteins affects the size of particles. Smaller particles possess higher surface to volume ratios which causes more proteins will bind a nanoparticle (relative to its mass) than larger particles. Consequently, particles that have become bigger may aggregate, become trapped in some organs and have lower filtration rates (31). Thus, the analysis of protein binding profiles and identification of possible candidates is essential to determine the nanoparticle safety and efficacy. The protein corona might be important to understand the pharmacokinetics and pharmacodynamics of nanoparticles in the body.

1.6 Characterization of nanoparticles for therapy

An adequate characterization of nanoparticles through a number of regulatory studies should be done before nanoparticles intended for clinical use can enter clinical trials. During the preclinical development, *in vitro* tests and *in vivo* animal studies are performed to analyze the

physicochemical properties, toxicity profile and pharmacokinetics (absorption, distribution, metabolism and excretion) of the particles of interest (Figure 6) (32). The first step in the preclinical characterization of nanoparticles is to evaluate the properties of the material through a physicochemical characterization. This study includes analysis of particle size, chemical composition, surface charge, shape, purity, stability and solubility (32). The assessment of these properties should be the proof that the particles retain their initial identity after being injected into the blood. A wide range of analytical methods are available today to extract, separate and detect nanoparticles in biological samples. These techniques allow examining the properties of nanoparticles and their fate in the body (33). For example, when analyzing particles in a complex matrix, a separation based on size is normally required. Different types of techniques are used for this purpose, such as liquid chromatography procedures, field flow fractionation (FFF) and capillary electrophoresis. However, when using these separation approaches the differentiation between nanoparticles and proteins of the same size is still a challenge (34). Moreover, a verification of the fractionation is often needed and thus, a further analysis of the size, using light scattering techniques such as dynamic light scattering (DLS) and electron microscopy (EM) techniques. The latter includes transmission and scanning-electron microscopy (TEM and SEM respectively). The advantage of using microscopy related techniques is that the shape and aggregation tendency can also be verified.

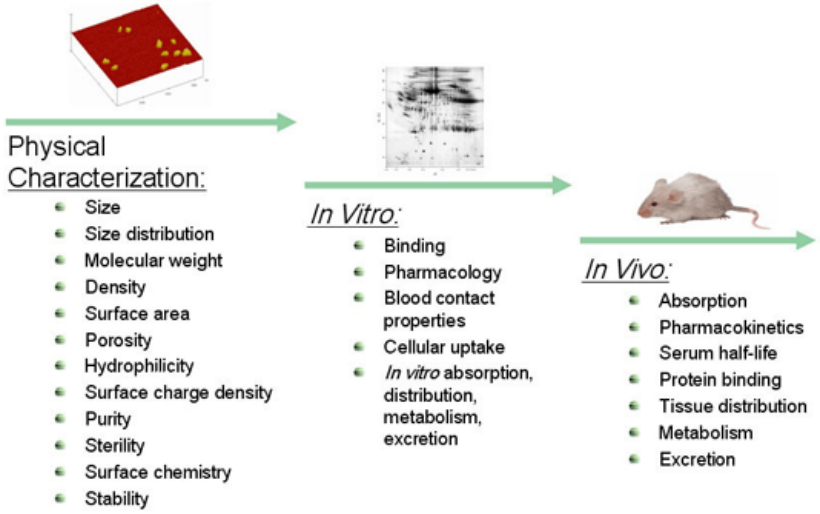

Figure 6. Currently strategy for the characterization of nanoparticles. It includes **A)** physicochemical characterization **B)** *in vitro* analysis of blood contact properties, cytotoxicity and safety aspects **C)** *in vivo* animal studies to evaluate biodistribution and toxicity (Image reproduced from http://nano.cancer.gov/action/news/featurestories/monthly_feature_2006_july.asp) (35).

However, in EM images it is difficult to completely identify particles or to evaluate if a complex nanoparticle retains its integrity during the metabolism within the body. Thus, one of the first challenges when choosing a method to characterize a nanomaterial is the ability to detect a specific element within a complex matrix. Compared to size and aggregation events, the elemental composition of a nanoparticle normally does not change in the biological matrix. Thereby, the composition “hallmark” can be examined to identify and quantify the particles in biological samples, as long as they can be detected. For particles that can be observed by EM, X-ray microscopy-based techniques, such as energy dispersive X-ray (EDX) can be used to detect the location of nanoparticles in tissues (34). Other element-specific modalities such as

inductively coupled plasma optical emission spectroscopy (ICP-OES) and inductively coupled plasma mass spectrometry (ICP-MS) offer higher sensitivity than X-ray-based techniques and can differentiate between distinct isotopes of the same element (36).

An alternative approach when the instrumental analysis offers poor resolution is the use of biological sensors which exploits the natural occurring interactions in the living organisms. Some examples of biosensors are the use of specific antibodies and enzymes such as in the enzyme-linked immunosorbent (ELISA) assays, interactions of particles with cell surface proteins and reporter genes that have a selective response to certain nanoparticles and coatings (37). Sampling methods are also a key step to further analyze the extracted particles. It is of high importance to determine the minimum sample volume required to have an illustrative sample according to the desired study (34).

A potential strategy to define the properties of nanoparticles is the combination of several high accurate techniques. In this project, a powerful combination of different methods to keep track of the nanomaterial identity after being exposed to biological matrices has been developed. This new procedure allows a rapid and inexpensive quantification of nanoparticles in a complex matrix, such as human serum, that can be implemented in blood and other tissues later on. Moreover, it offers high specificity and sensitivity in low concentration samples despite the presence of other molecules in the mixture.

2. Objectives of the project

The final goal to achieve in this project was to demonstrate that, when the nanoparticles are intravenously injected in animals during *in-vivo* trials, the identity of the material remains unaffected in the blood. Problems can arise if the content of the nanoparticles is released to the biological fluids or if particles aggregate and lodge somewhere in the body.

The aim of this project was to establish a combined method to extract, characterize and quantify nanoparticles from relevant biological matrices (e.g urine, serum, blood) using GPC-HPLC, ELISA and ICP-OES. A dummy particle made of an organosilicophosphonate core, coated with a hydrophilic, covalently attached coating and filled with gadolinium was used. The following issues were addressed:

- Prove presence of the nanomaterial in the biological matrix.

- Quantify how much of the starting nanomaterial remains in the matrix after incubation and extraction (prove concentration).

- Analyze if the nanomaterial retain its physical properties in the biological matrix (prove identity).

GPC fractions of smaller particles were also studied to provide information about released PEG or small fragments of nanoparticles present in the matrix after extraction.

The ability of the method to study the properties of the nanoparticles after being exposed to a biological matrix namely, size, composition and protein interactions was evaluated. Moreover, several parameters to validate the method for the intended use were investigated, specifically: accuracy and recovery, calibration curves, limits of optimal resolution and size stability.

3. Materials and Methods

3.1 Preparation of the nanomaterial

3.1.1 Metal loading of empty nanoparticles

Nanoparticles consisting of a central core of silicon (Si) and phosphorus (P) with a covalently attached polyethylene glicol (PEG) coating were synthesized by Spago Nanomedical AB. The Si and P contents were determined using ICP-OES. Concentrations of Si and P were 100.4 mM and 77.3 mM, respectively. The pH of the solution was 5.85.

Gd was loaded into the nanoparticles, which contained metal chelating groups. A solution of 100 mM Gd was prepared by dissolving Gd(III) chloride hexahydrate (Sigma-Aldrich) in Millipore Milli-Q (MQ) water. The Gd solution was then added in a molar ratio of 1:20 (Gd:P) to a nanoparticle solution of 77.3 mM P in MQ water. The solutions were mixed using a magnetic stirrer (FALC) at 2.5 rpm and room temperature for 1 hour. The pH was adjusted to 7.5 with 1 M Trizma Base. After the incubation, free Gd in the solution was removed by washing three times with MQ water on a 10 kDa centrifugal filter (Millipore) and centrifuging at 3500 rpm for 10 minutes and 25 ºC. Gd that was not bound to the nanoparticles passed through the filter whereas the particles did not go through and were retained.

3.2 Characterization of the nanomaterial

3.2.1 Determination of Gd-binding stability of nanoparticles

3.2.1.1 Theoretical background

Two procedures were used to determine Gd stability: ethylenediaminetetraacetic acid (EDTA)-based method and non-EDTA-based method. The former relies on a chelate effect and measures the affinity of the nanoparticles for Gd in comparison with EDTA which acts as a chelating agent that captures metal ions. Gd bound to EDTA passes through a 10 kDa spin filter in a centrifugation step whereas the nanoparticles are retained. The latter method does not contain any chelating agent. It comprises a filtration step where free Gd ions from the nanoparticle solution pass through a spin filter and are collected as permeate. Gd concentration in the permeate solution after filtration is compared to Gd concentration in the nanoparticle solution before filtration.

3.2.1.2 Methodology: EDTA-stability

Nanoparticles were diluted to a concentration of 1 mM Gd in MQ water. 150 µl of

1 mM EDTA in 50 mM Tris-HCl (pH 7.5, adjusted with 1 M HCl) was mixed with 150 µl of 1 mM Gd nanoparticle solution and incubated for 1 hour at room temperature. After incubation, 100 µl of the mixed solution was transferred to an eppendorf tube (pre filtration sample) and the remaining 200 µl of the mixture was placed into an Amicon® Ultra 0.5 ml 10 kDa centrifugal filter (Millipore) and centrifuged for 10 minutes at 13400 rpm. After filtration, 100 µl of permeate was transferred to an eppendorf tube (post filtration sample). Gd concentration was measured with ICP-OES in pre- and post-filtration samples.

The stability was calculated according to equation (1) as a percentage of the Gd that was still attached to the nanoparticles after incubation with EDTA.

$$Gd\ stability\ (\%) = 100 - \left(\frac{[Gd]\text{-}post}{[Gd]\text{-}pre}\right) \times 100 \qquad Eq\ (1)$$

3.2.1.3 Methodology: non-EDTA-stability

Nanoparticles were diluted to a concentration of 1 mM Gd in MQ water in a final volume of 300 µl. 100 µl of 1 mM Gd nanoparticle solution was transferred to an eppendorf tube (pre filtration sample) and the remaining 200 µl of the solution was placed into an Amicon® Ultra 0.5 ml 10 kDa centrifugal filter (Millipore) and centrifuged for 10 minutes at 13400 rpm. After filtration, 100 µl of permeate was transferred to an eppendorf tube (post filtration sample). Gd concentration was measured with ICP-OES in pre- and post-filtration samples. The stability was calculated using equation 1 as a percentage of the Gd that was still attached to the nanoparticles after filtration.

3.2.2 DLS size analysis

3.2.2.1 Theoretical background

DLS is one of the most common analytical techniques used for determination of particle size and size distribution in suspension. This method relies on the relationship between a particle´s movement in liquid and its size. It measures the intensity of light scattered at a given scattering angle assuming that particles move randomly. This is referred to as Brownian motion (38). The speed of a particle´s movement called the translational diffusion coefficient (D) is proportional to its hydrodynamic radius (R_H). R_H is defined as the size of a sphere that has the same D as the measured particles (33). This relationship is illustrated by the Stokes-Einstein equation shown in equation 2 where k_B is Boltzmann´s constant, T is temperature and η is viscosity.

$$D = \frac{k_B\, T}{6\pi\eta R_H} \qquad Eq\ (2)$$

Since the particles in suspension constantly move by Brownian motion, the intensity of light scattered will also fluctuate depending on the size, so that small particles will produce fast fluctuations and large particles will produce slow fluctuations (Figure 7). These signals are detected and used to calculate the diffusion coefficient from which the hydrodynamic radius can be determined using the Stokes-Einstein equation and knowing the temperature and viscosity of the solution.

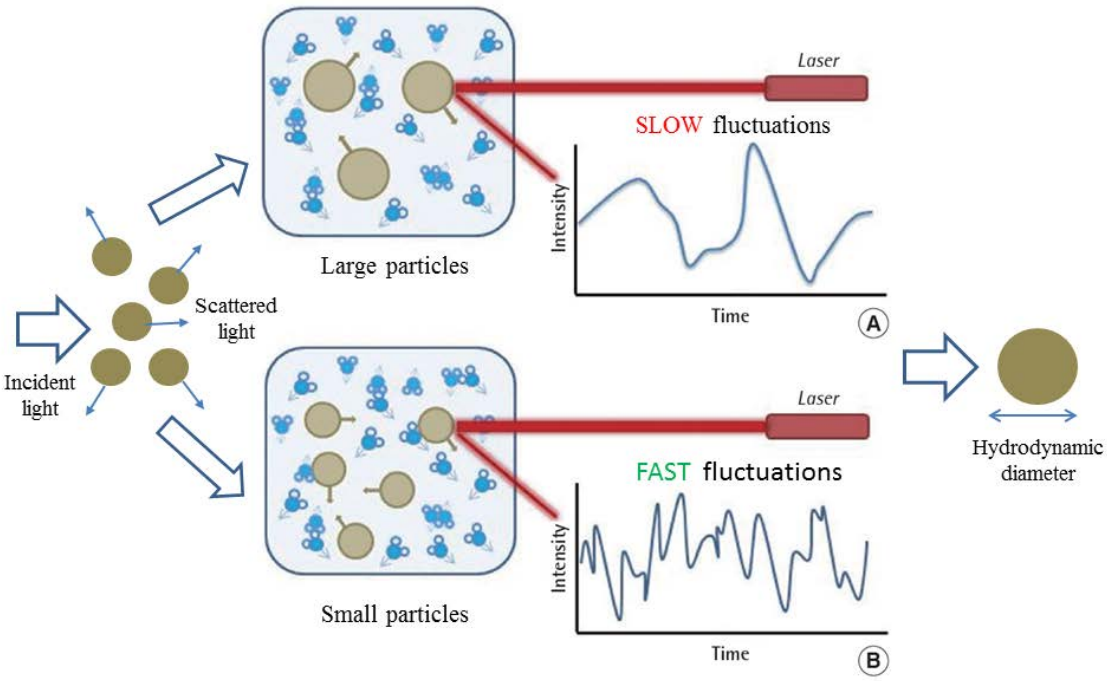

Figure 7. Intensity rate of fluctuations of scattered light from **A)** large particles and **B)** small particles in DLS. The intensity of the scattered light is measured over time (Image modified from Kim et al., 2014) (39).

3.2.2.2 Methodology

To determine the size of the nanomaterial, the size distribution by volume was examined by DLS using Zetasizer Nano ZS (Malvern Instruments) and the Zetasizer software. The size was measured as the volume mean diameter, defined as the diameter of a particle whose volume is equal to the volume of the sample when multiplied by the total number of particles. Changes in size distribution of nanoparticles with regards to two factors, storage time and storage temperature were measured (Table 1).

Table 1. DLS size measurements to study storage time and storage temperature effects. The different conditions used for each measurement are detailed.

Factor	Solution	Matrix	Incubation *	Storage temperature	Storage time	Measurement days
Time	1	Water	2h; 37ºC	Room t	16 days	0-5; 8; 16
	2	SBF	2h; 37ºC	Room t	16 days	0-5; 8; 16
Temperature	3	SBF	2h; 37ºC	Room t	5 days	0-5
	4	SBF	2h; 37ºC	4ºC	5 days	0-5
	5	SBF	2h; 37ºC	-20ºC **	5 days	0-5

* nanoparticles/matrix volume ratio=1. Incubation in water bath.
** aliquots were prepared to avoid size changes if the same sample was thawed and refrozen several times

DLS was also used to measure the size of the nanoparticles in the different matrices as well as the size of the fractionated material.

Nanoparticle solutions diluted in SBF and urine were measured as is, whereas the nanomaterial solutions in water and HS were diluted with 225 µl of 50 mM $(NH_4)_2CO_3$ (pH 7.4, adjusted with formic acid). All samples were placed in cell disposable cuvettes (ZEN 0040) with a final volume of 250 µl.

Some considerations were taken into account prior to DLS measurements: transparency of each sample, solution concentration for optimal measurements and careful preparation of the sample to avoid dirt or dust particles. When necessary, the solutions were filtered using 25 mm syringe filters with 0.2 µm GHP membrane (PALL, Life Science) to remove large particles prior to measurement.

An established standard operation procedure (SOP) for size measurement was followed and the reported size of nanoparticles was chosen following a standard procedure (Appendix I).

3.3 Incubation of nanoparticles with matrices

The matrices used to mix with the nanoparticles were water, urine, SBF and HS. SBF and HS were used as the matrices to mimic physiological conditions in human blood plasma. The SBF buffer was prepared as follows (Table 2).

Table 2. Chemical components and amount of each compound in the SBF buffer.

Chemical Compound	Formula	Purity or Concentration [% or M]	Company	Lot [#]	Amount (g or ml)
Sodium Chloride	NaCl	≥ 99.5 %	Sigma Aldrich	BCBF1709V	7,996
Sodium Bicarbonate	$NaHCO_3$	99.7 - 100.3 % (sic)	Sigma Aldrich	011M01472V	0,350
Potassium Chloride	KCl	≥ 99.5 %	Fluka	70320 13007C01	0,224
Potassium Phosphate Dibasic	K_2HPO_4	≥ 98 %	Sigma Aldrich	BCBC3668V	0.174*
Magnesium Chloride	$MgCl_2$	> 95 %	Aldrich Chemistry	MKBD7838V	0.143**
Calcium Chloride Dihydrate	$CaCl_2 \cdot 2H_2O$	99 - 103 % (sic)	Sigma Aldrich	SZBA181AV	0.368***
Sodium Sulphate Anhydrous	Na_2SO_4	≥ 99.0 %	Fluka Analytical	SZB93370	0,071
Hydrochloric Acid	HCl	1.0 M	Solution prepared		40 ml
Trizma Base (= "Tris")	$NH_2(CH_2OH)_3$	minimum 99.9 %	Sigma Life Science	128K5433	6,057
MQ water	H_20	100%	Millipore	-	1000

* instead of 0.228 g of $K_2HPO_4 \cdot H_2O$

** instead of 0.305 g of $MgCl_2 \cdot 6\ H_2O$

*** instead of 0.278 g of $CaCl_2$

One liter was prepared in a 1000 ml volumetric flask where all the reagents were dissolved in MQ water. The solution was mixed at room temperature using a magnetic stirrer. If the solution was not completely clear, it was sonicated with an ultrasonic cleaner (Branson 1510) for 5 minutes. The pH was then adjusted to 7.4 by adding 370 µl of 1 M HCl.

HS was purchased from Sigma Aldrich (H6914) from male AB clotted whole blood and stored at -20 ºC. After thawing it at room temperature, the serum was centrifuged for 2 minutes at 13400 rpm before use to avoid aggregation (40). Then, it was used as is or diluted 1:10 and 1:100 in distilled water due to the high concentration of proteins. All these matrices were incubated with the nanoparticles.

Urine was freshly donated by me and stored in the fridge at 4 ºC to avoid bacterial growth. It was filtered through a 25 mm syringe filter with 0.2 µm GHP membrane (PALL, Life Science) before incubation with the nanoparticles.

Three nanoparticle batches were used to incubate with the matrices. They were called GF0103 0.1R, GF01058 0.1R and GF01102 0.1R respectively when they were loaded with Gd. The starting concentration of each element was 77.3 mM, 100.4 mM and 3.7 mM of P, Si and Gd respectively. Nanoparticles were mixed at a volume ratio 1:1 with each of the five biological matrices. The solutions were incubated in a water bath with constant shaking for 2 hours at 37 ºC, the physiological body temperature. After that, solutions were concentrated with 10 kDa filters (Millipore) by centrifugation at 3500 rpm for 10 minutes and 25 ºC.

3.4 Preparative GPC of nanoparticles

3.4.1 Theoretical background

Gel Permeation Chromatography, a type of size exclusion chromatography (SEC), separates molecules by size.

GPC/SEC contains a static liquid in the pores of beads as the stationary phase and a running liquid acting as the mobile phase. The particles are differently retained in the pores of the polymer beads depending on their size. Large particles are eluted first, because they do not enter the beads at all, whereas small particles can enter pores in the beads, having a more tortuous path, so they will come out later in time (67). The equipment contains a pump to introduce the solvent, an injection needle, a column that holds the stationary phase, a detector for nanoparticles called evaporating light scattering detector (ELSD) and a software to control all the outputs (Figure 8).

Figure 8. Main components of GPC/SEC equipment: pump, injector, column, detector and software (Image reproduced from http://polymer.ustc.edu.cn/xwxx_20/xw/201109/P020110906263097048536.pdf) (41).

The goal, when using preparative GPC, is the isolation of particles in discrete fractions. A fraction collector is added to the components of the GPC/SEC equipment described in figure 8 (Figure 9A). The sample goes from the pump to the column and from the column the flow is split in two: 10% of the flow goes to the ELSD and 90% of the flow goes to the fraction collector, where it is divided for waste and collection. The tap, shown in figure 9B, regulates the flow direction and pressure changes occur when opening and closing this tap. Thus, it remained in a fixed position, as indicated in figure 9B. All the flow was coming down for collection and nothing was coming out for waste when the tap was in this position.

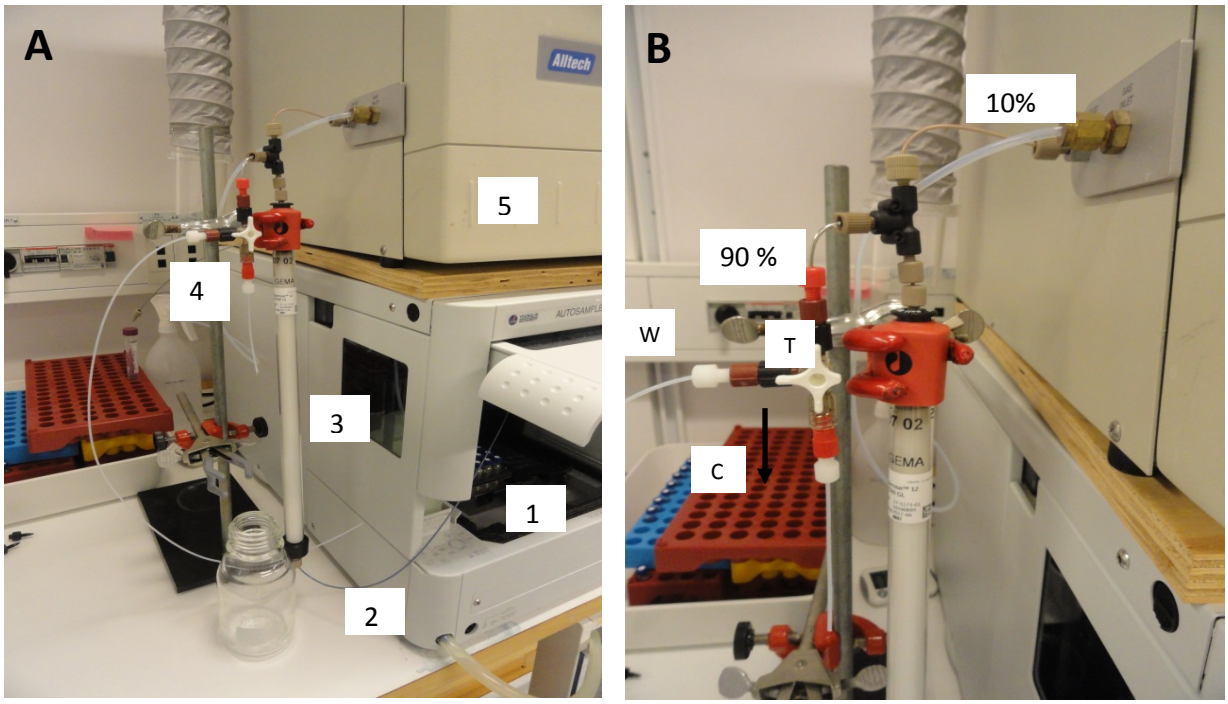

Figure 9. GPC/SEC equipment in the preparative mode **A)** Overview of the equipment arrangement **1.** Injector **2.** Cable connecting the pump with the column **3.** Column with the stationary phase inside **4.** Fraction collector **5.** ELSD where nanoparticles are detected **B)** Detailed figure of the fraction collector. 10% is going to the ELSD that will give a peak signal on the monitor and 90% is going to the fraction collector. The tap (T) regulates the direction of the flow that can be separated for waste (W) and collection (C).

3.4.2 Methodology

A YL9100 HPLC System (Dalco Chromtech) was used to collect the fractions from nanoparticles in water and nanoparticles mixed with SBF, HS and urine respectively. HPLC consisted of several parts: YL9101 (Vacuum Degasser), YL9110 (Quaternary Pump), YL9130 (Column Compartment) and ELSD 2000 (Alltech). The Clarity HPCL software was used to monitor ELSD signals from the nanoparticles.

A prepacked Tricorn column Superose^{TM} 12 10/300 (GE Healthcare) was used with freshly prepared 50 mM $(NH_4)_2CO_3$ buffer (pH 7.4, adjusted with formic acid) as mobile phase. The pH of the buffer was adjusted everyday before use.

First, a baseline for pressure and ELSD signals was established by purging with 100% of 50 mM $(NH_4)_2CO_3$ (pH 7.4, adjusted with formic acid) at a flow rate of 1 ml/min. This flow rate was running for approximately 30 minutes until both signals, pressure (± 0.1 MPa) and ELSD (± 0.2 mV), were stable. Nanoparticles suspended in a biological matrix were injected onto the column. The injection volume was 125 µl and the flow rate was 1 ml/min. The running time for each injection was 30 minutes. ELSD registered 10% of the signal on the monitor as different peaks representing the elution times. 90% of the flow was collected in 7 separate fractions during the running time for a total of 5-7 injections.

3.4.2.1 Determination of the delay between the fraction collector and the ELSD

The delay between the sample exiting to the collection tube and the sample giving an ELSD signal on the monitor was measured. This delay was taken into account when calculating the collection times for each fraction. A dye, Blue Dextran (Sigma, Life Science) stored at 4 ºC in the fridge, was used. It was diluted to 0.01 g/ml with distilled water and then filtered using a 25 mm syringe filter with 0.2 µm GHP membrane (PALL, Life Science). 50 µl of this solution was injected onto the GPC column in the preparative mode and fractions were collected each 15 seconds between 5.45 and 8 minutes. The absorbance of each collected sample was measured at 220 nm in a spectrophotometer (UV-1800 CE 230V, Shimadzu) to calculate the time point at which the absorbance was increasing. The sample was coming to the fraction collector 18 seconds before the ELSD signal (0.3 minutes in the decimal system that the software was using).

3.4.2.2 Fractionation of nanoparticles

Time-based and peak-detection fractionation methods were used to fractionate. 125 µl of the nanoparticle solution was injected onto the GPC column and collection times were decided upon the peak separation patterns observed. Special attention was paid to the peaks given by the nanoparticles, which were in the range between 10-17 minutes (see 4.2.1 of Results). Once these times were determined, column overloading strategy was followed to fractionate. 125 µl of the nanoparticle solution was injected onto the GPC column for 30 minutes at a flow rate of 1 ml/min. In total, 5-7 fractionation runs were performed for each matrix. The volume of each fraction correlated to the collection times. Peak separation patterns were changing due to fluctuations in pressure and matrix effects, so collection times were adjusted for each matrix (Table 3). HS as a blank matrix was also fractionated to further analyze protein-nanoparticle interactions. The fractionation was performed in the following order: water (1º), SBF, HS, urine, HS 1:10, HS 1:100 and water 2º (Appendix IX).

Table 3. Collection times and volumes of each fraction in the different matrices. Retention time from the software and the timer times in minutes are indicated.

Matrix	Fraction	Retention time (min)	*Timer time (min) **	Total volume collected (ml)
Water 1º /2º) (Injection volume= 500 µl)	# F1	5-10.5//5-10	3.42-9.12//3.42-8.42	22.0//20
	# F2	10.5-13.5//10-13	9.12-12.12//8.42-11.42	12.0//12.0
	# F3	13.5-15//13-14.8	12.12-13.42//11.42-13.12	6.0//7.2
	# F4	15.0-17.1//14.5-16.4	13.42-15.48//13.12-15.06	8.4//7.6
	# F5	17.1-18.7//16.4-18.1	15.48-17.24//15.06-16.48	6.5//6.8
	# F6	18.7-20.9//18.1-20.4	17.24-19.36//16.48-19.06	8.8//9.2
	# F7	20.9-25.0//20.4-25	19.36-23.42//19.06-23.42	16.5//18.4
SBF (Injection volume= 500 µl)	# F1	5.0-9.8	3.42-8.3	19.2
	# F2	9.8-12.0	8.3-10.42	8.8
	# F3	12.0-14.0	10.42-12.42	8.0
	# F4	14.0-16.8	12.42-15.30	11.2
	# F5	16.8-18.5	15.30-17.12	6.8
	# F6	18.5-21.2	17.12-19.54	10.8
	# F7	21.2-25.0	19.54-23.42	15.2
Matrix	**Fraction**	**Collection time (decimal system)**	**Timer time (metric system)**	**Total volume collected (ml)**
***HS//HS 1:10 and 1:100 (Injection volume = 500 µl)	# F1	5.0-9.0// 5-10.8	3.40-7.40//3.42-9.30	16.0//23.2
	# F2	9.0-11.6//10.8-13.4	7.40-10.16//9.30-12.06	10.4//10.4
	# F3	11.6-14.0//13.4-14.5	10.16-12.40//12.06-13.12	9.6//4.4
	# F4	14.0-16.3//14.5-16.8	12.40-14.58//13.12-15.30	9.2//9.2
	# F5	16.3-18.2//16.8-18.4	14.58-16.52//15.30-17.06	7.6//6.4
	# F6	18.2-21.2//18.4-20.8	16.52-19.52//17.06-19.30	12.0//9.6
	# F7	21.2-25.0//20.8-25	19.52-23.42//19.30-25	15.2//16.8
Urine (Injection volume= 600 µl)	# F1	5-0-10.5	3.42-9.12	27,5
	# F2	10.5-13.3	9.12-12.0	14.0
	# F3	13.3-14.5	12-0-13.12	6.0
	# F4	14.5-16.8	13.12-15.3	11.5
	# F5	16.8-18.3	15.3-17.0	7.5
	# F6	18.3-21.8	17.0-20.3	17.5
	# F7	21.8-25.0	20.3-23.42	16.0

* The delay time between ELSD and collector was taken into account (18´´)

** The timer was started at retention time 1.00 minute in the software

***Blank HS was also fractionated for further SDS-PAGE analysis

3.5 Analytical GPC of nanoparticles

3.5.1 Theoretical background

Analytical GPC is based on the same principles as explained for the preparative mode but it aims to quantify and identify different compounds based on their size. It relates elution times and sizes of particles compared to some standard references with known sizes (63). In the analytical GPC, a PDA Detector UV lamp is connected to detect proteins. These proteins are used as internal standards to measure the retention time of the samples. The sample goes from the pump to the column. From the column, it goes first to the UV lamp and from there to the ELSD without being collected. Since the sample amount applied is lower compared to the preparative GPC, the peaks maintain narrow and sharp profiles in an analytical chromatography due to a non-saturated column (42). Because of changes in the profile peaks in the preparative GPC, the analytical method is preferred when analyzing the size whereas the preparative mode is used only for fractionation. The equipment in an analytical set-up is depicted in figure 10.

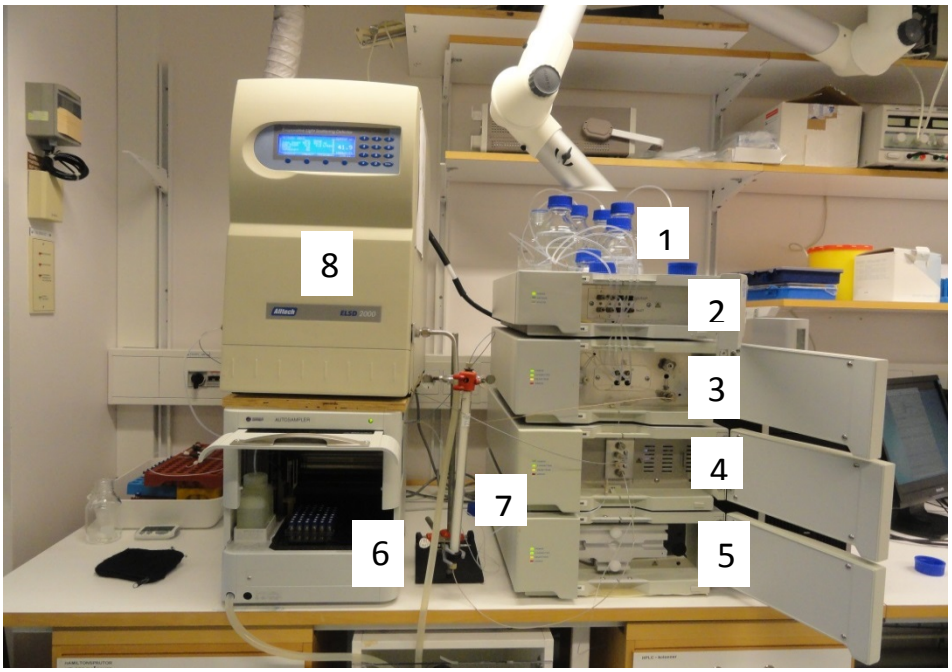

Figure 10. GPC/SEC equipment in the analytical mode **1.** Running buffer, 50 mM $(NH_4)_2CO_3$ (pH 7.4, adjusted with formic acid) **2**.Vacuum degasser **3.** Quaternary lamp **4.** PDA detector UV lamp **5.** Column compartment **6**. Injector **7.** Column **8.** ELSD

3.5.2 Methodology

The equipment in figure 10 was used to analyze both nanoparticle solutions and fractionated nanoparticles. First, a baseline for pressure and ELSD signals was established by purging with 100 % of 50 mM $(NH_4)_2CO_3$ (pH 7.4, adjusted with formic acid) at a flow rate of 1 ml/min. This flow rate was running for approximately 30 minutes until both signals, pressure (± 0.1

MPa) and ELSD (± 0.2 mV), were stable. Then, the samples were injected onto the column for a total running time of 30 minutes and a flow rate of 1 ml/min.

3.5.2.1 Size determination of nanoparticles

Retention time for nanoparticle solutions in different matrices was determined using two protein references, albumin and myoglobin. For nanoparticles in human serum, protein standards were not added. For nanoparticles in water, SBF and urine, two protein standard solutions (5 mg/ml) were prepared by dissolving bovine serum albumin (BSA) (≥ 98 % ; Sigma, Life Science) and myoglobin from equine heart (≥ 90 % ; Sigma Life Science) in 50 mM $(NH_4)_2CO_3$ (pH 7.4, adjusted with formic acid). A solution of 200 µl was prepared by mixing 180 µl of nanoparticles with 10 µl of each protein standard solution, albumin and myoglobin, respectively. 50 µl of this sample was injected onto the GPC column with the conditions mentioned above. The delay between the UV and ELSD signals was 0.3 min in the software (previously determined). This delay was used to adjust ELSD peak signals and calculate the retention time using the albumin peak as a reference.

3.5.2.2 Analysis of the fractionated nanoparticles

The fractionated nanoparticles in the different matrices were analyzed by GPC/SEC to test if the fractionation was successful. 125 µl of each fraction was injected onto the GPC column without any protein standards. In this case, the internal reference was the corresponding nanoparticle solution used for fractionation. The peak separation patterns from the nanoparticles were compared with the peaks obtained from the fractions to check if the retention times were the same.

3.6 Elemental analysis of components: ICP-OES

3.6.1 Theoretical background

ICP-OES is an analytical procedure used to quantify the concentration of a wide variety of materials in a sample. The equipment contains two main components: an ICP torch and the spectrometer detector. Argon gas is directed through the torch connected to a radio frequency generator. As electrical power is applied, electrical and magnetic fields are created on the top of the torch allowing the release of electrons from argon atoms. These electrons acquire high energy levels due to the magnetic field and this is known as inductive coupling. The excited electrons hit argon atoms and disintegrate the gas into plasma containing argon atoms, electrons and ions (43). The sample of interest, in liquid form, is carried through a pump into a nebulizer that converts the sample into aerosol drops. The analyte, in the form of an aerosol, is introduced into the hot plasma by a second argon gas flow. The high temperature causes the sample to be, first converted into solid particles and then vaporized. The resulting gas is atomized and ionized, releasing atoms and ions respectively (44). When these ions are excited, they emit light at characteristic wavelengths typical for each element. This light is detected and quantified through a spectrometer with a monochromator that converts the light into a spectrum with its constituent wavelengths (34).

3.6.2 Methodology

The concentration of Si, P and Gd in the nanoparticles and the fractionated material was determined by Nooshin Yousefpour and Olof Björnberg from Spago Nanomedical using ICP-OES 710 from Agilent. Samples contained in water, SBF and urine were diluted in 1% HNO_3 whereas samples dissolved in HS were diluted in 0.1% HNO_3. Standard curves of the different elements were made in 1% HNO_3, with concentration ranges that encompassed the sample concentration. Limits of quantification (LOQ) for Si, P and Gd were 0.1 mg/l, 0.2 mg/l and 0.048 mg/ml respectively. The concentrations of Si, P and Gd in the nanoparticle solution, obtained using ICP-OES, were used for comparison with the Si, P and Gd concentrations in each fraction. The amount of recovered material after fractionation was calculated.

3.7 Anti-PEG ELISA assay

3.7.1 Theoretical background

Enzyme-linked immunosorbent assay (ELISA) is a biochemical test used to detect and quantify a molecule through antibodies, enzymes and color development. A competitive-based ELISA was used to quantify the concentration of PEG in the fractionated material. In this assay, an enzyme called PEG-Horseradish peroxidase (HRP) is mixed with the PEGylated samples and transferred to the wells. PEGylated molecules and PEG-HRP compete for the binding to anti-PEG antibodies that are attached to the bottom of the well-plate. If the sample contains a low PEG concentration, more PEG-HRP can bind to the antibodies whereas if PEG concentration in the sample is high, less PEG-HRP will bind. A substrate for the enzyme HRP, 3, 3', 5,5'-Tetramethylbenzidine (TMB), is added to produce color. When PEG-HRP cleaves the substrate, a blue color is produced. A stop solution to end this reaction is added changing the color from blue to yellow (Figure 11). The absorbance of the solution at 450 nm is inversely proportional to the amount of PEG in the samples. If the amount of PEG in the sample is low, more enzyme can bind to the wells, cleaving more substrate and producing an intense color. A higher PEG concentration in the samples will result in a weak or absent color.

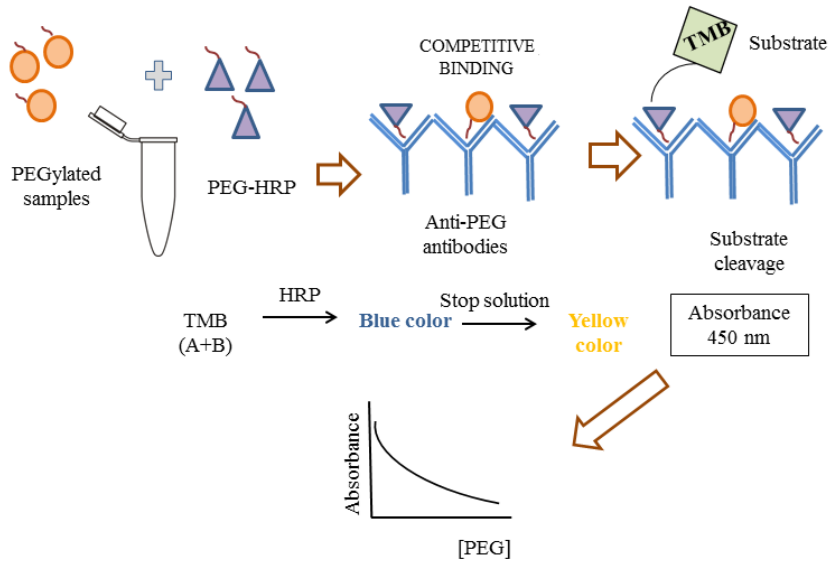

Figure 11. Competitive ELISA assay between PEGylated samples and PEG-HRP. PEGylated samples and PEG-HRP compete for the binding to anti-PEG antibodies. As a result of this competition, different amounts of PEG-HRP will bind to the antibodies and more or less amount of substrate will be cleaved. Thus, different color intensity will be obtained giving different absorbance values at 450 nm.

3.7.2 Methodology

To quantify the amount of PEG contained in each fraction, a competitive ELISA assay was performed using the PEG ELISA Kit RabMab ab138914 (Abcam) following the instructions for use provided by the manufacturer (Appendix II). The fractions were mixed with PEG-HRP and then placed into a microtiter plate where the anti-PEG antibodies were attached. Then, the mixture was incubated for 45 minutes in a shaker at room temperature and washed 3 times with the ELISA washing buffer provided. After that, 100 µl of a chromogenic substrate, TMB, was added to each well and incubated for 15 minutes protected from the light, at room temperature. Finally, the mixture was placed into a V-bottomed 96-well plate (Nunc TM, Thermo Scientific) and the optical density was measured at 450 nm using a microplate reader (SoftMax® Pro Microplate Reader and Analysis software). Water, SBF, HS and urine were used as the respective blanks for each matrix.

A nanoparticle solution, in which the Si concentration was already determined by ICP-OES, was used as a reference to build a standard curve in each matrix (water, SBF, HS and urine). This standard solution was diluted to a concentration range between 0.2-4 µM Si. PEG monomer (mPEG 550, MKBR 1665V, Sigma Aldrich) was also used as another internal reference for PEG concentration (data not shown). Then, each fraction was diluted to 0.2-4 µM and the absorbance values were used to calculate PEG concentration using three different standard equations depending on the matrix. For the first fractionation in water and for SBF and HS, equation 3 was used; for the second fractionation in water, equation 4 was used and for the urine fractionation equation 5 was used. In all these equations, x is the PEG concentration (µM) and y is the absorbance.

$$y = 0.3473e^{-2.336x} \qquad Eq\ (3)$$
$$y = 1.1303e^{-3.267x} \qquad Eq\ (4)$$
$$y = 0.0918x^{0.702} \qquad Eq\ (5)$$

3.8 SDS-polyacrylamide gel electrophoresis

3.8.1 Theoretical background

Sodium dodecyl sulphate polyacrylamide gel electrophoresis (SDS-PAGE) separates proteins only according to their size. Then, the molecular weight can be identified using standard proteins with known molecular weights.

SDS is an anionic detergent that denatures the proteins by interacting with hydrophobic amino acids in the proteins. These amino acids are responsible for the tertiary and quaternary structures of the proteins. When mixed with SDS, proteins become linear polypeptide chains that are negatively charged and will migrate towards a positive electrode (45).

3.8.2 Methodology

SDS-PAGE was performed using pre-cast 12 % NuPAGE® Bis-Tris Mini Gels (Life Technologies). Each nanoparticle fraction (HS andHS+NPs) 1-7 was mixed in a ratio 1:4 with NuPAGE® LDS Sample Buffer (4x) and deionized water if needed, up to a total volume of 10 µl. Then, the samples were heated and shaken, to further denature the proteins, using a heating

block (IKA® KS 130) for 10 minutes at 80 ºC and 240 rpm. 1X NuPAGE® MES-SDS running buffer was prepared by adding 50 ml of 20X NuPAGE® MES-SDS running buffer to 950 ml of deionized water. 12 µl per sample was loaded onto a 12 % NuPAGE® Bis-Tris Mini Gel and 12 µl of PageRuler Prestained Protein Ladder 10-170 kDa (LifeTechnologies) was loaded as a protein standard to follow the molecular weight of the proteins. The gel was run for different times (35 min, 1h 30 min and 1h 45 min) at 200 V with 1X NuPAGE® MES-SDS as running buffer.

Then, the gel was washed 3 times for 5 minutes with distilled water and stained with Simply Blue Safe Stain (Coomassie Blue, Life Technologies) for 1 hour with a balance shaking at low speed (Grant-Bio, PMR 30). Finally, it was destained overnight with distilled water and washed again with distilled water the next day for 1 hour. Then, it was dried and analyzed with the softwares GIMP 2 and Inkscape 0.91. Fractionation of HS and SDS-PAGE were carried out together with Evelina Folkesson at Spago Nanomedical.

3.9 Determination of protein concentration: the Bradford assay

3.9.1 Theoretical background

The Bradford assay is a fast and accurate method for determination of protein concentration. It is based on the binding of the dye Coomassie Blue G250 to the proteins. The assay reagent Coomassie Plus™ contains Coomasie Blue G250 dye, methanol, phosphoric acid and distilled water. The free dye can exist in different ionic forms. Two of the predominant ionic forms in the acidic reagent are the brown and blue forms with absorbance values at 465 and 595 nm respectively. In the acidic conditions of the assay reagent, proteins bind to the dye and cause a change in the absorbance from 465 nm to 595 nm associated with a color change. Therefore, protein concentration is estimated by determining the amount of dye in the blue ionic form. A high protein concentration will give an intense blue color and a higher absorbance. Protein concentration in unknown samples can be calculated from a standard series of known protein dilutions of BSA.

3.9.2 Methodology

Protein concentration in four matrices (HS, HS 1:10, HS 1:100 and urine) was determined by the Coomassie Plus™ (Bradford) assay kit (Thermo Scientific). Standard dilution series of BSA were prepared in 50 mM $(NH_4)_2CO_3$ (pH 7.4, adjusted with formic acid). After preparation of the standards, the Coomassie Plus Reagent was mixed several times by inverting the bottle and placed at room temperature. Then, 0.05 ml of each standard or unknown sample (previously diluted if needed) was mixed with 1.5 ml of the Coomassie Plus Reagent and incubated for 10 minutes at room temperature.

The spectrophotometer (UV-1800 CE 230V, Shimadzu) was used to measure the absorbance at 595 nm. First, it was set to zero using 1 ml of distilled water placed in a UV-cuvette. Then, 1 ml of 50 mM $(NH_4)_2CO_3$ (pH 7.4, adjusted with formic acid) was placed in a UV-cuvette and used as a blank. After that, 1 ml of each sample was placed in a UV-cuvette and the absorbance was measured.

The absorbance measurement for the blank was subtracted from the measurements of all the samples and two standards curves with the BSA standards were created (absorbance measurement vs. concentration in µg/ml) (Figure 12). Equation 6 was used to calculate the protein concentration of the unknown samples in the concentration range of 0-800 µg/ml and equation 7 was used to calculate the protein concentration of the unknown samples with a concentration range of 900-2000 µg/ml. In both equations, x is the protein concentration (µg/ml) and y is the absorbance.

$$y = 0{,}0011x + 0{,}0196 \qquad Eq\ (6)$$

$$y = 0{,}3206\ln(x) - 1{,}2882 \qquad Eq\ (7)$$

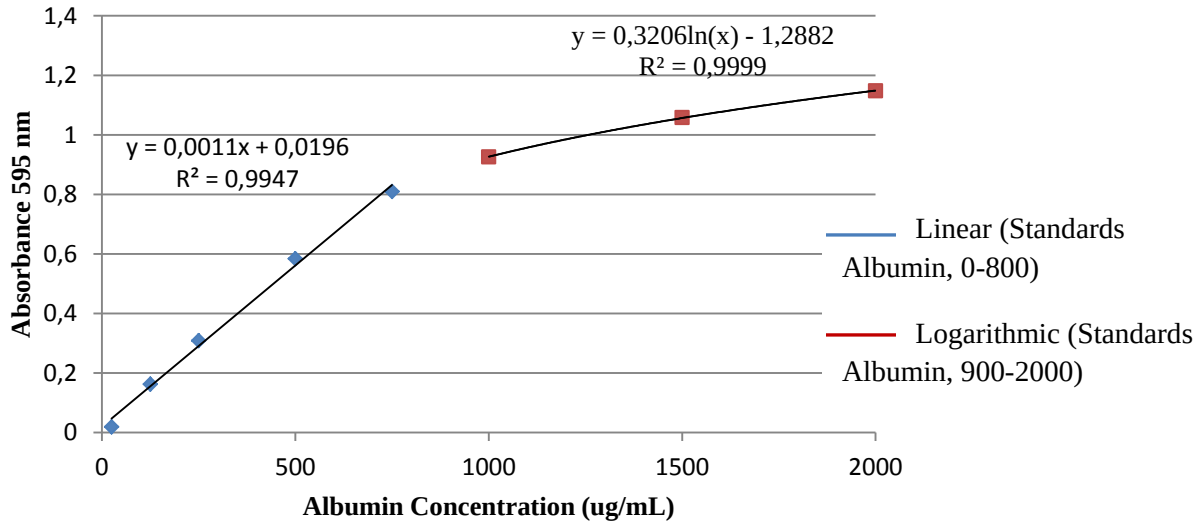

Figure 12. Standard curve for BSA samples. Absorbance values at 595 nm for each BSA standard were corrected with the blank and plotted against its concentration in µg/ml.

4. Results and Discussion

4.1 Characterization of nanoparticles in different matrices

The ultimate aim of the project was to establish a new approach to extract and characterize nanoparticles first from blood and urine samples and then possibly from liver and tumors. Since blood was a very complex matrix to start with, I chose SBF and HS which have similarities in composition with blood. I proved that the nanoparticles retained their physical properties in the matrices and I also quantified how much of the injected material remained after extraction. After separating the material using GPC, I was able to prove identity and concentration of the extracted nanoparticles in the matrices using ICP-OES and ELISA. To prove identity, I characterized the nanomaterial, before and after separation, in order to compare the pre-and post-fractionated particles. To prove concentration, I measured Si, Gd and PEG concentrations of the fractions in the different matrices. First, I studied the viability of IXGp-Gd nanoparticles in water by analyzing the core structure, metal ion stability, PEG coating and size.

4.1.1 Core structure

The main structure consists of organosilicophosphonate polymers which constitute the central core containing Si and P atoms. An external coating made of PEG silane is covalently attached to the core. The core contains chelating sites with ligand binding atoms that chelate metal ions. The nanoparticle precursor was loaded with Gd to mimic the current nanoparticles used today for MRI (Figure 13). An elemental analysis of the core was performed to characterize its composition.

4.1.1.1 Elemental analysis

ICP-OES was used to perform the elemental analysis of the core with respect to Si and P concentrations. The core of the nanoparticles was made of cross-linked monomers. Each monomer contained two atoms of P and two atoms of Si (Figure 13). However, total P concentration was expected to be less than total Si concentration because Si also accounted for the PEG coating. Thus, the ratio Si/P was expected to be higher than 1.

In fact, P and Si concentrations were 77.3 mM and 100.4 mM respectively for nanoparticles in water. The ratio Si/P was 1.3. P was only measurable in water because the other matrices contained significant amounts of P, in concentrations of 3.2 mg/dl and 0.5 mg/dl in serum and urine respectively (46). ICP-OES also accounted for this P concentration and gave background signal when measuring P concentration in nanoparticles. Therefore, P was only measured for the particles in water whereas Si and Gd concentrations were measured in all matrices and were used to compare among these matrices.

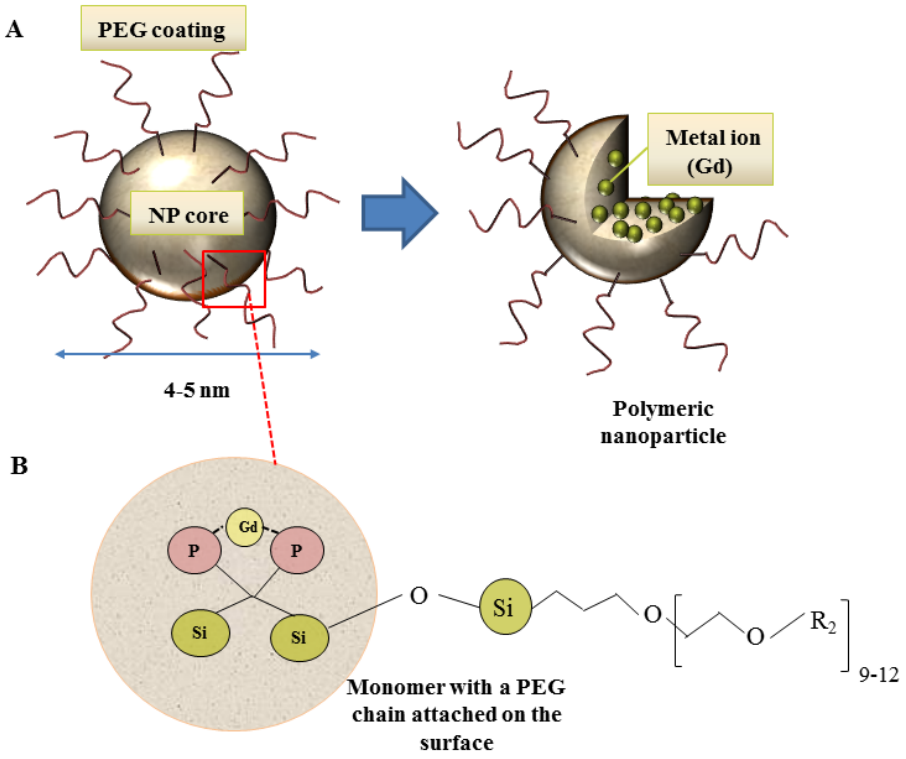

Figure 13. Schematic representation of the nanoparticle structure used in this project **A)** General overview of the different components of the nanomaterial: core with chelated metal ions (Gd) and the coating, consisting on several PEG chains (9-12 monomers) covalently attached to the core **B)** Simplified illustration showing in detail the composition of both the core (Si, P and Gd) and the PEG coating (PEG silane).

4.1.2 Metal ion

4.1.2.1 Elemental analysis

Gd concentration, measured with ICP-OES, was 3.7 mM and it was loaded in molar ratios of 1:20 with respect to P. Since the ratio Si/P expected in the core of each monomer in the nanoparticles was 1, the expected Si/Gd ratio was, thus, 1:20. Calculated Si/Gd ratio (n=3 samples) was between 21.5 and 23. Si/Gd ratio was accounted for all the matrices (Figure 14; Appendix IIIA and B).

The measured Si/Gd ratio was higher than the expected value. This difference implied that there was less Gd in the core. Therefore, not all Gd was incorporated into the core since after the loading, the free Gd was removed. However, the Si/Gd ratio was constant for all matrices which meant that the amount of Gd in the core was the same for all of them.

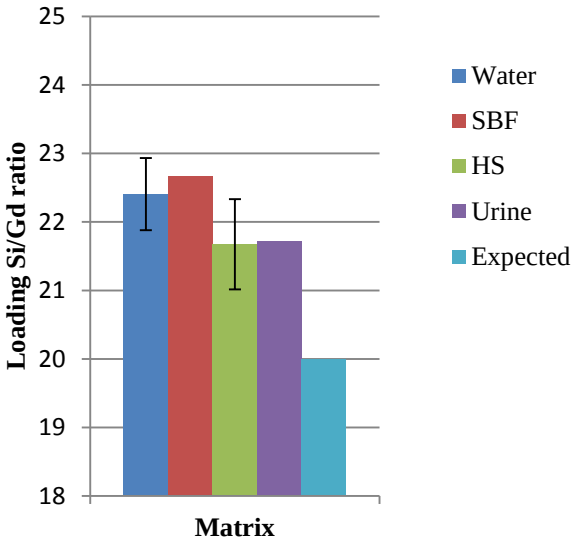

Figure 14. Calculated Si:Gd ratio in different matrices (water, SBF, HS and urine) measured with ICP-OES. (n=3 samples for water and HS; error bars represent the standard error of the mean (SEM)

4.1.2.2 Chelating ability of nanoparticles

Leakage of toxic ions from metal nanoparticles has been related to significant toxicity both *in vitro* and *in vivo* (47). Stable particles have shown low levels of toxicity compared to the ones that are more soluble. Thus, a stability test of metal-containing nanoparticles is used to assess stability related to safety levels in nanoparticles (48).

To analyze the affinity of the nanoparticles for Gd and the strength of the binding, two stability tests of Gd-containing nanoparticles were performed: in the presence of EDTA and in the absence of a chelating agent, respectively. The first method was based on a chelation effect in which EDTA acted as a chelating agent that captured Gd ions. Two different concentrations of EDTA, 1 and 10 mM, were used to incubate with the nanoparticles. The second test was performed to test if the metal ion was leaking from the nanoparticle´s core without a chelate effect.

The stability of Gd was expected to be close to 100% in the absence of a chelating agent because the nanoparticles have chelating sites for Gd. In the presence of EDTA, nanoparticles and EDTA compete for chelation of Gd. Thus, Gd ions are captured by EDTA and the core will contain lower Gd concentration than it normally has. This chelate effect should be higher with increasing EDTA concentrations.

The limitation of this technique is that it cannot be used for nanoparticles contained in solutions with other metal ions such as calcium or magnesium because they will compete with Gd for the binding to EDTA giving wrong results. Therefore, the stability was only checked for the nanoparticles in water with reliable results (Figure 15). As expected, the stability was inversely proportional to the concentration of EDTA. In the presence of EDTA 1 mM, Gd stability was 69.1% whereas it decreased to 38% when EDTA 10 mM was added.

In the experiment free of EDTA, the stability was 97.7% indicating that almost all Gd remained inside of the core and that the binding to the core was strong enough to avoid release of toxic Gd ions. According to the results, the nanomaterial had a strong ability to chelate Gd and thus, it migh not have toxic effects related to the release of free metal ions.

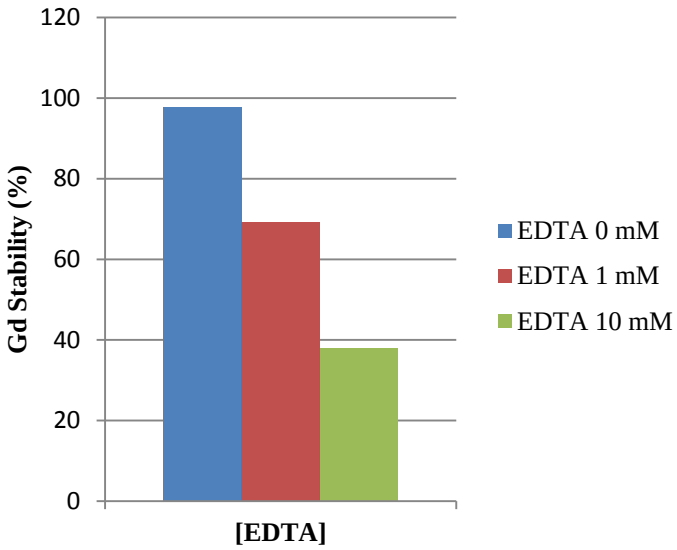

Figure 15. Gd stability in percentage for different concentrations of EDTA. The stability is inversely correlated to the presence of EDTA. Gd stability was 69.1 % in the presence of 1 mM EDTA and 38 % in the presence of 10 mM EDTA. In the absence of EDTA Gd stability was 97.7 %.

It has been demonstrated that unstable nanoparticles which are diluted in biological media have high levels of toxicity causing the release of harmful metal ions to the extracellular media (48). One study done with two different soluble nanoparticles, ZnO and TiO_2 incubated with mammalian cells, revealed that the more toxic particles were those showing a higher solubility in the growth media such as ZnO compared to the ones with low solubility like TiO_2 (49). Another study with two copper oxide particles with similar size, demonstrated that those coated and stabilized with carbon were less toxic than the soluble ones in cell culture. In the last case, copper ions were released to the extracellular media giving toxic effects similar to the ones caused by treatment of cells with equal amounts of isolated copper ions (50). These studies also highlight the importance of having a coating in the particles that isolates the core structure.

4.1.3 PEG coating

PEG-silane coating with 9-12 monomers was covalently attached to the surface of nanoparticles by Spago Nanomedical. The addition of this coating plays an important role in the stabilization of the nanoparticles avoiding aggregation and interaction in biological fluids (26). Quantification of the amount of PEG present on the surface of nanoparticles is a key step in the characterization of the behavior of these particles in the body. Changes in the concentration of PEG such as the release of PEG from the surface of nanoparticles can lead to toxic effects as well as to some undesired interactions and a decrease in the circulation half-life (27). To test this issue, I used PEG coating that was not tightly attached to the core of the

particles so that it could start to fall off. The aim was to study whether I could detect the shedding of coating with ELISA.

4.1.3.1 Elemental and ELISA analysis

Si:P ratio, measured with ICP, was used to calculate PEG concentration in the nanoparticles. Si/P ratio in the nanoparticle was expected to be higher than 1 since Si concentration was the largest. In fact, the measured Si/P ratio was 1.3 (Figure 16; Appendix IIIB).

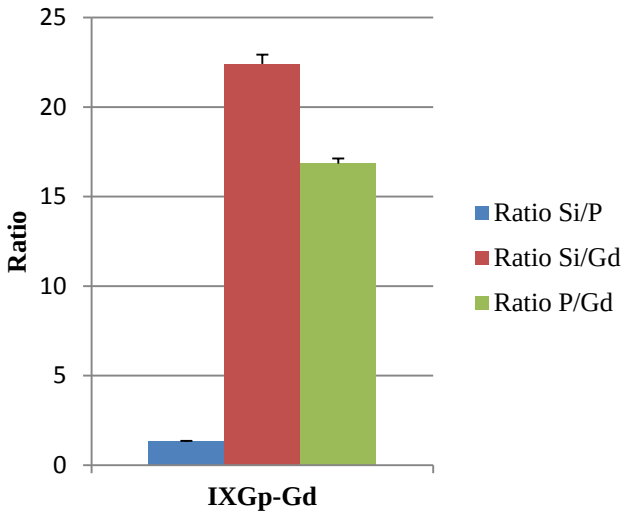

Figure 16. Calculated ratios in nanoparticles from Si, P and Gd concentrations measured with ICP-OES. Si/P ratio was 1.3, Si/Gd was 22.4 and P/Gd was 16.8 (n=3samples; error bars represent the SEM).

PEG coating was calculated as the remaining Si concentration which was not forming part of the core. It was determined as mol percentage of PEG in proportion to mol percentage of the core following equation 8.

$$\%\ PEG = \frac{[Si] - [P]}{[P]} x\ 200\ \% \qquad Eq\ (8)$$

The percentage of PEG for nanoparticles in all matrices was 63.8 %. This equation uses the concentrations measured by ICP-OES. Moreover, ELISA was used to measure PEG concentration using *Eq (3)* for water, SBF and HS (Figure 17). The percentage of PEG obtained from the measured values with ELISA was between 66-77 % which correlates with the calculated value using *Eq (8).*

After evaluating the core and coating, I performed a size characterization of the material to determine stability.

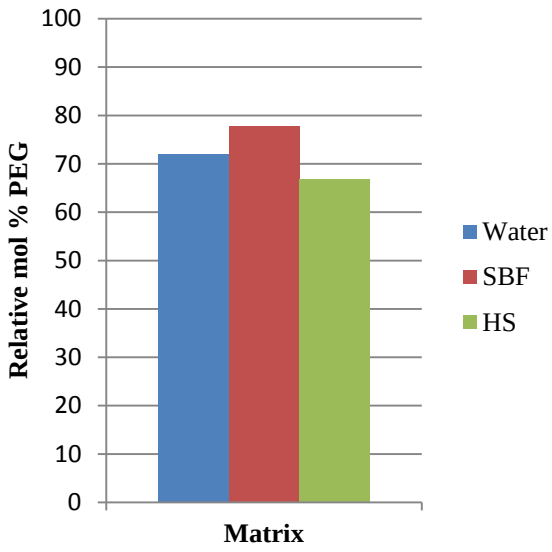

Figure 17. Relative mol % PEG coating with respect to mol % core for different matrices measured using ELISA and *Eq(3)* as the standard curve.

4.1.4 Size analysis

DLS was used to measure the size of the nanoparticles after metal loading and compare it with the sizes obtained from the incubation with different biological matrices (SBF, HS and urine) to assess any differences. The volume mean diameter of the particles in water was between 4.9 (±0.4) and 5.1 (±0.4) nm, similar to the volume mean diameter in SBF about 5.2 (±0.3) nm. However, the size increased up to 6.2 (±0.7) when particles were placed in urine which might be an indication of aggregation (Appendix IIIC). When measuring the size in serum the values obtained were not accurate due to high polydispersity in the samples (data not shown).

The size of nanoparticles stored in water or SBF at room temperature for 16 days was followed to see if the size remained constant for a long period of time and there was not any aggregation occurring (Figure 18A; Appendix IIID). Size stability at room temperature was important to measure to confirm that particles stored at room temperature for a certain period of time did not change their size so they could still be used for *in vitro* tests. Also, to discard that any other possible observed effect was due to size changes. As shown in figure 18A, the size was stable around 5 to 5.7 (±0.4) nm and did not experience notable changes.

The storage temperature of the nanoparticles and how changes in the temperature could cause size alterations was also analyzed. The reason behind was to confirm that when a blood sample was stored in the freezer, the nanoparticles conserved their original size. If some changes were seen in the sample, it was not because of the size changing due to storage in the freezer. The size of particles stored at different temperatures: room temperature, 4 ºC and -20 ºC was approximately the same, between 4.8 and 5.5 (±0.3) nm so the particles were considerably stable when stored at different temperatures for long periods of time (Figure 18B; Appendix IIIE).

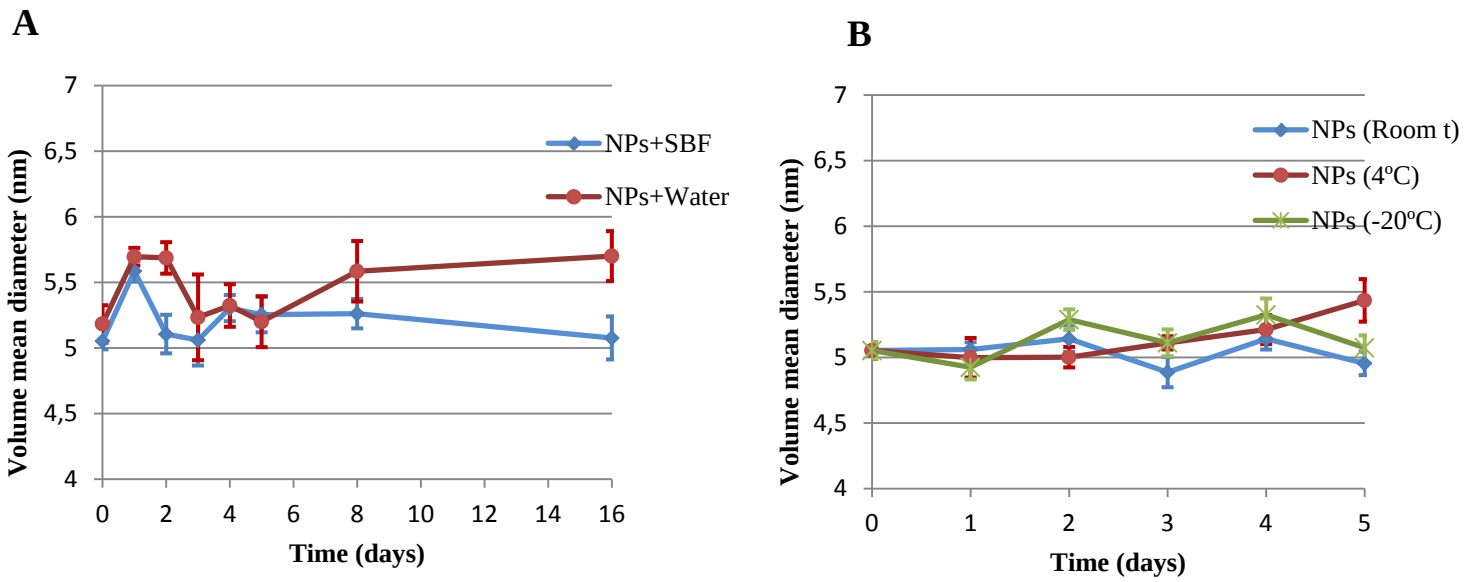

Figure 18. Volume mean diameter (nm) of NPs measure
or water at 37ºC for 2 hours and then stored at room temperature for 16 days (n=8-9 measurements) **C)** Mean diameter of NPs incubated in SBF at 37ºC for 2 hours and then stored at different temperatures (n=8-9 measurements). Error bars represent the SEM. Any statistical test was used to analyze the significance of the study because more measurements were needed in order to conduct such study.

In conclusion, the nanoparticles used had a volume mean diameter of 5 nm (n=7; standard deviation=0.37) where 92 volume % of the population was within a size range comprised between 2.5 and 6.5 nm (Figure 19).

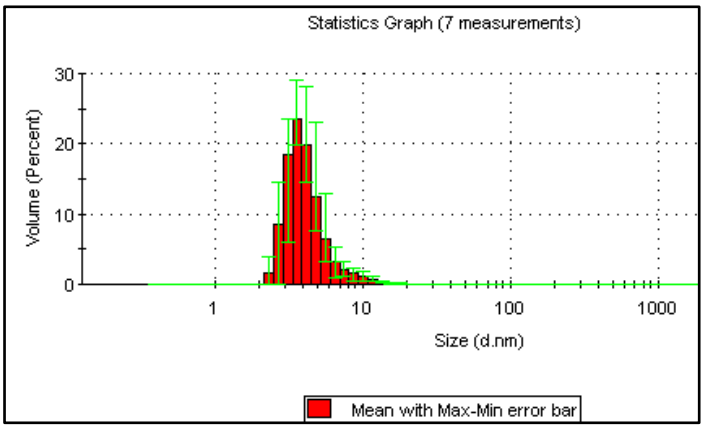

Figure 19. Mean volume percent of NPs in water measured with DLS. The size range for 92 volume % of the particles was between 2.5 and 6.5 nm.

DLS was chosen because it provides a fast and simple way to measure the size even though it also has some limitations. The main disadvantage is that the method is highly sensitive to dust and impurities in the samples. Another limitation is that the size measured depends especially on salt concentration (39). Increasing size particles also increase the polydispersity, with a wide range of size distributions. High polydispersity does not provide accurate size for

particles. When measuring nanoparticles in serum, the larger proteins were masking the signal of the small nanoparticles, increasing the polydispersity so that the size could not be estimated in a reliable way (39). Several techniques are available to measure the size of nanoparticles and can complement DLS measurements. One is TEM which offers high resolution of the size and shape and direct visualization. However, the preparation of the sample can lead to aggregation and there is a preference for high electron dense atoms, such as Gd, reporting an overall size predominated by these atoms. Other methods are the nanoparticle tracking analysis and analytical centrifugation that offer high resolution for size distribution but longer measurement times (51).

The nanoparticle size was also determined through GPC-HPLC as retention time compared to two reference proteins: albumin and myoglobin and their respective elution peaks (Appendix IVA-G). The retention time is defined as the amount of time it takes for the sample to pass through the column. It is measured as the time interval between the injection of the compound into the column and its detection as a peak on the monitor. Since albumin and myoglobin sizes are known, 7 and 4 nm, respectively, the nanoparticles size can be estimated by comparing the retention time between the nanoparticles and the proteins. The elution peak for the nanoparticles in water was located between the peaks of the two proteins (Figure 20). Thus, the estimated size for the nanoparticles using this technique was between 4-7 nm. This result correlates with the size obtained using DLS.

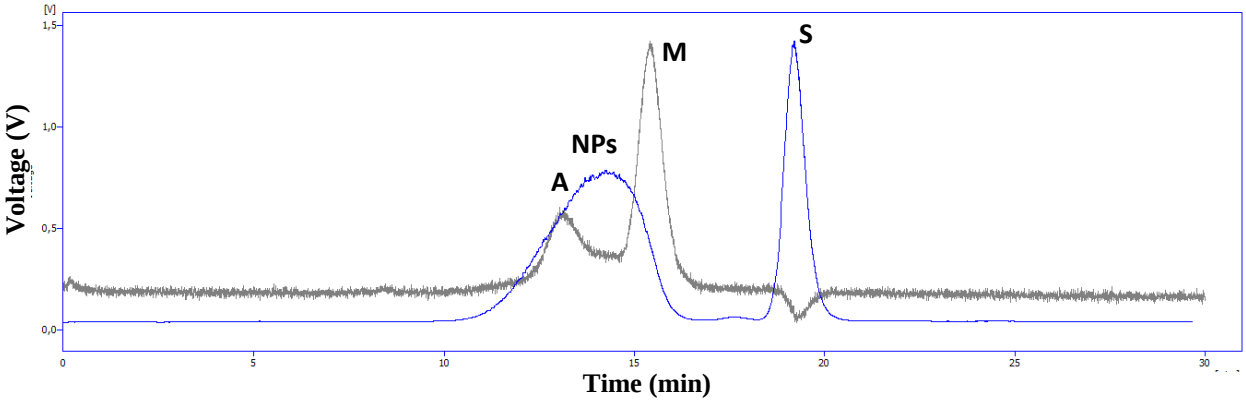

Figure 20. Chromatogram from GPC-HPLC analysis showing the UV (grey) and ELSD (blue) signals from proteins and NPs in water respectively. A: albumin; M: myoglobin; NPs: nanoparticles: S: salts. Nanoparticle´s peak was coming out 1.2 minutes after the albumin peak.

Besides, the pH of the nanoparticle solution was considered as another factor affecting the size through changes in the zeta potential and surface charge. Therefore, when loading the nanoparticles with Gd, an acid pH of 5.2 was measured and adjusted to 7.5, the physiological pH. Even though the analysis of the pH was not the main objective in this project, it was measured when incubated with the different matrices and adjusted to 7.5 when needed. A tendency of a decrease in the pH when the nanoparticles were standing for a certain period of time at room temperature was observed and this was translated into a slightly bigger size, which could be explained through nanoparticle aggregation.

When entering the body, the uptake of the nanoparticles in the cells is dependent on the size, shape and surface charge of particles which will determine its biodistribution, retention and clearance rate (51). Particle size is one of the key determinants to describe the stability and

behavior of particles in a given biological matrix. A decrease in size could mean a dissociation of particles in solution whereas an increase might be caused by aggregation (33). A constant size means stability and that has to be achieved when engineering nanoparticles with medical purposes. Matrix effect arises from the biological solution properties that might differ among the biological fluids. Consequently, size can be different in water than in the rest of the biological matrices, such as in serum or urine, where the presence of proteins and other biomolecules will increase the hydrodynamic radius of the nanoparticles (51).

After testing that the material intended to be used for the project was viable, I used three different techniques (GPC, ELISA and ICP-OES) to establish the bioanalytical method.

4.2 Development and validation of the bioanalysis method

When a new compound is being developed with an intended clinical use, different analytical methods, for quantitative and qualitative evaluation of the molecule, are conducted to perform clinical and toxicology studies. The aim of any bioanalytical method validation is to ensure that an established quantitative procedure to detect some analytes in a biological sample is reliable and sensitive (52). In this project, an optimized method to assay the behavior of nanoparticles in different biological matrices was developed according to FDA and ICH guidelines on validation of bioanalytical methods for new drugs applications and registration in human clinical pharmacology (52) (53).

The main parameters for a bioanalytical method validation are accuracy, precision, selectivity, sensitivity, reproducibility and stability according to FDA and ICH guidelines (52) (53). Some of the parameters analyzed in this project for the method development and validation include: accuracy and recovery, selectivity, calibration curves, limits of optimal resolution and stability. Here, the main focus will be the determination of accuracy, recovery, calibration curves and limits for optimal resolution. Stability of nanoparticles was analyzed in terms of size in the previous section and selectivity will be introduced in the next section.

4.2.1 *GPC-HPLC method for separation of nanoparticles by size*

A preparative mode in the HPLC equipment was assembled in order to separate the starting batch of nanoparticles by size in discrete fractions (F) that were further analyzed. The delay time between the fraction collector and the ELSD was measured using the dye Blue Dextran (see 3.4.2.1 Materials and Methods). Blue Dextran solution was injected onto the GPC column to analyze its retention time in the preparative mode.

The elution peak from Blue Dextran was detected at 7.8 min on the software which corresponded to 7´ 48´´ on the timer (Figure 21). The dye was reinjected onto the column and fractions were collected, using the timer, between 5´ 45´´ and 8´´ each 15´´. The absorbance of each collected sample was measured to see absorbance changes (Table 4). The higher the concentration of the dye in the solution, the greater the amount of light absorbed. An increase in the absorbance was detected at 7´ 30´´ which meant that the particles were starting to be eluted at that time. Thus, the sample was coming to the fraction collector 18´´ before the ELSD signal (0.3 minutes in the software). The software detecting the signals (Clarity program) was using a decimal time system. However, the timer used to collect the fractions

was in minutes and seconds. The decimal time system was converted into the metric time applicable for the timer.

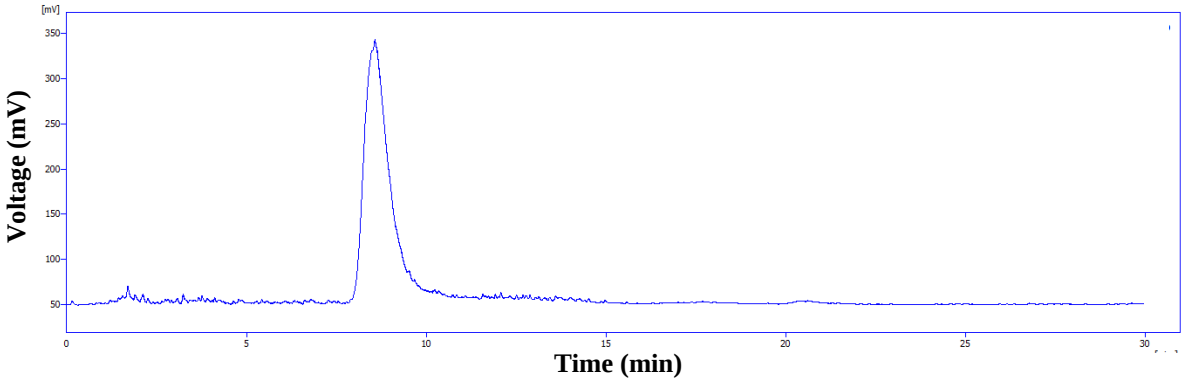

Figure 21. Chromatogram from GPC-HPLC analysis showing the elution peak (ELSD signal) from Blue Dextran (7.8 min on the software corresponding to 7´ 48´´ on the timer).

Table 4. Absorbance values from the Blue Dextran measured at 220 nm

Collection times timer (min and sec)	Absorbance 220 nm	Collection times timer (min and sec)	Absorbance 220 nm
5´45´´- 6´ 00´´	0.018	7´ 00´´- 7´ 15´´	0.018
6´ 00´´- 6´ 15´´	0.014	7´ 15´´- 7´ 30´´	0.016
6´ 15´´- 6´ 30´´	0.008	7´ 30´´- 7´ 45´´	0.038
6´ 30´´- 6´ 45´´	0.009	7´ 45´´- 8´ 00´´	0.096
6´ 45´´- 7´ 00´´	0.010	8´ 00´´- 8´ 15´´	0.101

To successfully separate the nanoparticles in fractions according to size, the analytical mode of the GPC was first used to determine the peak separation patterns and further decide the collection times. First, 50 µl of the nanoparticles contained in the matrix was injected onto the GPC column to measure the retention time of the nanoparticles using the albumin peak as a reference. Then, 125 µl of the nanoparticles was reinjected onto the GPC column (see 3.4.2 Materials and Methods). The aim was to determine the maximum amount of sample volume that could be injected without losing resolution and check changes in the retention time with increasing injection volumes. When increasing the amount of sample applied to the column, the peak height and peak area also increase. However, the peak width and symmetry have to remain unchanged. If more and more sample volume is injected, it reaches a point where the peak height does not increase and the peaks become broader. In that situation, resolution can be lost and the results are not reliable anymore. To determine the collection times, first, the peak symmetry when overloading the column with the maximum amount of sample volume that could be injected (125 µl) was compared with the peak symmetry in the analytical mode. The collection times were then decided according to the desired peaks to be collected. The ELSD signal from nanoparticles was separated in 7 fractions where fractions 1 and 7 were the baselines, fractions 2, 3 and 4 contained the nanomaterial, fraction 5 contained the PEG chains of the coating and fraction 6 represented the salts (Figure 22).

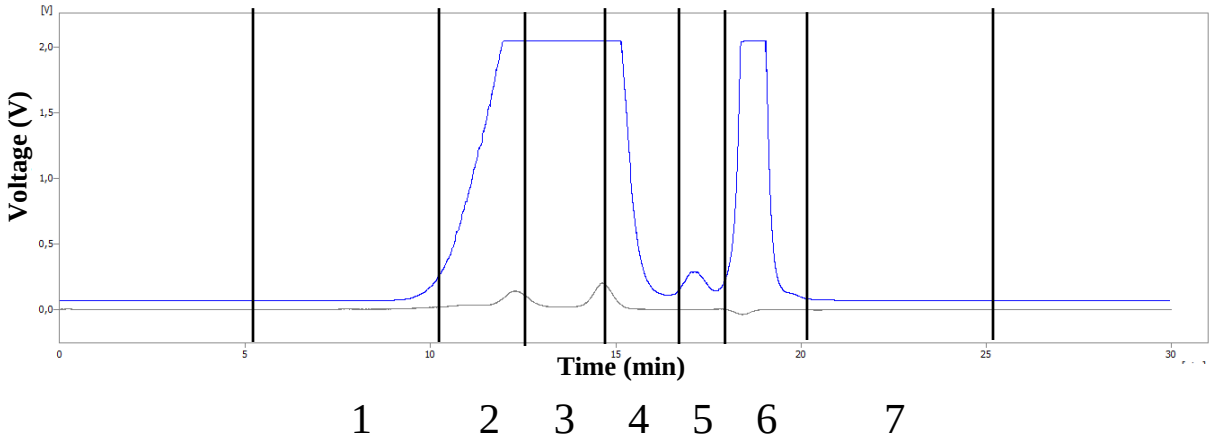

Figure 22. Chromatogram from GPC-HPLC analysis showing the UV (grey) and ELSD (blue) signals from proteins and NPs in water respectively and the time intervals during which the fractions (1-7) were collected.

Once these times were determined, the HPLC equipment was arranged for the preparative mode. 125 µl of the sample was injected onto the column and the peak separation patterns checked again. If some changes with respect to the analytical times occurred, the times were adjusted according to the chromatogram in the preparative mode. Collection times were decided based on the decimal system in the software with the range of collection from 5-25 minutes. Then, the delay time between collector and ELSD, (0.3 minutes on the software) was subtracted and the time was converted into the metric system used in the timer (see 3.4.2.2 Materials and Methods). To correlate the software and timer times more precisely, the timer was started 1 minute later from the software. Thus, all collection times were recalculated one minute ahead to compensate for the timer delay. The collection times were first set for the nanoparticles in water. However, peak separation patterns were changing due to fluctuations in pressure and matrix effects, so collection times needed to be modified for each matrix (Table 3). A total of 5-7 fractionation runs were performed depending on the amount of volume sample needed for further analysis. The volume collected of each fraction correlated with the time span of the fraction considering that the flow was 1 ml/ min and the sample was running for a total time of 30 minutes.

Column performance analysis was assessed in terms of yield since according to the FDA guideline, recovery of the analyte is one of the essential parameters for method validation (52). The yield was calculated in percentage as the amount of material recovered from the injected sample as shown in equation 9 where $n(F_i)$ was the number of moles in each collected fraction and n_{inj} was the number of moles injected into the column.

$$Yield\ (\%) = \frac{\sum_{i=1}^{7} n(F_i)}{n_{inj}} \times 100 \qquad Eq\ (9)$$

The yield was calculated with respect to Si and Gd recovery in each matrix. The aim was to determine the highest performance of the column in each matrix and test if any matrix was causing the material be stuck in the column (Tables 5A and B). The overall performance of the column was considerably good since in all matrices it was working over 50 % and the

recovery was between 70-100 % of the injected material. This recovery was similar for Si and Gd. One of the lowest yields was observed in HS which can be explained by the fact that it is a denser medium and contains quite a lot of proteins that might affect the flow of the sample through the column. It could also be because of a possible interference between the serum and the mobile phase causing precipitation that slow down the mobility through the column (54). The majority of the yield was represented by fractions 2, 3 and 4 which indicates that nanoparticles elute in these fractions.

Table 5. Summary of the yields (%) obtained in each fraction and for each matrix. **A)** Yield (%) for Si **B)** Yield (%) for Gd.

A

	Yield (%) Si			
Fraction	Water	SBF	HS	Urine
F1	0.19	0.69	1.13	0.50
F2	16.20	20.41	12.40	37.45
F3	38.47	38.80	30.51	27.50
F4	26.83	26.11	27.30	24.02
F5	2.27	1.61	1.62	2.77
F6	0.46	0.34	0.29	0.67
F7	0.06	0.09	0.08	0.12
Total	84.48	88.06	73.37	93.03

B

	Yield (%) Gd			
Fraction	Water	SBF	HS	Urine
F1	1.03	0.65	0.65	2.79
F2	36.42	23.94	42.21	57.42
F3	55.61	42.26	30.22	22.89
F4	11.94	10.78	4.67	3.77
F5	0.17	0.16	0.25	0.38
F6	0.13	0.11	0.20	0.32
F7	0.21	0.11	0.30	0.27
Total	105.50	78.02	78.51	87.83

One of the problems that can arise when loading the column in excess is that some material is getting stuck in the column. Also, when overloading the column, its efficiency might decrease leading to variability in the retention time, loss of reproducibility and pressure increase. To further test the column efficiency, washing steps with 50 mM $(NH_4)_2CO_3$ (pH 7.4, adjusted with formic acid) were done before and after a fractionation experiment and in between one fractionation run and the next one. These washings were done to elute any remaining material stuck in the column. The washing samples were collected, stored at room temperature and analyzed with ICP-OES. The results confirmed that there was not carry-over of sample since Si and Gd concentrations were below the detection limit. The column performance assessed here revealed that the method was accurate and precise, two of the parameters required for validation of a bioanalytical method.

After fractionation, 125 µl of each fraction was reinjected in the analytical GPC mode. These samples were diluted in 50 mM $(NH_4)_2CO_3$ (pH 7.4, adjusted with formic acid) according to their volumes. Analytical GPC allowed the comparison of the elution times between the fractions and the nanoparticle solution used for fractionation (Figures 23A and B). When the elution peaks from the nanoparticle solution and the fractionated material were overlapping, a successful fractionation was performed.

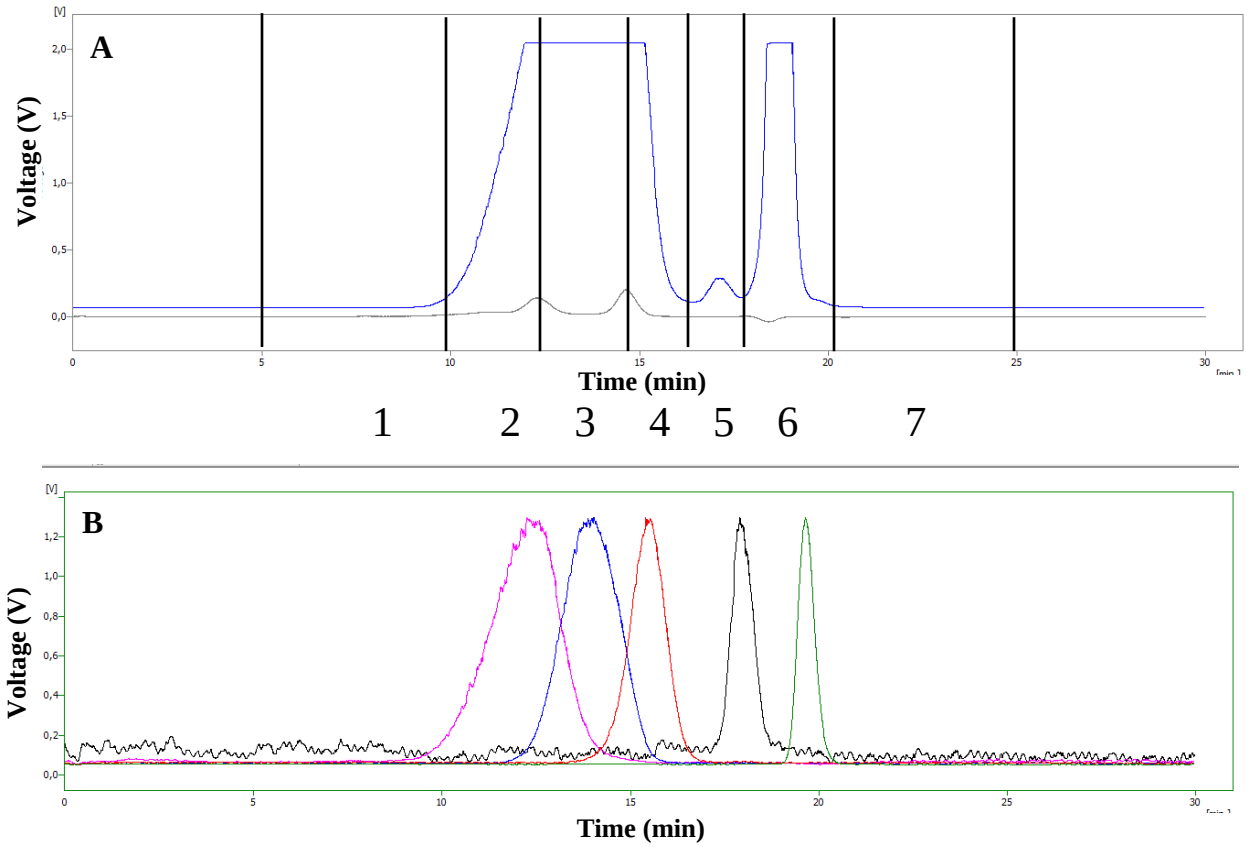

Figure 23. Chromatogram from GPC-HPLC analysis showing **A)** the ELSD signal (blue) and the UV signal (grey) from NPs and proteins in water respectively and the time intervals during which the fractions (1-7) were collected **B)** isolated material from 2-6 fractions (2 in pink, 3 in blue, 4 in red, 5 in black and 6 in green). A successful fractionation was performed since the elution time of NPs and the elution times of the fractionated material correlated.

When extracting and analyzing nanoparticles from blood samples post-injection a key issue is the presence of proteins in high concentrations. In the fractions from the nanoparticles incubated with HS, the presence of proteins was masking the ELSD signal from the nanoparticles in the GPC-HPLC chromatograms (Figures 24 A and B). Consequently, HS was diluted, 10 or 100 times, in distilled water before being incubated with the nanoparticles. By diluting the serum, protein concentration was 10 or 100 times lower and more optimal fractionation was achieved (Figures 24 C and D). However, to separate the fractions and have a better resolution in blood samples, removal of the most abundant proteins would be required.

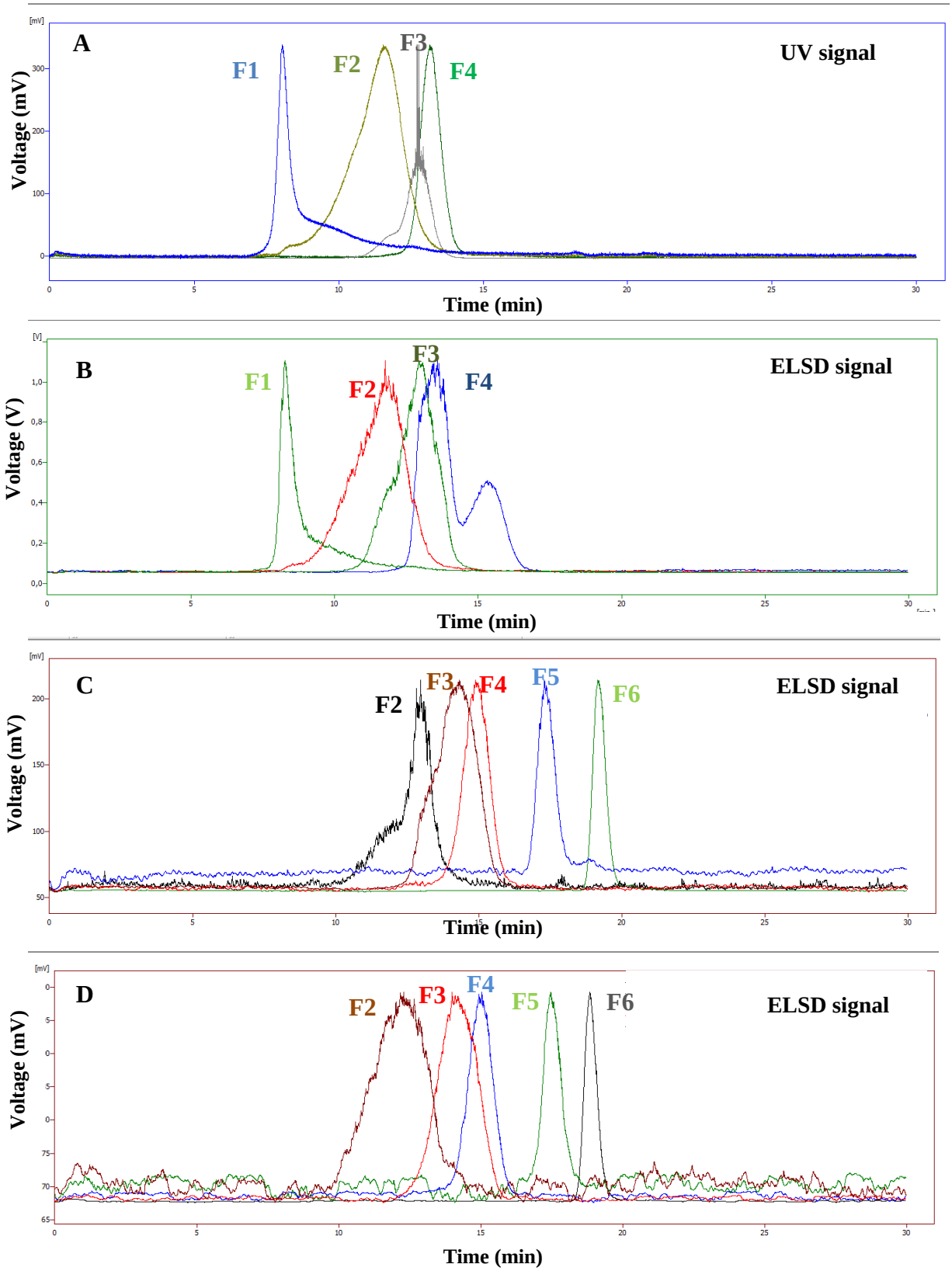

Figure 24. Chromatograms from GPC-HPLC analysis showing the UV and ELSD signals fromproteins and NPs fractions respectively incubated with HS **A)** UV signal from fractions 1-4 in HS (blue, light green, grey and dark green respectively) **B)** ELSD signal from fractions 1-4 in HS (light green, red, dark green and blue respectively) The ELSD signal is the same as the UV signal because the presence of proteins is masking the nanoparticle signal **C)** ELSD signal from fractions 2-6 in HS 1:10 (black, brown, red, blue and green respectively) **D)** ELSD signal from fractions 2-6 in HS 1:100 (brown, red, blue, green and grey

To sum up, a preparative GPC-HPLC method with ELSD detection was developed and validated for the extraction of nanoparticles in different matrices, namely water, SBF, HS and urine. Delay time, column performance, highest injection volume for optimal detection and matrix-dependent limitations were studied. The results showed a delay of 18´´ between the ELSD and the fraction collector. Column performance was efficient and the recovery of the injected material was adequate for the purpose of the method according to the FDA guideline, which states that "recovery need not to be 100 % but should be consistent, precise and reproducible" (52). However, the highest injection volume that still allowed optimal column performance was too small for the intended experiment, since a considerable volume of each fraction was required for further analysis by ICP. The maximum injection volume of 125 µl was a limitation of the extraction method, as several fractionation runs were required to achieve a significant amount of material. Thus, sample volume constitutes here the main limitation factor. Besides, overloading of the column caused an increase in the pressure and therefore, some instability in the elution times, leading to variability and difficulty when collecting the samples at fixed times. The presence of a dense matrix with high protein concentration, such as serum, posed a problem masking the ELSD signal of the nanoparticles that avoided the analytical analysis. Some improvements would involve protein removal such as a protein precipitation step with, for example, 5-sulfosalicylic acid that allowed the purification and quantification of a drug in plasma patients (55). To further improve the sensitivity and selectivity of the method, plasma matrix interference with the mobile phase around the retention time of nanoparticles could be studied (54). A good strategy to follow will consider to have an adequate HPLC preparative column that could optimize the process and conditions.

4.2.2 *ELISA assay for PEG quantification*

ELISA assay was used after separation of the particles through GPC-HPLC to quantify the amount of PEG in each fraction. Si/P ratio could not be used in this case to calculate PEG concentration since P could not be measured in the biological matrices. A dilution series of nanoparticles diluted with known concentration of PEG (Si) were done. Standards curves were prepared in the same matrix as the samples in the analysis to verify matrix effects. Nanoparticles were incubated with SBF, HS and urine as described in section 3.3 of Material and Methods. An inverse correlation between the absorbance values and PEG concentration was used to build the standard curves (Figure 25). One unique standard curve was used for the control, SBF and HS because similar absorbance values were obtained for the same PEG concentration which indicated high robustness. In the case of urine, a new standard curve was used due to different absorbance values for the same PEG concentration used in the first standard curve. The reason behind this difference could be a tendency of aggregation due to a high concentration of salts in urine. Another reason could be that the coating of these particles might have partially fallen off the nanoparticles. A different absorbance for PEG monomer or PEG on nanoparticles hence changed absorbance signal. Therefore, a new standard curve using the same batch of particles in water that was incubated with urine was done to allow comparison. The samples used as a blank were the appropriate matrix in each case (water, SBF, HS and urine).

From these standard curves, an evaluation of the accuracy of the ELISA assay was done through determination of a standard deviation between the expected PEG concentration and the actual measurement of PEG concentration with the ELISA (Appendix V). ELISA was successfully working within the range of PEG concentrations used, except for the lowest concentration, 0.04 µmol/l, where the higher standard deviations were found. Therefore, the accuracy of the method decreases as PEG concentration become lower. To determine the analytical range in which the ELISA was working accurately, the limits of detection and quantitation (LOD and LOQ respectively) were calculated using the calibration curves.

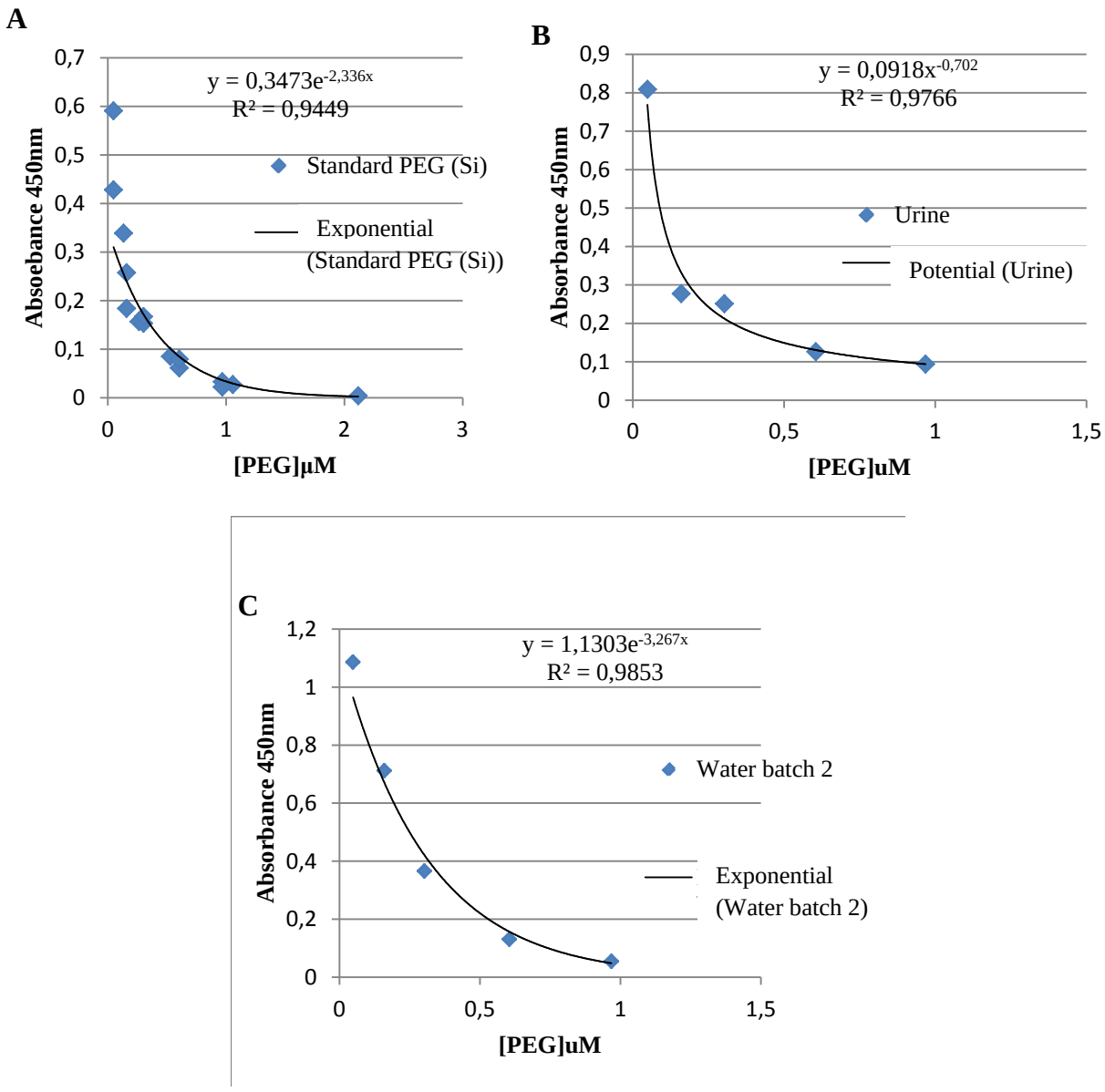

Figure 25. Standard curves obtained through anti-PEG ELISA assay **A)** Standard curve for the first batch of nanoparticles in water and particles incubated in SBF and HS **B)** Standard curve for the particles incubated in urine **C)** Standard curve for the second batch of particles in water.

ELISA was a highly accurate method able to quantify low concentrations of PEG. LOD and LOQ were calculated according to the ICH guidelines for validation of analytical procedures (53). LOD is defined as "the lowest amount of analyte in a sample which can be detected but not necessarily quantitated" (53) whereas LOQ is defined as "the lowest amount of analyte in a sample which can be quantitatively determined with suitable precision and accuracy" (53).

LOD and LOQ were calculated using low concentrations of PEGylated particles added to the blank matrices (water, SBF and HS) and the resulting standard curves (A and B). Urine was excluded from these calculations due to the different behavior that could cause deviations in the estimations.

LOD was determined as the lowest PEG concentration that produced a response three times the standard deviation of the mean signal from the blank. The absorbance values obtained using the different biological matrices as a blank were similar in all cases within a range between 0.035 and 0.038. Thus, an average of the absorbance values obtained from the blanks in water, SBF and HS was done and the standard deviation was calculated. LOD value was 0.04 μmol/l. The calculated LOD correlated with the first observation based on the comparison between expected and measured PEG concentration.

LOQ was calculated as the lowest concentration of the standard curve that can be measured precisely. From the calibration curves, 0.1 μmol/l was estimated as the lowest concentration with an acceptable standard deviation. The calculated LOQ agrees with the FDA bioanalytical method validation guideline where it is stated that "LOQ should be at least 5 times the response compared to blank response" (52).

Thus, the lowest analytical range of this assay in which the method is precise might be between 0.04 and 0.1 μmol/l of PEG concentration. It can be concluded that this method is highly accurate, precise and robust for the intended use.

4.2.3 *ICP-OES method for Si, P and Gd quantification*

ICP-OES was used to determine the Si, P and Gd concentrations in the particles incubated with the matrices and in the resulting fractions (P only in water). All ICP-OES measurements were done by Nooshin Yousefpour and Olof Björnberg from Spago Nanomedical. The most important parameter to consider here is the reproducibility and reliability of the measurements. Some deviations between the expected and measured concentrations were observed.

Prior to the measurement, samples were diluted in HNO_3, at different concentrations depending on the matrix. Matrix effects are extremely important to consider because they can affect the accuracy of trace elemental analysis (56). It is known that increasing acid concentrations can lead to a decrease in the signal and that low concentrations of the samples can cause problems in terms of quantitation and detection limits (44). According to the established SOP, samples were normally diluted in 1% HNO_3 but 0.1% HNO_3 was used for serum samples. Some interference effects such as interactions between the proteins and the acid matrix might occur when using higher acid concentrations.

A spiking test was performed to evaluate the accuracy of the method (Appendix VI). Correction factors to adjust the measured values and possible matrix effects were determined.

All matrices were spiked with a known concentration of nanoparticles covering the range of concentrations detected in the fractions. These samples were measured with ICP-OES and deviations between the measured and expected concentrations were studied. The analyzed concentration range of Si and Gd was between 23-6900 μM and 1-300 μM respectively which covered the concentration range measured in the fractions. Two HNO_3 concentrations were used: 1% for water, SBF and urine samples and both, 0.1 and 1% for HS. Triplicates of standard nanoparticles in water with known concentrations of Si, P and Gd were used as an internal reference to adjust the measured values. Si and Gd measurements (and P in water) were performed and the ratio between the expected and the measured value was used to generate correction factors for each element that were applied for all ICP measurements (Table 6). The average of the calculated correction factors in the range of concentrations 10-300 μM Gd for water, SBF, HS and urine was done whereas in HS in the range of concentrations 1-300 μM Gd and in all matrices for 1 μM Gd, different correction factors were used because they showed distant values from the other matrices and concentrations.

Table 6. Mean correction factors for Si, P and Gd respectively applied for ICP measurements depending on their concentration, biological matrix and HNO_3 concentration.

Biological matrix	**HNO_3 concentration**	**Element concentration range (based on Gd, μM)**	**Si**	**Gd**	**P**
All	1%	10-300	0.98	0.97	0.90
HS	0.1%	10-300	1.09	1.36	-
Water	1%	1	1.09	1.77	-
SBF	1%	1	1.09	1.74	-
HS	1%	1	0.99	1.55	-
HS	0.1%	1	1.38	1.73	-
Urine	1%	1	1.00	1.61	-

The importance of this optimized method resides in the ability to detect and quantify the nanoparticles in blood samples in a rapid and effective way, avoiding high costs and using the lowest amount of sample possible. For ICP-OES method, two main limitations were found: LOQ and volume of the fractions needed.

The LOQ of the method for each element according to the previously established standard curves were: Si 0.1 mg/l, P 0.2 mg/l and Gd 0.048 mg/l. Concentration of samples should be higher than LOQ for an accurate quantification. In fact, some concentrations in the fractions were detected but they were below the LOQ and they were not quantifiable. LOQ values correlated with the amount of volume needed to achieve an accurate measurement. Total volumes needed for Si and Gd quantification in ICP-OES were 4 and 6 ml respectively. If the sample was enough concentrated, it could be diluted to get to these volumes whereas if it was too diluted, a large volume of sample was required. Using the fractionated material from the nanoparticles contained in HS, a theoretical calculation for the amount of blood sample needed for ICP-OES was done. According to some *in vivo* experiments performed by Spago Nanomedical, a dose of 20 μmol/kg (2 mM Gd) is injected in a 30 g mouse. Plasma volume in the mouse is 56.1 ml/kg so the concentration of nanoparticles found in the blood after injection at time 0 is around 5355 μM Si and 357 μM Gd. These concentrations were used for both Si

and Gd to calculate the amount of blood sample needed to measure these elements (Tables 7A and B). The concentration of some fractions originated from blood nanoparticles could be below LQ. This limitation would need to either pool blood from several mice or inject a higher dose in the animals.

Table 7. Expected concentrations and volumes needed for ICP-OES measurement of Si and Gd in fractions from a hypothetical blood sample containing 5355 µM of Si **(A)** and 357 µM Gd **(B)**.

A							
Sample	**Injected [Si] µM**	**Dilution factor**	**Collected [Si] µM**	**LOQ [Si] µM**	**Concentration factor to reach LOQ**	**Volume needed for ICP after concentration (ml)**	**Dose increase**
F1	5355	10465.84	0,51	3.6	6,96	28,14	281
F2	5355	60.22	88,92	3.6	-	0,16	2
F3	5355	32.71	163,72	3.6	-	0,09	1
F4	5355	73.77	72,59	3.6	-	0,20	2
F5	5355	501.89	10,67	3.6	-	1,35	13
F6	5355	3631.01	1,47	3.6	2,41	9,76	98
F7	5355	64044.39	0,08	3.6	42,58	172,22	1722
B							
Sample	**Injected [Gd] µM**	**Dilution factor**	**Collected [Gd] µM**	**LOQ [Gd] µM**	**Concentration factor to reach LOQ**	**Volume needed for ICP after concentration (ml)**	**Dose increase**
F1	357	2036.34	0,18	0.3	-	10,61	106
F2	357	45.64	7,82	0.3	-	0,24	2
F3	357	39.04	9,14	0.3	-	0,20	2
F4	357	410.96	0,87	0.3	-	2,14	21
F5	357	4867.67	0,07	0.3	-	25,36	254
F6	357	8267.35	0,04	0.3	7,18	43,07	431
F7	357	11164.67	0,03	0.3	9,69	58,17	582

For the quantification of the nanoparticles using ICP-OES, the most important fractions are 2, 3 and 4. For both Si and Gd, the dose would need to be increased 2 times to be able to detect the particles in F2 and F3. In F4, the dose would need to be increased 2 and 20 times to detect Si and Gd respectively. These numbers are reasonable considering that the current dose used is the therapeutic dose that can be increased up to 10-100 times in toxicology studies.

Some studies have overcome these problems about sample volume and interferences between the matrix and detection signal with a convenient sample pretreatment before ICP-OES measurement. A combination of magnetic solid phase extraction with ICP-OES detection was offering a simple method for determination of trace elements in environmental and biological samples (57). This approach could be useful to detect Gd amounts in the samples but not for PEG or Si quantification.

4.3 Characterization of the fractionated material

After separation of the nanoparticles contained in different matrices, the fractionated material was further analyzed in terms of size using DLS, composition (Si and Gd) through ICP-OES and presence of nanoparticle coating (PEG) through ELISA. The study was performed for all fractions. However, the data shown in some sections is only for F2-F5 which were the samples containing the nanoparticles and coating. Here, the selectivity or specificity of the method was evaluated. Thus, the ability of the methods used to quantify the particles in the presence of other components, such as endogenous matrix components, was assessed. From this analysis, several issues can be proved: presence (detection), concentration of the nanomaterial in the matrix and changes in the composition such as in the coating when compared to the nanoparticles in water.

4.3.1 *Size analysis*

From the recovered material in each matrix, fractions 2, 3 and 4 were the samples containing the nanoparticles separated by size. Thus, these samples were analyzed using DLS to determine the size and the correlation with the chromatograms obtained from the analytical GPC-HPLC (Appendix VII A-F). The fractionated material was injected onto the GPC column to determine the relative size of each fraction containing the nanoparticles. F2 was the first sample eluted and F4 the last. F1 and F7 are not shown because they were the baselines and they did not contain any particle. From the chromatograms, it was concluded that F2 contained the largest particles whereas F4 contained the smallest ones. DLS was then used to determine the size of the fractionated material containing the nanoparticles (F2-F4). F2 encompassed the largest particles bigger than 15 nm, F3 consisted of the particles between 8-10 nm and F4 contained the smallest particles below 8 nm (Figure 26). These results were consistent for water, SBF and urine. F2 was the most variable among the matrices and contained larger particles whereas F3 and F4 showed similar sizes in the different matrices. In urine, particles seem to be larger in F2 compared to the other matrices which correlates with the results shown in Appendix IIIC. The obtained sizes for each fraction matched the elution peaks from the chromatograms in GPC-HPLC method which indicated that the separation of nanoparticles was successful.

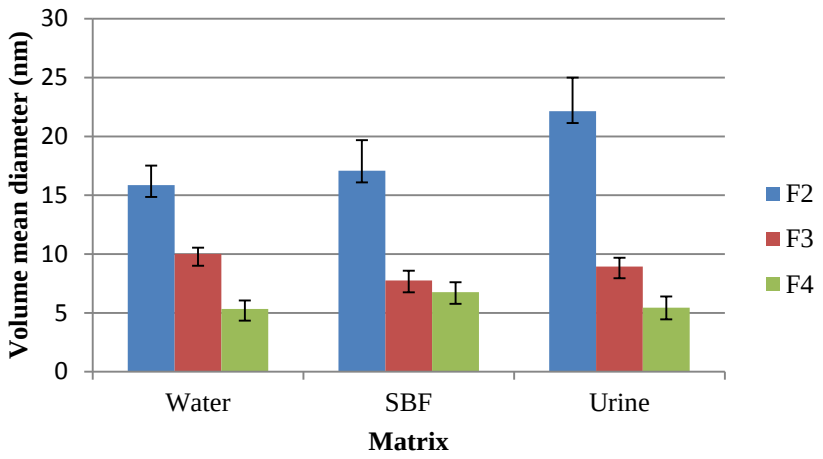

Figure 26. Volume mean diameter (nm) of F2, F3 and F4 in water, SBF, and urine measured with DLS. n=7 measurements. Error bars represent the standard deviation. Data was not tested with a statistical test because the number of experiments was insufficient to have a reasonable n.

An elemental analysis using ICP-OES was performed in order to measure Si, P (when possible) and Gd concentrations in each fraction and for each matrix. For selectivity analysis, Si and Gd concentrations in the blank matrices (before incubation with nanoparticles) were measured to avoid interference with already existing Si and Gd in the matrices. Si and Gd content in the blank matrices were not significant enough to cause interference (data not shown). The aim was to analyze the ability of the analytical method to quantify the nanoparticles in the matrix and detect possible changes in Si and Gd content among the different fractions and compared along the matrices. These differences could indicate alterations in the nanoparticles identity due to matrix effects. The relative abundance of Si and Gd in percentage per fraction was determined. The relative amount of each element was calculated as the percentage of Si or Gd content in each fraction with respect to the total Si or Gd amount respectively. The total amount was calculated as the sum of Si or Gd concentrations in all fractions. (Figures 27A and B)

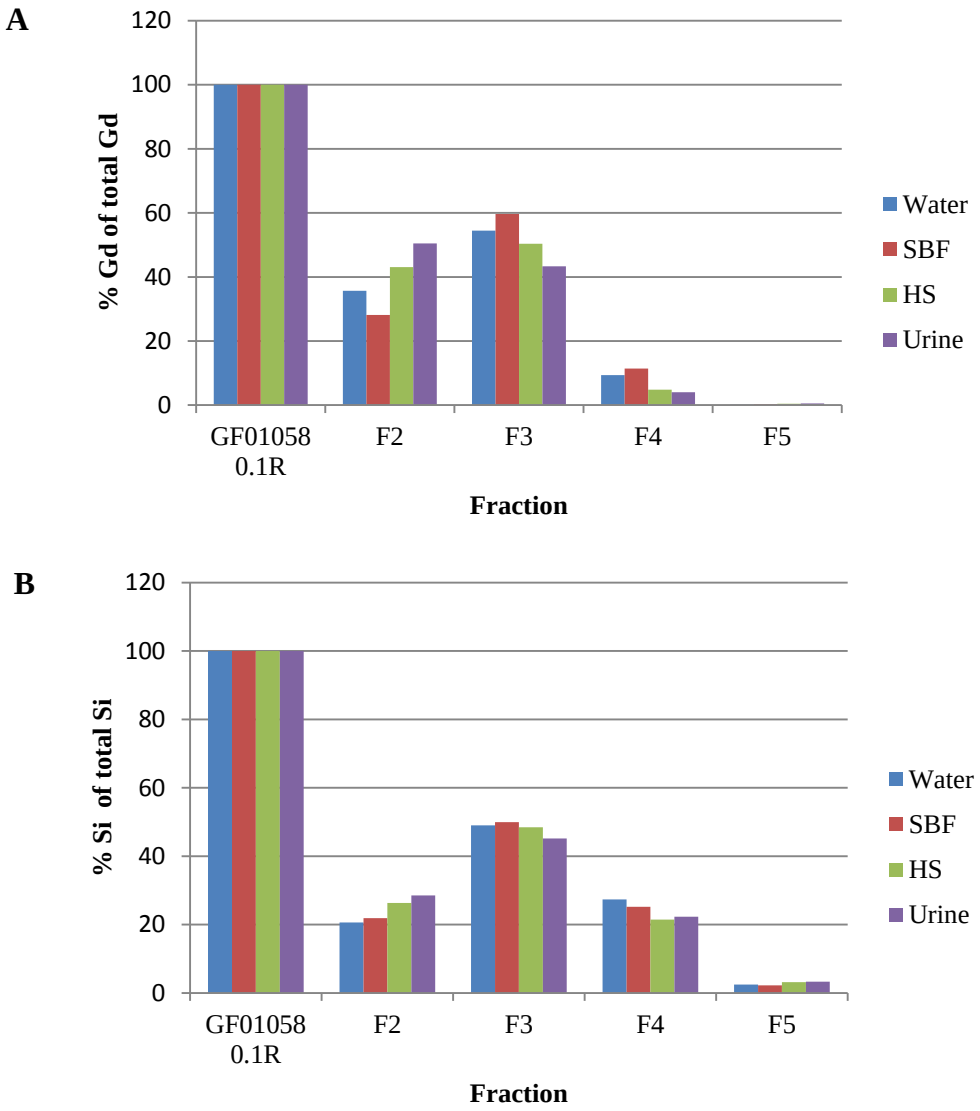

Figure 27. Gd or Si content per fraction (%) with respect to the total sum of Si or Gd content in the fractionated material, considered as 100% . Calculations based on concentrations measured with ICP **A)** %Si of total Si injected for F2-F5 **B)** % Gd of total Gd injected for F2-F5. The relative Si or Gd content was calculated with respect to the total sum of Si or Gd content in all fractions even though the data only shows results obtained for F2-F5.

The fraction value was assessed in terms of Si and Gd concentrations. The most representative fraction was the sample containing the highest Si and Gd concentrations. F3 was, among all fractions, the most representative and valuable, accounting for almost 50% of both Si and Gd contents. Besides, it was the most even fraction among all matrices. F2 and F4 contained around 20% of Si each. However, F2 contained around 30% of Gd whereas F3 around 10%. F5 encompassed 3% of Si and 0.5 % of Gd.

F2 was the most variable fraction throughout the matrices, especially in urine and HS. Both matrices were enclosing the highest Si and Gd contents in F2 and the lowest in F4. These increased concentrations might be explained through an increase in size of some nanoparticles

due to possible interactions with other molecules present in the matrix or aggregation of particles. If that is possible, there would be larger particles in the sample and these larger nanoparticles would elute first from the column. In other words, the nanoparticles that were supposed to be collected in F4, became bigger and were collected in F2. Most probably, these interactions are due to the presence of proteins and other molecules like salts in serum and urine (58).

Recently, it has been demonstrated that some of these interactions are caused by the adsorption of proteins to the surface of nanoparticles which determines biodistribution *in vivo* (30). As a result of the binding of proteins to the surface of nanoparticles, a protein corona is created (40).

4.3.3 *Coating analysis: PEG quantification*

PEG concentration was measured in each fraction using ELISA. The aim was to quantify the coating of the nanoparticles upon incubation with the matrix. These changes were calculated as percentage of PEG (Si) with respect to the amount of core in each fraction measured by ICP-OES (Figure 28).

The most representative fraction for PEG coating was F5 which accounted for 70-80 % of the PEG coating compared to the core. However, in the case of urine F5 only represented a 15% having the majority of PEG in F2. Thus, F2 in urine accounted for half of the PEG coating content with respect to the core. These results might indicate that the identity of the particles in urine had changed and that probably there was an aggregation that caused a larger proportion of PEG to appear in F2. However, the method was sensitive enough to assess the identity of the particles in this matrix and showed that it had changed. The aggregation event was also seen in the chromatogram from the GPC (Appendix IVG). Another possible explanation might be translated into PEG coating falling off from the nanoparticle´s surface causing aggregation of loose PEG molecules. Released PEG molecules interacting with each other were eluted in F2 which gave the highest PEG concentration in this fraction. In HS, a lower amount of PEG in F5 compared to the other matrices was observed. In this case, the presence of proteins may have caused some interference effect. Proteins can adsorb to the surface of the nanoparticles but they might also interact with the PEG chains from the coating. Protein adsorption to the PEG chains could interfere with any specific interaction such as the binding of PEG to anti-PEG antibodies in the ELISA assay. This protein-PEG interaction may have caused a decrease in the detection of PEG by ELISA. In fact, it has been reported that PEG chains can bind proteins and that these attractive forces are linked to changes in the polymer configuration (59).

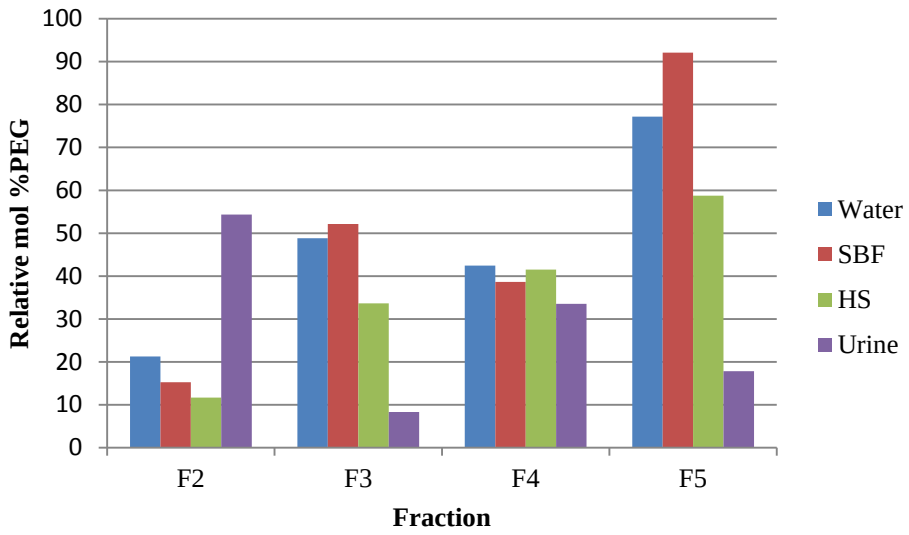

Figure 28. %PEG Si with respect to the core component in each fraction. Calculations based on PEG concentration measured with ELISA and Si concentration measured by ICP-OES. Data shown for F2-F5 in each matrix

4.3.4 *Identity of nanoparticles: summary*

Overall, it was demonstrated that the PEG, Gd and Si contents were exhibiting the same trend in all matrices except for the urine (for PEG and Gd) (Figures 29 A, B and C). In water, SBF and HS, most of the PEG coating remained attached to the nanoparticles (F2-F4) whereas some PEG coating was falling off and appeared in F5. In HS a higher amount of PEG in F4 indicated that PEG might be starting to fall off from the nanoparticles. In urine it seemed that there was a tendency of aggregation since most of the PEG coating was in F2. Urine was the last matrix tested and so, the first hypothesis was that the nanoparticles were losing their stability with time, changing their identity. For that reason, a second batch of nanoparticles in water was prepared. As shown in figure 29A, the second batch of nanoparticles in water (shown in orange) had the majority of the coating in the same fractions where the nanoparticles were collected. Thus, the changes observed in urine were not due to an "aging" effect of the nanoparticles but an effect that the urine had on the nanoparticles. In fact, the method developed was able to detect these changes. Also, the DLS measurements in urine samples gave a similar indication (Figure 26). In SBF and HS, PEG, Gd and Si contents remained unaffected when compared to the nanoparticles in water. The same trend as with PEG was observed for Gd in urine (Figure 29B). However, when analyzing the Si content, the differences were not that obvious (Figure 29C). Therefore, using a powerful combination of ELISA and ICP-OES, identity of the nanoparticles was proved. The method was sensitive enough to also detect changes in the identity such as in urine. Further experiments would be necessary using a freshly prepared batch of nanoparticles incubated with all matrices at the same time.

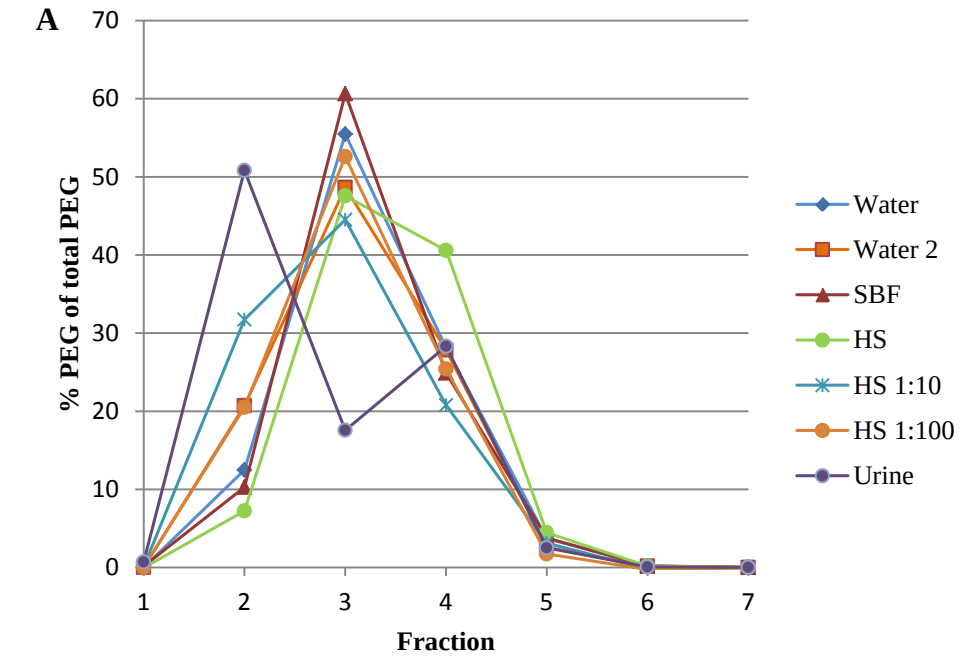
A
% PEG of total PEG
Fraction
Water
Water 2
SBF
HS
HS 1:10
HS 1:100
Urine

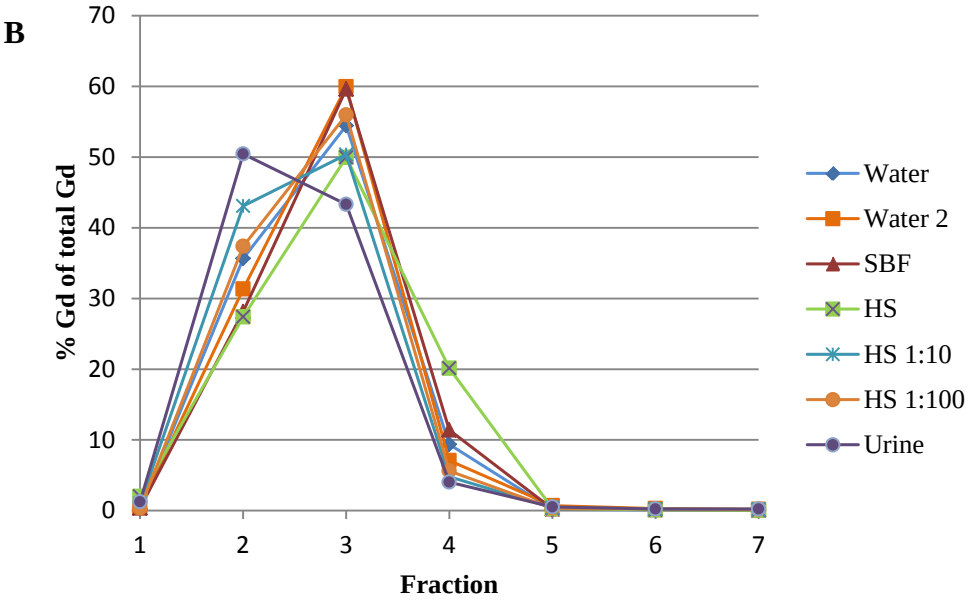
B
% Gd of total Gd
Fraction
Water
Water 2
SBF
HS
HS 1:10
HS 1:100
Urine

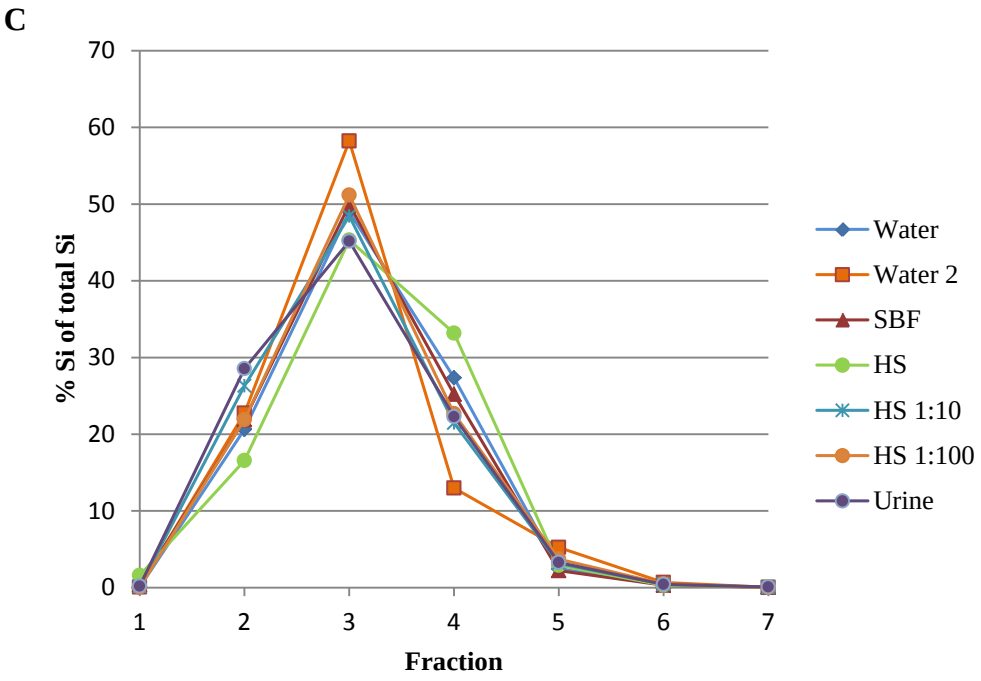

Figure 29. Analysis of PEG, Gd and Si contents for NPs incubated with different matrices
A) %PEG of total PEG content in F1-F7 for the two runs in water and for SBF, HS, HS 1:10 and HS 1:100 **B)** % Gd of total Gd content in F1-F7 for two runs in water and for SBF, HS, HS 1:10 and HS 1:100 **C)** % Si of total Si content in F1-F7 for two runs in water and for SBF, HS, HS 1:10 and HS 1:100

Specificity of the method was achieved through a combination of various analytical assays. Two of the methods that achieved more selectivity were ELISA and ICP-OES. ELISA was a highly sensitive assay for the intended use. It was able to detect the coating of the nanoparticles over other components in the matrix for all the media analyzed. ICP-OES was suitable for quantifying the elemental composition of the particles (Si, Gd). However, the innate presence of P in the matrices did not allow a precise measurement of P. Both procedures maintained their specificity in a range of low concentrations. Moreover, it was possible to isolate particles in three main fractions (F2. F3 and F4) using GPC-HPLC where the ELSD signal was detected over other components of the matrix. However, some selectivity problems arose in HS due to a predominant presence of proteins. This issue was partially solved but an optimal protocol to achieve higher discrimination would be needed. The same scenario was obtained using DLS, which was able to measure the required particles of small size but in the presence of proteins, it was mainly measuring the size of the proteins.

Thereby, specificity was not achieved in all cases and especially in serum, where several improvements would be required to minimize the interference caused by endogenous components in this matrix.

4.4 Nanoparticle-protein interaction: the protein corona

Upon introduction into the body, nanoparticles are exposed to biological fluids such as plasma. In this environment, nanoparticles can selectively bind proteins. These interactions

depend on the surface properties and size of nanoparticles but also on the type of proteins and physiological medium (60).

Nanoparticle-protein interactions are dynamic and different proteins participate in the formation of the protein corona. The amount and type of proteins bound to the surface of nanoparticles is variable depending on plasma proteins concentration (29).

Studying these interactions is crucial to determine the fate of nanoparticles *in vivo*. Adsorption of proteins to nanoparticles might impact cellular uptake, biodistribution and clearance of the nanomaterial leading to possible toxic effects. Quantification and identification of proteins attached to nanoparticles is required to understand these interactions.

4.4.1 *Protein size changes in human serum*

One-dimensional gel electrophoresis was used for protein separation after incubation of nanoparticles with serum at a volume ratio 1:1 and subsequent fractionation. HS without nanoparticles was the internal reference used to compare protein size profiles. HS was fractionated using GPC-HPLC as the same way as the serum containing the nanomaterial and with the same collection times (see 3.4.2.2 of Material and Methods).

Fractions 1-7 from HS and HS+NPs were applied to SDS-PAGE for separation of the proteins according to their molecular weight. The aim was to analyze possible shifts in the bands indicating a delay in the migration of the proteins by particle interactions. Besides, a "jump" of a band from one fraction to another was studied. Although fractions 1-7 were used, only data for fractions 2, 3 and 4 is shown where the most notable changes were observed (Figures 30 A and B).

A

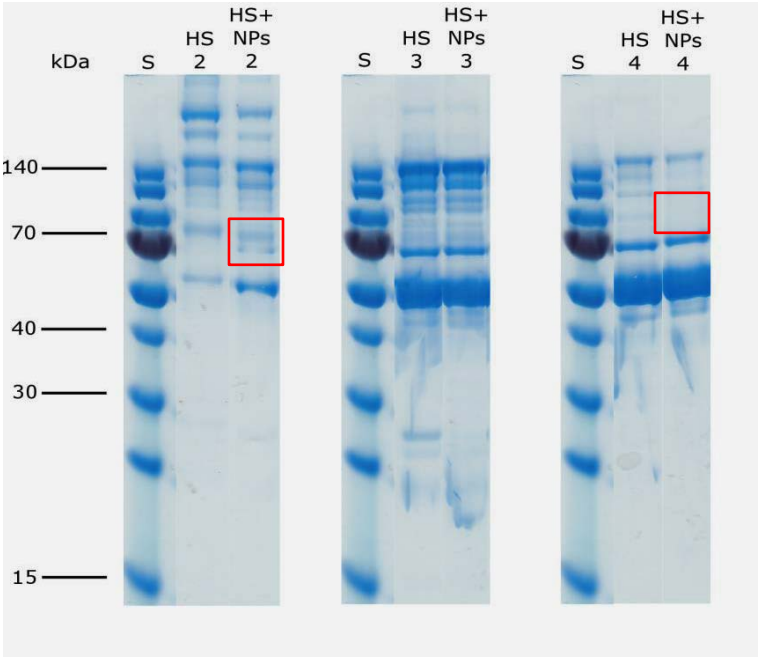

B

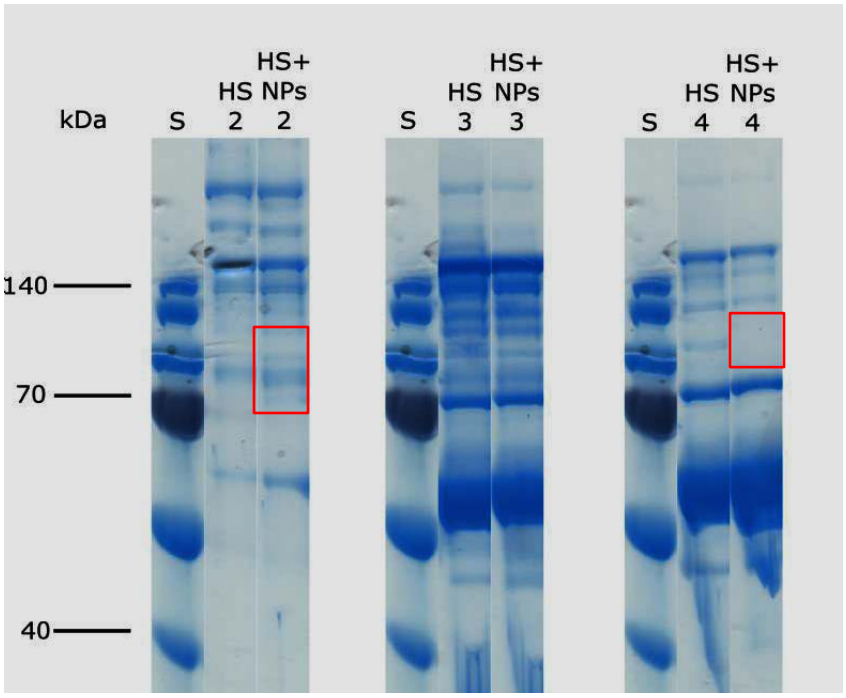

Figure 30. SDS-PAGE of fractions 2, 3 and 4 from HS and HS+NPs **A)** Running time 1 hour **B)** Running time 1 h 45 minutes. Noticeable changes are shown in red. S= standards; HS= human serum; NPs= nanoparticles.

The nanoparticles seemed to affect the protein-band patterns in some fractions such as F2 and F4 (red marks in figure 30). A protein band between 70-80 kDa disappeared in F4 (HS+NPs) whereas an additional band around the same molecular weight appeared in F2 (HS+NPs). These changes were noticed only in the fractions containing the nanoparticles. The HS fractions did not experience any appreciable change. These effects were reproducible for at least three experiments. This movement of bands among fractions might be explained due to some interactions between proteins and nanoparticles. If a protein-nanoparticle complex is formed, it will be eluted in an earlier fraction due to an increase in size. Thus, the protein adsorbed to the surface of the nanoparticle will be collected in a different fraction compared to when it is separated in the reference serum (HS). Therefore, the band of that protein will disappear in the HS+NPs fraction that contained the protein and a new band will appear in another fraction according to the size of the complex.

However, the protein band remained in the same weight range as before even though it appeared in another fraction. The reason why the protein remained at the same weight was that all proteins were denatured when treated with SDS causing all tertiary and quaternary structures and hence, the NP-protein interactions, to be lost. Thus, the proteins are separated from nanoparticles and become a linear polypeptide chain with the same molecular weight as before. In fact, interactions that bring together different subunits from a protein are also broken. This means that these results might not be a proof of nanoparticle-protein interaction but rather a proof of interactions between nanoparticles and single subunits of a protein.

Native gels should be used instead to detect these interactions with complete proteins. Using this method, proteins maintain their tertiary and quaternary structures and each band in the gel

represents a protein. After separation, the bands of interest can be directly submitted to trypsin digestion and further identification using mass spectrometry techniques such as Matrix Assisted Laser Desorption/Ionization Time of Flight Mass Spectrometry (MALDI-TOF-MS) (Figure 31). However, for an accurate quantitative analysis of the protein of interest, Western blot or immunoblotting methods are more suitable.

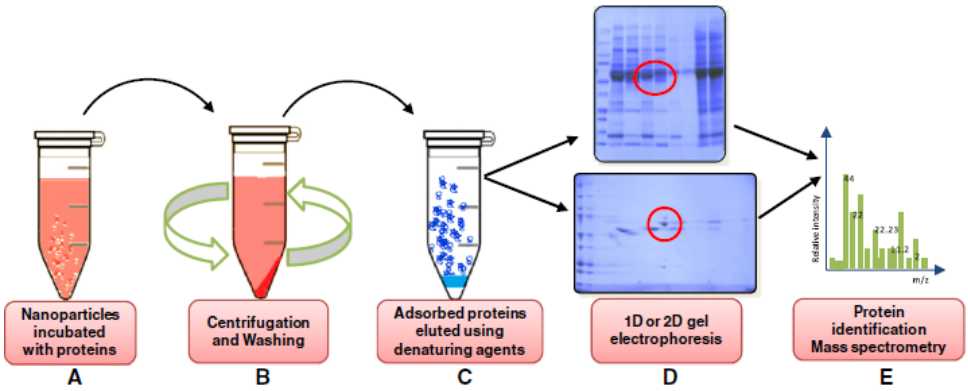

Figure 31. Schematic overview of the procedure most commonly followed to isolate and identify proteins interacting with nanoparticles. **A)** NPs are incubated with serum or plasma proteins that will bind to the surface of NPs. **B)** The sample is centrifuged to remove the unbound proteins and the remaining NP-protein pellet is washed several times. **C)** Laemmli buffer containing SDS denatures the proteins and release them from the nanoparticles. **D)** Released proteins are further separated using one or two dimension electrophoresis**. E)** The bands of interest are digested with trypsine and the proteins identified using mass spectroscopy (Image reproduced from Saptarshi et al., 2013) (29).

If the previous results shown in figure 31 were true, a nanoparticle-protein complex was formed and a shift from F4 to F2 occurred. This would result in an increasing protein and nanoparticle concentration in F2 which correlates with the results obtained from the ICP-OES analysis of the fractions in serum and urine (Figures 27A and B). Using ICP-OES, an increase in Si and Gd contents was observed in F2 whereas a decrease occurred in F4. Thus, a higher nanoparticle concentration resulted in F2.

Using nanoparticles with different properties, such as super-paramagnetic iron oxide nanoparticles (SPIONs), gold particles and metal oxide particles (ZnO, TiO_2 and SiO_2), a more accurate characterization of the protein corona has been made in several studies (29) (40). Albumin, apolipoproteins, fibrinogen, immunoglobulins and complement proteins are the most common proteins found in the protein corona. Complement proteins are opsonising proteins that can lead to an undesired immune recognition (29).

4.4.2 *Relative distribution of proteins and nanoparticles in human serum*

A quantitative analysis of protein and nanoparticle concentrations and their relative distribution in serum and urine fractions was performed. Relative distribution was calculated as the percentage of protein concentration in each fraction with respect to the total protein concentration in all the fractions. The aim was to study the effect of protein concentration in each fraction since it has been reported that the amount of proteins available to interact with NPs can affect the protein corona formation and composition (31). The relative distribution of proteins among the different fractions in human serum and urine showed a different protein composition in these matrices (Figure 32).

In human serum, albumin is the most abundant protein with a concentration of approximately 40-50 mg/ml and represents around 55% of the total protein content (61). This 66 kDa protein is eluted in F3 and the rest of the proteins are distributed almost exclusively among F1, F2 and F4. Thus, human serum mostly contains proteins within a range of 80-250 kDa because they have a native molecular weight larger than the kidney filtration cutoff (around 45 kDa) (62). Ig G, Ig A, transferrin, haptoglobin and antitrypsin are the other five proteins with the highest concentrations. Together with albumin, these six highly abundant proteins represent over 85% of the human serum proteome (63). Therefore, the overwhelming presence of these proteins, makes difficult the separation and identification of low abundance serum proteins (64).

However, normal total protein concentration in human urine is much lower than in human serum. It is not usually more than 0.1 mg/ml with an excretion rate of less than 150 mg per day (58). Urine contains proteins coming from blood plasma, kidneys and the urogenital tract. It also has components from body filtrates such as water, high salt content, electrolytes and nitrogenous waste elements (65). Individual samples are very heterogeneous in composition depending on the body flow and filtration rates. Thus, these results might be different when analyzing other samples. The proteins in urine were distributed more evenly among all the fractions containing molecules from a wide range of molecular weights. A high salt content together with other components such as electrolytes and nitrogenous derivatives were collected in the "smallest" fractions (F6 and F7) and might interfere when analyzing the proteome. Thus, the first step reported to prepare urine samples for protein analysis is always the removal of salts with gel filtration and further protein concentration by ultrafiltration (65).

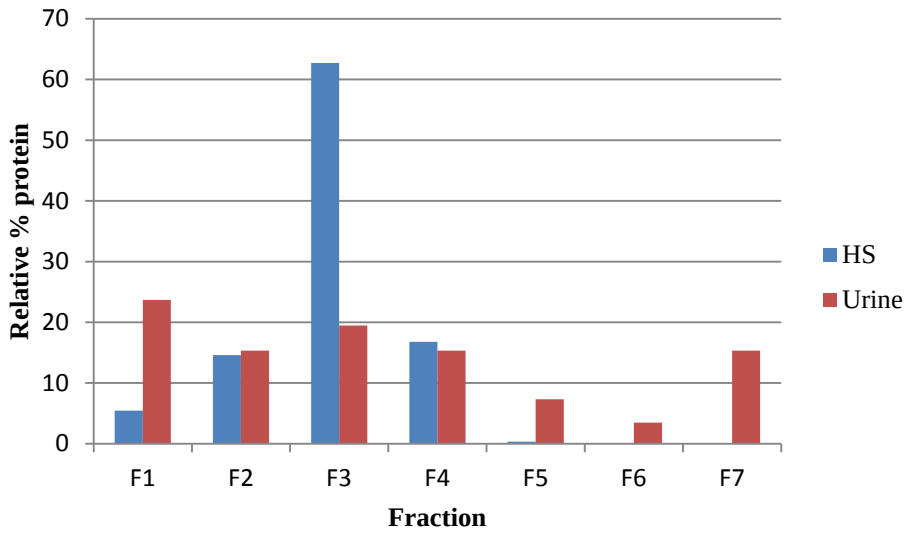

Figure 32. Relative abundance of proteins (%) in human serum and urine fractions. A different proteomic composition of both matrices is clearly seen. A more even protein distribution among all fractions is observed in urine whereas in serum, most of the proteins are located in F1-F4.

To determine the ratio between proteins and nanoparticles in each fraction, nanoparticle and protein concentrations (in µg/ml) were measured (Appendix VIII A-D). For the nanoparticles, Si composition and weight were considered to calculate the concentration in each fraction. For the proteins, the Bradford assay was used to measure the protein amount based on a series of BSA standards with known concentrations (Figure 12).

When fractionating nanoparticles in serum, 125 µl of a sample containing 50 mg /ml of proteins was injected onto the GPC column. This protein concentration value was obtained with the Bradford assay in reference to BSA standards and was in agreement with the normal concentration range of serum albumin (35-50 mg/ml) reported in several studies (61) (62). Thus, 6.25 mg of protein was injected. Knowing the relative protein percentage that should go in each fraction (figure 32) and fraction volumes, the expected protein concentration was calculated (Figure 33).

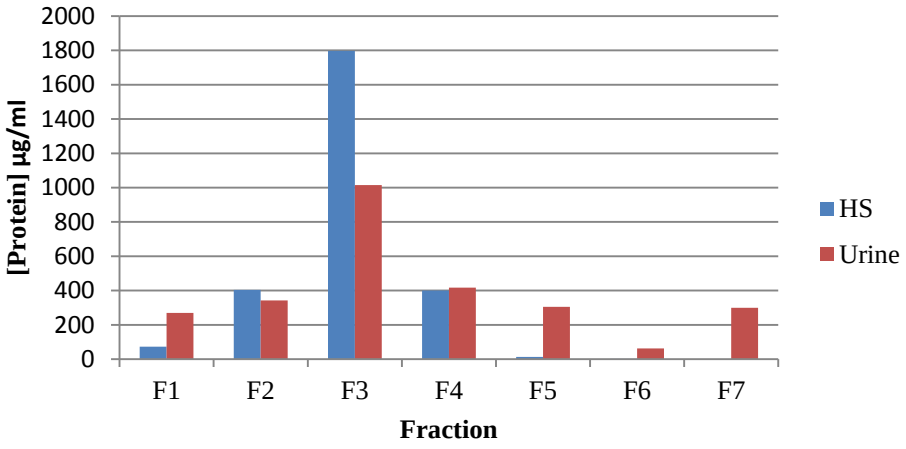

Figure 33. Expected protein concentration (µg/ml) in each serum and urine fraction calculated using the amount of protein injected, the relative protein abundance in each fraction and the fraction volumes.

F3 contained the largest protein concentration although the protein amount in serum is almost twice the amount in urine. Serum albumin concentration in normal urine is 2.2-3.3 mg/l (58) which is more than a thousand times lower than in serum. F3 accounted for the most significant differences between both matrices. F1-F4 contained similar protein concentrations whereas F5-F7 encompassed filtration products in urine (salts, waste products) that are smaller than 45 kDa (kidney cutoff).

Therefore, depending on the desired aim different strategies can be followed. To characterize nanoparticles alone, removal of high abundant proteins would make it easier. However, if nanoparticle-protein interactions want to be analyzed, all proteins should be present in the sample.

5. Future work

In this project, the first steps towards the development and validation of a bioanalysis method to extract and characterize nanoparticles from biological matrices were performed. However, to achieve a complete validation and implementation of this method as proof of identity of particles in biological samples, more work needs to be done.

The next step would be the extraction of nanoparticles from different biological samples such as blood and liver. These particles are injected into the blood during *in vivo* experiments. Then, a sample is withdrawn from the animal and is used to study the properties of the nanoparticles post-injection with this method. The results would be compared with a nanoparticle solution in water that is not injected. The concentration of nanoparticles injected into the body is much lower than the concentrations used for this project. Moreover, the amount of sample extracted from the animal cannot be higher than 100 µl each time. Thereby, the limitations of the method could be studied in a better way in terms of sample volume needed and further sample concentration to better discriminate the nanoparticles out of the matrix components. It would also be interesting to study the recovery of nanoparticles from cell cultures.

Some improvements to scale-up the fractionation method would be required. The acquisition of a preparative HPLC column would allow increasing the size in the analysis conditions by incrementing the column size, flow rate or sample load (injection volume). It would also be important to review the eluent (mobile phase) composition to make sure there is not interferences with the matrix components that could lead to precipitation or aggregation of particles. Since the obtained fractions are dissolved in the eluent, it is necessary to confirm that the components of the eluent do not pose a problem when analyzing the fractions by using other assays. Most probably, it would be required the development of a protocol for sample concentration after separation by size to be able to detect particles through ICP-OES. Another alternative could be to increase the dose in the *in vivo* animal studies. Also, removal of the highest abundant proteins through protein precipitation would allow a more “clean “signal from the GPC-HPLC. However, if the nanoparticle-protein interactions are further studied, a different procedure would be followed. Samples would contain all the plasma proteins and alternatively to denaturing gels, native gels would be run to keep the proteins in their original structure. Protein bands of interest would be identified through mass spectroscopy. After identification of proteins, Western blot could be used to further detect these proteins and quantify their expression. It would be interesting to study the effects of time incubation and protein concentration on protein binding to nanoparticles.

To further study the presence of PEG in the isolated fractions, Western blot using an anti-PEG antibody could be done. The presence of PEG would appear in bands of different molecular weights in each fraction according to the size of nanoparticles.

6. Conclusion

This study presents a powerful bioanalytical method to extract nanoparticles from different matrices (water, SBF, serum and urine). Firstly, I characterized the nanomaterial in water in terms of chelate ability, composition and size. The results show that the size of the nanomaterial is 5 nm and it is composed of Si, P and Gd and 60% PEG coating. I demonstrated the stability of Gd inside the nanoparticles. Also, I proved long-term and short-term size stability of these particles at different storage times and temperatures. Secondly, I investigated the efficiency of the methods used. I revealed a high performance of the GPC column with 80% of the material recovered and high sensitivity of ELISA measuring PEG concentrations efficiently in a low range of concentrations up to 0.1 μ/mol. Thirdly, I characterized the fractionated material. F3 showed the highest Si and Gd content and was the fraction where the intermediate particles were collected (6-8 nm). F5 was the most representative fraction for PEG coating. In all matrices, most PEG coating remained attached to the nanoparticles in F2-F4. However, in urine it seemed that there was a tendency of aggregation. Nanoparticles in serum also showed some variable results. Finally, this variable behavior leads us to study possible nanoparticle-protein interactions in serum. Results showed a potential change in some protein bands but any definitive conclusion can be drawn. In fact, more experiments should be done to confirm these results.

7. Acknowledgments

First of all, I would like to thank Spago Nanomedical for giving me the opportunity to perform my thesis at their laboratory and providing me with all the necessary equipment I needed to develop my experiments. This project was a challenge for me since I was discovering for the first time the amazing but unknown world of nanotechnology and all the new concepts that implied. Now I can say that all the effort was worthy. Thanks to all the members of Spago for sharing with me your valuable knowledge and vast experience in this field. Since the very beginning you embraced me and accepted me as one of your own. I would specially like to thank Sania for encouraging and guiding me through this, sometimes, tortuous path until the end. Thanks for your support and endless patience and for having always a smile that was making those dark days in winter a little bit easier. I would also like to thank Oskar. Thank you for inspiring me with your great knowledge, shedding me light on the chemistry concepts and listen to my ideas. And for always having this sense of humor that has helped me to see that everything, even the most difficult things, have a funny side. I do not want to miss the chance to thank all the people who has helped me throughout all these last months. Thanks Rodrigo, Petter and Frank, the HPLC experts, for your great help when teaching me all the technical aspects of the HPLC equipment. Especially to you Rodrigo, for always giving me your time to fix every problem I was having even in a Friday evening. I will also be eternally grateful to Nooshin and Olof who have been an essential part in this project. Thanks for teaching me all the secrets about the ICP and for been always available for me. I also want to thank Emil, for bringing me the best biology-related discussions ever that I really needed for giving sense to all the work I have done. I would like to thank Gabriel for being my Swedish and chemistry teacher all this time and for all the valuable advice in both, academic and personal levels. Last but not least, thanks Evelina for being the best lab partner everyone could wish for and for all the Swedish lessons during the fractionation time.

8. References

1. World Health Organization 2015 [2015-05-25]. Available from: http://www.who.int/cancer/en/.
2. World Cancer Research Fund International 2015 [2015-05-25]. Available from: http://www.wcrf.org/int/cancer-facts-figures/worldwide-data.
3. Cancer research UK 2015 [2015-05-25]. Available from: http://www.cancerresearchuk.org/cancer-info/cancerstats/world/cancer-worldwide-the-global-picture.
4. Frangioni JV. New technologies for human cancer imaging. J Clin Oncol. 2008;26(24):4012-21.
5. Chen ZY, Wang YX, Lin Y, Zhang JS, Yang F, Zhou QL, et al. Advance of molecular imaging technology and targeted imaging agent in imaging and therapy. Biomed Res Int. 2014;2014:819324.
6. Mandelblatt JS, Cronin KA, Bailey S, Berry DA, de Koning HJ, Draisma G, et al. Effects of mammography screening under different screening schedules: model estimates of potential benefits and harms. Ann Intern Med. 2009;151(10):738-47.
7. Recht A, Come SE, Henderson IC, Gelman RS, Silver B, Hayes DF, et al. The sequencing of chemotherapy and radiation therapy after conservative surgery for early-stage breast cancer. N Engl J Med. 1996;334(21):1356-61.
8. Gore JC, Manning HC, Quarles CC, Waddell KW, Yankeelov TE. Magnetic resonance in the era of molecular imaging of cancer. Magn Reson Imaging. 2011;29(5):587-600.
9. Gallagher FA. An introduction to functional and molecular imaging with MRI. Clin Radiol. 2010;65(7):557-66.
10. Pautler RG. Mouse MRI: concepts and applications in physiology. Physiology (Bethesda). 2004;19:168-75.
11. Strijkers GJ, Mulder WJ, van Tilborg GA, Nicolay K. MRI contrast agents: current status and future perspectives. Anticancer Agents Med Chem. 2007;7(3):291-305.
12. Shokrollahi H. Contrast agents for MRI. Mater Sci Eng C Mater Biol Appl. 2013;33(8):4485-97.
13. Zhou Z, Lu ZR. Gadolinium-based contrast agents for magnetic resonance cancer imaging. Wiley Interdiscip Rev Nanomed Nanobiotechnol. 2013;5(1):1-18.
14. Swanson SD, Kukowska-Latallo JF, Patri AK, Chen C, Ge S, Cao Z, et al. Targeted gadolinium-loaded dendrimer nanoparticles for tumor-specific magnetic resonance contrast enhancement. Int J Nanomedicine. 2008;3(2):201-10.
15. Leach MO, Brindle KM, Evelhoch JL, Griffiths JR, Horsman MR, Jackson A, et al. Assessment of antiangiogenic and antivascular therapeutics using MRI: recommendations for appropriate methodology for clinical trials. Br J Radiol. 2003;76 Spec No 1:S87-91.
16. van der Molen AJ. Nephrogenic systemic fibrosis and the role of gadolinium contrast media. J Med Imaging Radiat Oncol. 2008;52(4):339-50.
17. Grobner T, Prischl FC. Gadolinium and nephrogenic systemic fibrosis. Kidney Int. 2007;72(3):260-4.
18. Prchal D, Holmes DT, Levin A. Nephrogenic systemic fibrosis: the story unfolds. Kidney Int. 2008;73(12):1335-7.
19. Dawidczyk CM, Russell LM, Searson PC. Nanomedicines for cancer therapy: state-of-the-art and limitations to pre-clinical studies that hinder future developments. Front Chem. 2014;2:69.
20. Nazir S, Hussain T, Ayub A, Rashid U, MacRobert AJ. Nanomaterials in combating cancer: therapeutic applications and developments. Nanomedicine. 2014;10(1):19-34.
21. Yezhelyev MV, Gao X, Xing Y, Al-Hajj A, Nie S, O'Regan RM. Emerging use of nanoparticles in diagnosis and treatment of breast cancer. Lancet Oncol. 2006;7(8):657-67.

22. Pan D, Caruthers SD, Senpan A, Schmieder AH, Wickline SA, Lanza GM. Revisiting an old friend: manganese-based MRI contrast agents. Wiley Interdiscip Rev Nanomed Nanobiotechnol. 2011;3(2):162-73.
23. Eriksson PO, Aaltonen E, Petoral R, Lauritzson P, Miyazaki H, Pietras K, et al. Novel nano-sized MR contrast agent mediates strong tumor contrast enhancement in an oncogene-driven breast cancer model. PLoS One. 2014;9(10):e107762.
24. Greish K. Enhanced permeability and retention (EPR) effect for anticancer nanomedicine drug targeting. Methods Mol Biol. 2010;624:25-37.
25. Nakamura H, Jun F, Maeda H. Development of next-generation macromolecular drugs based on the EPR effect: challenges and pitfalls. Expert Opin Drug Deliv. 2015;12(1):53-64.
26. Jokerst JV, Lobovkina T, Zare RN, Gambhir SS. Nanoparticle PEGylation for imaging and therapy. Nanomedicine (Lond). 2011;6(4):715-28.
27. Knop K, Hoogenboom R, Fischer D, Schubert US. Poly(ethylene glycol) in drug delivery: pros and cons as well as potential alternatives. Angew Chem Int Ed Engl. 2010;49(36):6288-308.
28. Zhang X, Wang H, Ma Z, Wu B. Effects of pharmaceutical PEGylation on drug metabolism and its clinical concerns. Expert Opin Drug Metab Toxicol. 2014;10(12):1691-702.
29. Saptarshi SR, Duschl A, Lopata AL. Interaction of nanoparticles with proteins: relation to bio-reactivity of the nanoparticle. J Nanobiotechnology. 2013;11:26.
30. Aggarwal P, Hall JB, McLeland CB, Dobrovolskaia MA, McNeil SE. Nanoparticle interaction with plasma proteins as it relates to particle biodistribution, biocompatibility and therapeutic efficacy. Adv Drug Deliv Rev. 2009;61(6):428-37.
31. Mahmoudi M, Lynch I, Ejtehadi MR, Monopoli MP, Bombelli FB, Laurent S. Protein-nanoparticle interactions: opportunities and challenges. Chem Rev. 2011;111(9):5610-37.
32. Hall JB, Dobrovolskaia MA, Patri AK, McNeil SE. Characterization of nanoparticles for therapeutics. Nanomedicine (Lond). 2007;2(6):789-803.
33. Cho EJ, Holback H, Liu KC, Abouelmagd SA, Park J, Yeo Y. Nanoparticle characterization: state of the art, challenges, and emerging technologies. Mol Pharm. 2013;10(6):2093-110.
34. von der Kammer F, Ferguson PL, Holden PA, Masion A, Rogers KR, Klaine SJ, et al. Analysis of engineered nanomaterials in complex matrices (environment and biota): general considerations and conceptual case studies. Environ Toxicol Chem. 2012;31(1):32-49.
35. Institute) NCLNNC. [2015-06-02]. Available from: http://nano.cancer.gov/action/news/featurestories/monthly_feature_2006_july.asp.
36. Poitras EP, Levine MA, Harrington JM, Essader AS, Fennell TR, Snyder RW, et al. Development of an analytical method for assessment of silver nanoparticle content in biological matrices by inductively coupled plasma mass spectrometry. Biol Trace Elem Res. 2015;163(1-2):184-92.
37. Tiede K, Boxall AB, Tear SP, Lewis J, David H, Hassellov M. Detection and characterization of engineered nanoparticles in food and the environment. Food Addit Contam Part A Chem Anal Control Expo Risk Assess. 2008;25(7):795-821.
38. Pecora R. Dynamic Light Scattering Measurement of Nanometer Particles in Liquids. Journal of Nanoparticle Research. 2000;2(2):123-31.
39. Kim HA, Seo JK, Kim T, Lee BT. Nanometrology and its perspectives in environmental research. Environ Health Toxicol. 2014;29:e2014016.
40. Deng ZJ, Mortimer G, Schiller T, Musumeci A, Martin D, Minchin RF. Differential plasma protein binding to metal oxide nanoparticles. Nanotechnology. 2009;20(45):455101.
41. Polite LN. Fundamentals of Liquid Chromatography (HPLC). In: Agilent Technologies I, editor. 2014. p. 37.
42. Huber U, Majors R. Principles in preparative HPLC In: Agilent Technologies I, editor. 2007. p. 2-6.

43. Naseem U. Functionalized gold nanoparticles for specific generation of oxidative stress. Lund (Sweden): Lund University; 2012.
44. I. Stewart I, W. Olesik J. Steady state acid effects in ICP-MS. Journal of Analytical Atomic Spectrometry. 1998;13(12):1313-20.
45. Shapiro AL, Viñuela E, Maizel JV. Molecular weight estimation of polypeptide chains by electrophoresis in SDS-polyacrylamide gels. Biochem Biophys Res Commun. 1967;28(5):815-20.
46. Dominguez JR, Kestenbaum B, Chonchol M, Block G, Laughlin GA, Lewis CE, et al. Relationships between serum and urine phosphorus with all-cause and cardiovascular mortality: the Osteoporotic Fractures in Men (MrOS) Study. Am J Kidney Dis. 2013;61(4):555-63.
47. Sabella S, Carney RP, Brunetti V, Malvindi MA, Al-Juffali N, Vecchio G, et al. A general mechanism for intracellular toxicity of metal-containing nanoparticles. Nanoscale. 2014;6(12):7052-61.
48. Auffan M, Rose J, Bottero JY, Lowry GV, Jolivet JP, Wiesner MR. Towards a definition of inorganic nanoparticles from an environmental, health and safety perspective. Nat Nanotechnol. 2009;4(10):634-41.
49. Brunner TJ, Wick P, Manser P, Spohn P, Grass RN, Limbach LK, et al. In vitro cytotoxicity of oxide nanoparticles: comparison to asbestos, silica, and the effect of particle solubility. Environ Sci Technol. 2006;40(14):4374-81.
50. Studer AM, Limbach LK, Van Duc L, Krumeich F, Athanassiou EK, Gerber LC, et al. Nanoparticle cytotoxicity depends on intracellular solubility: comparison of stabilized copper metal and degradable copper oxide nanoparticles. Toxicol Lett. 2010;197(3):169-74.
51. Shang L, Nienhaus K, Nienhaus GU. Engineered nanoparticles interacting with cells: size matters. J Nanobiotechnology. 2014;12:5.
52. Guidance for Industry. Bioanalytical Method Validation. In: Administration FaD, editor. 2001.
53. Validation of Analytical Procedures: Text and Methodology Q2(R1). In: use. ICoHIotrfropfh, editor. 1996.
54. Lee YZ, Ming-Tatt L, Lajis NH, Sulaiman MR, Israf DA, Tham CL. Development and validation of a bioanalytical method for quantification of 2,6-bis-(4-hydroxy-3-methoxybenzylidene)-cyclohexanone (BHMC) in rat plasma. Molecules. 2012;17(12):14555-64.
55. Chin DL, Lum BL, Sikic BI. Rapid determination of PEGylated liposomal doxorubicin and its major metabolite in human plasma by ultraviolet-visible high-performance liquid chromatography. J Chromatogr B Analyt Technol Biomed Life Sci. 2002;779(2):259-69.
56. Gaines P. ICP Operations Guide. A guide for using ICP-OES and ICP-MS.: Inorganic Ventures; 2011. 4-8 p.
57. Cheng G, He M, Peng H, Hu B. Dithizone modified magnetic nanoparticles for fast and selective solid phase extraction of trace elements in environmental and biological samples prior to their determination by ICP-OES. Talanta. 2012;88:507-15.
58. Adachi J, Kumar C, Zhang Y, Olsen JV, Mann M. The human urinary proteome contains more than 1500 proteins, including a large proportion of membrane proteins. Genome Biol. 2006;7(9):R80.
59. Sheth SR, Leckband D. Measurements of attractive forces between proteins and end-grafted poly(ethylene glycol) chains. Proc Natl Acad Sci U S A. 1997;94(16):8399-404.
60. Elodie S, Julien D, Fernando R-L, Jean-Marie D. Nanoparticle-protein interactions: from crucial plasma proteins to key enzymes. Journal of Physics: Conference Series. 2011;304(1):012039.
61. Fan J, de Lannoy IA. Pharmacokinetics. Biochem Pharmacol. 2014;87(1):93-120.
62. Anderson NL, Anderson NG. The human plasma proteome: history, character, and diagnostic prospects. Mol Cell Proteomics. 2002;1(11):845-67.

63. Chromy BA, Gonzales AD, Perkins J, Choi MW, Corzett MH, Chang BC, et al. Proteomic analysis of human serum by two-dimensional differential gel electrophoresis after depletion of high-abundant proteins. J Proteome Res. 2004;3(6):1120-7.
64. Tirumalai RS, Chan KC, Prieto DA, Issaq HJ, Conrads TP, Veenstra TD. Characterization of the low molecular weight human serum proteome. Mol Cell Proteomics. 2003;2(10):1096-103.
65. Tantipaiboonwong P, Sinchaikul S, Sriyam S, Phutrakul S, Chen ST. Different techniques for urinary protein analysis of normal and lung cancer patients. Proteomics. 2005;5(4):1140-9.

1. World Health Organization 2015 [2015-05-25]. Available from: http://www.who.int/cancer/en/.
2. World Cancer Research Fund International 2015 [2015-05-25]. Available from: http://www.wcrf.org/int/cancer-facts-figures/worldwide-data.
3. Cancer research UK 2015 [2015-05-25]. Available from: http://www.cancerresearchuk.org/cancer-info/cancerstats/world/cancer-worldwide-the-global-picture.
4. Frangioni JV. New technologies for human cancer imaging. J Clin Oncol. 2008;26(24):4012-21.
5. Chen ZY, Wang YX, Lin Y, Zhang JS, Yang F, Zhou QL, et al. Advance of molecular imaging technology and targeted imaging agent in imaging and therapy. Biomed Res Int. 2014;2014:819324.
6. Mandelblatt JS, Cronin KA, Bailey S, Berry DA, de Koning HJ, Draisma G, et al. Effects of mammography screening under different screening schedules: model estimates of potential benefits and harms. Ann Intern Med. 2009;151(10):738-47.
7. Recht A, Come SE, Henderson IC, Gelman RS, Silver B, Hayes DF, et al. The sequencing of chemotherapy and radiation therapy after conservative surgery for early-stage breast cancer. N Engl J Med. 1996;334(21):1356-61.
8. Gore JC, Manning HC, Quarles CC, Waddell KW, Yankeelov TE. Magnetic resonance in the era of molecular imaging of cancer. Magn Reson Imaging. 2011;29(5):587-600.
9. Gallagher FA. An introduction to functional and molecular imaging with MRI. Clin Radiol. 2010;65(7):557-66.
10. Pautler RG. Mouse MRI: concepts and applications in physiology. Physiology (Bethesda). 2004;19:168-75.
11. Strijkers GJ, Mulder WJ, van Tilborg GA, Nicolay K. MRI contrast agents: current status and future perspectives. Anticancer Agents Med Chem. 2007;7(3):291-305.
12. Shokrollahi H. Contrast agents for MRI. Mater Sci Eng C Mater Biol Appl. 2013;33(8):4485-97.
13. Zhou Z, Lu ZR. Gadolinium-based contrast agents for magnetic resonance cancer imaging. Wiley Interdiscip Rev Nanomed Nanobiotechnol. 2013;5(1):1-18.
14. Swanson SD, Kukowska-Latallo JF, Patri AK, Chen C, Ge S, Cao Z, et al. Targeted gadolinium-loaded dendrimer nanoparticles for tumor-specific magnetic resonance contrast enhancement. Int J Nanomedicine. 2008;3(2):201-10.
15. Leach MO, Brindle KM, Evelhoch JL, Griffiths JR, Horsman MR, Jackson A, et al. Assessment of antiangiogenic and antivascular therapeutics using MRI: recommendations for appropriate methodology for clinical trials. Br J Radiol. 2003;76 Spec No 1:S87-91.
16. van der Molen AJ. Nephrogenic systemic fibrosis and the role of gadolinium contrast media. J Med Imaging Radiat Oncol. 2008;52(4):339-50.
17. Grobner T, Prischl FC. Gadolinium and nephrogenic systemic fibrosis. Kidney Int. 2007;72(3):260-4.
18. Prchal D, Holmes DT, Levin A. Nephrogenic systemic fibrosis: the story unfolds. Kidney Int. 2008;73(12):1335-7.
19. Dawidczyk CM, Russell LM, Searson PC. Nanomedicines for cancer therapy: state-of-the-art and limitations to pre-clinical studies that hinder future developments. Front Chem. 2014;2:69.
20. Nazir S, Hussain T, Ayub A, Rashid U, MacRobert AJ. Nanomaterials in combating cancer: therapeutic applications and developments. Nanomedicine. 2014;10(1):19-34.
21. Yezhelyev MV, Gao X, Xing Y, Al-Hajj A, Nie S, O'Regan RM. Emerging use of nanoparticles in diagnosis and treatment of breast cancer. Lancet Oncol. 2006;7(8):657-67.
22. Pan D, Caruthers SD, Senpan A, Schmieder AH, Wickline SA, Lanza GM. Revisiting an old friend: manganese-based MRI contrast agents. Wiley Interdiscip Rev Nanomed Nanobiotechnol. 2011;3(2):162-73.
23. Eriksson PO, Aaltonen E, Petoral R, Lauritzson P, Miyazaki H, Pietras K, et al. Novel nano-sized MR contrast agent mediates strong tumor contrast enhancement in an oncogene-driven breast cancer model. PLoS One. 2014;9(10):e107762.

24. Greish K. Enhanced permeability and retention (EPR) effect for anticancer nanomedicine drug targeting. Methods Mol Biol. 2010;624:25-37.
25. Nakamura H, Jun F, Maeda H. Development of next-generation macromolecular drugs based on the EPR effect: challenges and pitfalls. Expert Opin Drug Deliv. 2015;12(1):53-64.
26. Jokerst JV, Lobovkina T, Zare RN, Gambhir SS. Nanoparticle PEGylation for imaging and therapy. Nanomedicine (Lond). 2011;6(4):715-28.
27. Knop K, Hoogenboom R, Fischer D, Schubert US. Poly(ethylene glycol) in drug delivery: pros and cons as well as potential alternatives. Angew Chem Int Ed Engl. 2010;49(36):6288-308.
28. Zhang X, Wang H, Ma Z, Wu B. Effects of pharmaceutical PEGylation on drug metabolism and its clinical concerns. Expert Opin Drug Metab Toxicol. 2014;10(12):1691-702.
29. Saptarshi SR, Duschl A, Lopata AL. Interaction of nanoparticles with proteins: relation to bio-reactivity of the nanoparticle. J Nanobiotechnology. 2013;11:26.
30. Aggarwal P, Hall JB, McLeland CB, Dobrovolskaia MA, McNeil SE. Nanoparticle interaction with plasma proteins as it relates to particle biodistribution, biocompatibility and therapeutic efficacy. Adv Drug Deliv Rev. 2009;61(6):428-37.
31. Mahmoudi M, Lynch I, Ejtehadi MR, Monopoli MP, Bombelli FB, Laurent S. Protein-nanoparticle interactions: opportunities and challenges. Chem Rev. 2011;111(9):5610-37.
32. Hall JB, Dobrovolskaia MA, Patri AK, McNeil SE. Characterization of nanoparticles for therapeutics. Nanomedicine (Lond). 2007;2(6):789-803.
33. Cho EJ, Holback H, Liu KC, Abouelmagd SA, Park J, Yeo Y. Nanoparticle characterization: state of the art, challenges, and emerging technologies. Mol Pharm. 2013;10(6):2093-110.
34. von der Kammer F, Ferguson PL, Holden PA, Masion A, Rogers KR, Klaine SJ, et al. Analysis of engineered nanomaterials in complex matrices (environment and biota): general considerations and conceptual case studies. Environ Toxicol Chem. 2012;31(1):32-49.
35. Institute) NCLNNC. [2015-06-02]. Available from: http://nano.cancer.gov/action/news/featurestories/monthly_feature_2006_july.asp.
36. Poitras EP, Levine MA, Harrington JM, Essader AS, Fennell TR, Snyder RW, et al. Development of an analytical method for assessment of silver nanoparticle content in biological matrices by inductively coupled plasma mass spectrometry. Biol Trace Elem Res. 2015;163(1-2):184-92.
37. Tiede K, Boxall AB, Tear SP, Lewis J, David H, Hassellov M. Detection and characterization of engineered nanoparticles in food and the environment. Food Addit Contam Part A Chem Anal Control Expo Risk Assess. 2008;25(7):795-821.
38. Pecora R. Dynamic Light Scattering Measurement of Nanometer Particles in Liquids. Journal of Nanoparticle Research. 2000;2(2):123-31.
39. Kim HA, Seo JK, Kim T, Lee BT. Nanometrology and its perspectives in environmental research. Environ Health Toxicol. 2014;29:e2014016.
40. Deng ZJ, Mortimer G, Schiller T, Musumeci A, Martin D, Minchin RF. Differential plasma protein binding to metal oxide nanoparticles. Nanotechnology. 2009;20(45):455101.
41. Polite LN. Fundamentals of Liquid Chromatography (HPLC). In: Agilent Technologies I, editor. 2014. p. 37.
42. Huber U, Majors R. Principles in preparative HPLC In: Agilent Technologies I, editor. 2007. p. 2-6.
43. Naseem U. Functionalized gold nanoparticles for specific generation of oxidative stress. Lund (Sweden): Lund University; 2012.
44. I. Stewart I, W. Olesik J. Steady state acid effects in ICP-MS. Journal of Analytical Atomic Spectrometry. 1998;13(12):1313-20.
45. Shapiro AL, Viñuela E, Maizel JV. Molecular weight estimation of polypeptide chains by electrophoresis in SDS-polyacrylamide gels. Biochem Biophys Res Commun. 1967;28(5):815-20.
46. Dominguez JR, Kestenbaum B, Chonchol M, Block G, Laughlin GA, Lewis CE, et al. Relationships between serum and urine phosphorus with all-cause and cardiovascular mortality: the Osteoporotic Fractures in Men (MrOS) Study. Am J Kidney Dis. 2013;61(4):555-63.
47. Sabella S, Carney RP, Brunetti V, Malvindi MA, Al-Juffali N, Vecchio G, et al. A general mechanism for intracellular toxicity of metal-containing nanoparticles. Nanoscale. 2014;6(12):7052-61.
48. Auffan M, Rose J, Bottero JY, Lowry GV, Jolivet JP, Wiesner MR. Towards a definition of inorganic nanoparticles from an environmental, health and safety perspective. Nat Nanotechnol. 2009;4(10):634-41.

49. Brunner TJ, Wick P, Manser P, Spohn P, Grass RN, Limbach LK, et al. In vitro cytotoxicity of oxide nanoparticles: comparison to asbestos, silica, and the effect of particle solubility. Environ Sci Technol. 2006;40(14):4374-81.
50. Studer AM, Limbach LK, Van Duc L, Krumeich F, Athanassiou EK, Gerber LC, et al. Nanoparticle cytotoxicity depends on intracellular solubility: comparison of stabilized copper metal and degradable copper oxide nanoparticles. Toxicol Lett. 2010;197(3):169-74.
51. Shang L, Nienhaus K, Nienhaus GU. Engineered nanoparticles interacting with cells: size matters. J Nanobiotechnology. 2014;12:5.
52. Guidance for Industry. Bioanalytical Method Validation. In: Administration FaD, editor. 2001.
53. Validation of Analytical Procedures: Text and Methodology Q2(R1). In: use. ICoHIotrfropfh, editor. 1996.
54. Lee YZ, Ming-Tatt L, Lajis NH, Sulaiman MR, Israf DA, Tham CL. Development and validation of a bioanalytical method for quantification of 2,6-bis-(4-hydroxy-3-methoxybenzylidene)-cyclohexanone (BHMC) in rat plasma. Molecules. 2012;17(12):14555-64.
55. Chin DL, Lum BL, Sikic BI. Rapid determination of PEGylated liposomal doxorubicin and its major metabolite in human plasma by ultraviolet-visible high-performance liquid chromatography. J Chromatogr B Analyt Technol Biomed Life Sci. 2002;779(2):259-69.
56. Gaines P. ICP Operations Guide. A guide for using ICP-OES and ICP-MS.: Inorganic Ventures; 2011. 4-8 p.
57. Cheng G, He M, Peng H, Hu B. Dithizone modified magnetic nanoparticles for fast and selective solid phase extraction of trace elements in environmental and biological samples prior to their determination by ICP-OES. Talanta. 2012;88:507-15.
58. Adachi J, Kumar C, Zhang Y, Olsen JV, Mann M. The human urinary proteome contains more than 1500 proteins, including a large proportion of membrane proteins. Genome Biol. 2006;7(9):R80.
59. Sheth SR, Leckband D. Measurements of attractive forces between proteins and end-grafted poly(ethylene glycol) chains. Proc Natl Acad Sci U S A. 1997;94(16):8399-404.
60. Elodie S, Julien D, Fernando R-L, Jean-Marie D. Nanoparticle-protein interactions: from crucial plasma proteins to key enzymes. Journal of Physics: Conference Series. 2011;304(1):012039.
61. Fan J, de Lannoy IA. Pharmacokinetics. Biochem Pharmacol. 2014;87(1):93-120.
62. Anderson NL, Anderson NG. The human plasma proteome: history, character, and diagnostic prospects. Mol Cell Proteomics. 2002;1(11):845-67.
63. Chromy BA, Gonzales AD, Perkins J, Choi MW, Corzett MH, Chang BC, et al. Proteomic analysis of human serum by two-dimensional differential gel electrophoresis after depletion of high-abundant proteins. J Proteome Res. 2004;3(6):1120-7.
64. Tirumalai RS, Chan KC, Prieto DA, Issaq HJ, Conrads TP, Veenstra TD. Characterization of the low molecular weight human serum proteome. Mol Cell Proteomics. 2003;2(10):1096-103.
65. Tantipaiboonwong P, Sinchaikul S, Sriyam S, Phutrakul S, Chen ST. Different techniques for urinary protein analysis of normal and lung cancer patients. Proteomics. 2005;5(4):1140-9.
66. Athar M, Das AJ. Therapeutic nanoparticles: State-of-the-art of nanomedicine. Adv. Mater. Rew. 2014, 1(1):25-37.
67. Malawer EG, Senak L. Handbook of Size Exclusion Chromatography and Related Techniques, 2nd ed. C.S. Wu, Ed. Marcel Dekker, New York, NY, 2004, p 13.

Appendix I

SOP for DLS size measurements: Zetasizer Nano Malvern Instrument

- **Sample**
  - Material: silica

    Refractive index (RI): 1,450

    Absorption: 0,001
  - Dispersant: Water

    Temperature: 25ºC

    Viscosity: 0,8872 centipoise (cP)

    RI: 1,330

    Use dispersant viscosity as sample viscosity
  - General temperature: 25 ºC
  - Equilibration time (seconds): 180
  - Cell type: Disposable cuvettes (ZEN 0040)
  - Volume: 250 µl

    Water and HS: 25 µl + 225 µl $(NH_4)_2CO_3$ (pH 7.4, adjusted with formic acid)

    SBF and urine: 250 µl
- **Measurement**
  - Angle of detection: 173º Backscatter (NIBS default)
  - Measurement duration (automatic):

    Number of runs: 11

    Run duration (seconds): 10
  - Measurements:

    Number of measurements: 10

    Delay between measurements (seconds): 0
  - Measurement settings: Automatic attenuation selection

    Allow the software to seek for the best position

- **Data processing**
  - Analysis model: Multiple narrow modes (high resolution)

The size of the nanoparticles was reported following the procedure below.

- The quality of the correlogram was checked (it could not be below 0.5 and good quality was considered above 0.8). It should have a sigmoidal shape.
- In the Volume PSD (M) window, the measurements deviating from the average were removed (by looking at the size distribution by volume graph).
- In the Volume stats table (M) window, the size range of the nanoparticle population was determined including all sizes (d.nm) with a mean volume percent above 5.
- In the records view, the volume mean (d.nm) was chosen to report the size by selecting the mean and standard deviation of 5-10 measurement values of volume mean.

Appendix II

ELISA assay protocol (Abcam)

- Bring the necessary amount of well strips to room temperature. Keep the rest of reagents and wells at 4 ºC while not in use.
- Bring ELISA 10X Washing Buffer (12 ml) to room temperature and dilute it to 1X by adding 108 ml of deionized water. Mix the buffer by inverting the solution several times.
- Dilute 60X PEG-HRP to 1X with 1X Antigen/Antibody Diluent Buffer. The volume needed will depend on the amount of samples.
- Mix 27 µl of 1X PEG-HRP with 27 µl of PEGylated samples (standards, unknown samples). It is important to make more volume than will be needed.
- Add 50 µl of the mixture to each well and incubate for 45 minutes at room temperature on a shaker.
- Aspirate each well and wash 3 times with 250 µl 1X washing buffer.
- Mix TMB A and TMB B (1:1). Add 100 µl of combined substrate solution to each well.
- Cover to protect from light and incubate for 15 minutes at room temperature without any shaking.
- Add 100 µl of stop solution to each well and make sure that it is mixing properly.
- Transfer the solution from each well to a V-bottomed 96-well plate (Nunc TM, Thermo Scientific).
- Determine the absorbance at 450 nm using a microplate reader (SoftMax® Pro Microplate Reader and Analysis Software).

Appendix III

Element ratios and volume mean diameters

A) Element Ratios of IXGp-Gd particles in different biological matrices

Matrix	Volume (ml)	Si (µM)	Gd (µM)	Ratio Si/Gd	Average Si/Gd	Std. Deviation	*SEM
SBF	0.50	208455.80	9195.60	22.67	-	-	-
HS	0.50	225172.20	11056.80	20.37	21.67	1.14	0.66
HS	0.50	69744.35	3106.91	22.45			
HS	0.50	68522.48	3085.47	22.21			
Urine	0.63	64874.73	2987.31	21.72	-	-	-

*Standard error of the mean

B) Element ratios of IXGp-Gd in water

Sample	Volume (ml)	Si (µM)	P (µM)	Gd (µM)	Ratio Si/Gd	Ratio Si/P	Ratio P/Gd
GF0103 0.1R	0.5	134522.64	105796.80	6134.28	21.93	1.27	17.25
GF01058 0.1R	0.5	131680.93	98235.90	6031.47	21.83	1.34	16.29
GF01102 0.1R	0.5	128095.80	92844.00	5461.10	23.46	1.38	17.00
Average	-	-	-	-	22.41	1.33	16.85
Std.Deviation	-	-	-	-	0.91	0.05	0.50
SEM	-	-	-	-	0.53	0.03	0.29

C) Volume mean diameter (nm) in different matrices

Matrix	Average size (nm)	Std deviation	Range
Water	4.9	0.4	2.7-6.5
SBF	5.1	0.3	3.1-6.5
Urine	6.2	0.90	3.1-10.1

D) Volume mean diameter (nm) of IXGp-Gd in SBF o water at room temperature

Matrix	SBF	SBF	SBF	Water	Water	Water
Day	Mean diam	Std.Deviation	SEM	Mean diam	Std.deviation	SEM
0	5.1	0.2	0.06	5.2	0.5	0.14
1	5.6	0.3	0.08	5.7	0.2	0.07
2	5.1	0.5	0.15	5.7	0.4	0.12
3	5.1	0.6	0.19	5.2	1.0	0.33
4	5.3	0.3	0.10	5.3	0.5	0.16
5	5.3	0.4	0.14	5.2	0.6	0.19
8	5.3	0.4	0.11	5.6	0.7	0.23
16	5.1	0.5	0.16	5.7	0.6	0.19

E) Volume mean diameter (nm) of IXGp-Gd in SBF at different storage temperatures

T ºC	Room t	Room t	Room t	-20	-20	-20	4	4	4
Day	Mean diam	Std deviation	SEM	Mean diam	Std deviation	SEM	Mean diam	Std deviation	SEM
0	5.1	0.2	0.06	5.1	0.2	0.06	5.1	0.2	0.06
1	5.1	0.2	0.05	4.9	0.3	0.09	5.0	0.5	0.15
2	5.1	0.3	0.10	5.3	0.3	0.08	5.0	0.3	0.08
3	4.9	0.4	0.11	5.1	0.3	0.10	5.1	0.2	0.05
4	5.1	0.3	0.08	5.3	0.4	0.12	5.2	0.4	0.11
5	5.0	0.3	0.09	5.1	0.3	0.10	5.4	0.5	0.16

Appendix IV

GPC-HPLC chromatograms of nanoparticles

A) IXGp-Gd water nanoparticles (batch 1)

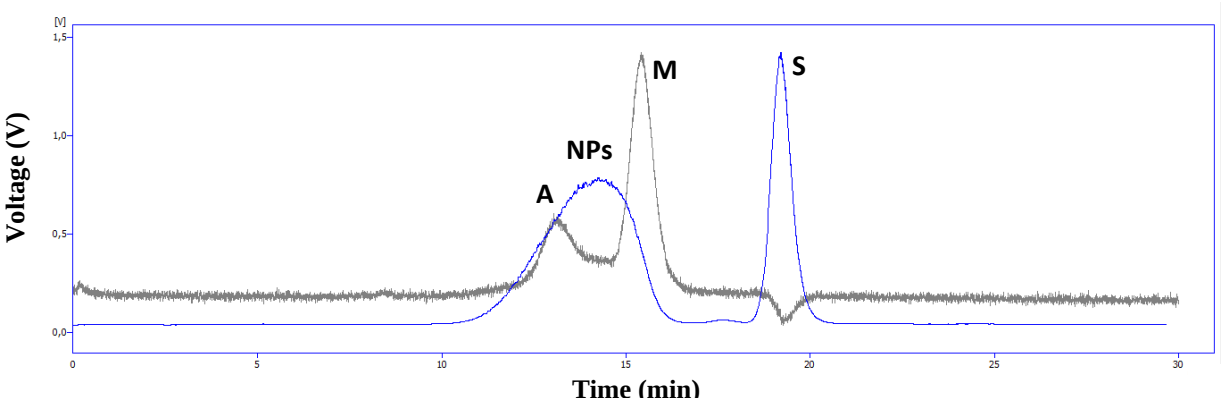

Figure 1. Chromatogram from GPC-HPLC analysis showing the UV (grey) and ELSD (blue) signals from proteins and NPs in water respectively. A: albumin; M: myoglobin; NPs: nanoparticles: S: salts. Nanoparticle´s peak was coming out 1.2 minutes after the albumin peak.

B) IXGp-Gd nanoparticles in SBF

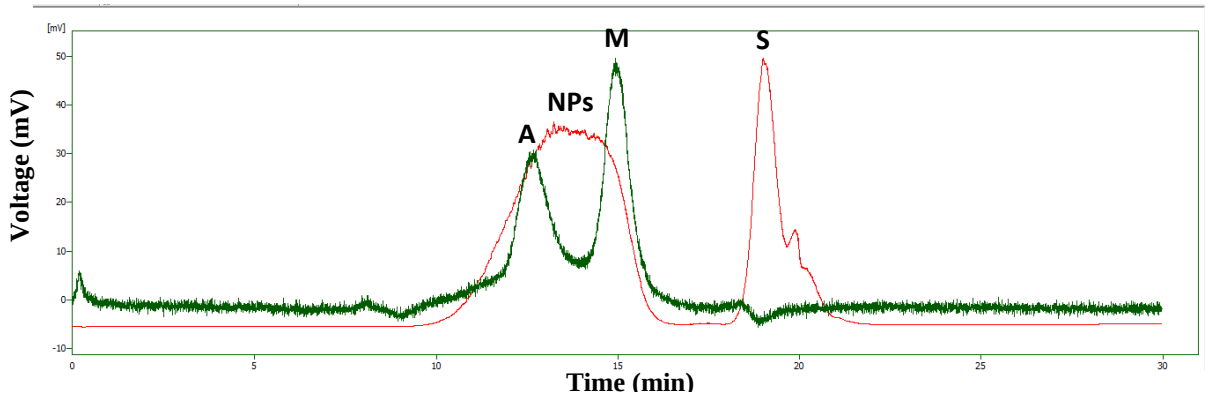

Figure 2. Chromatogram from GPC-HPLC analysis showing the UV (green) and ELSD (red) signals from proteins and NPs in SBF respectively. A: albumin; M: myoglobin; NPs: nanoparticles: S: salts. Nanoparticle´s peak was coming out 0.8 minutes after the albumin peak.

C) IXGp-Gd nanoparticles in HS

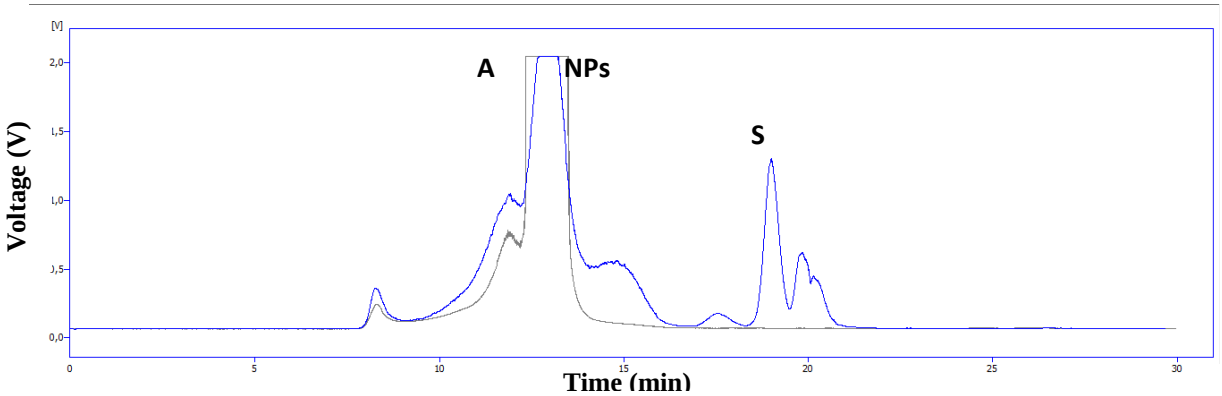

Figure 3. Chromatogram from GPC-HPLC analysis showing the UV (green) and ELSD (red) signals from proteins and NPs in HS respectively. A: albumin; M: myoglobin; NPs: nanoparticles: S: salts. The presence of proteins in high concentrations masks the nanoparticle signal.

D) IXGp-Gd nanoparticles in HS (diluted 1:10)

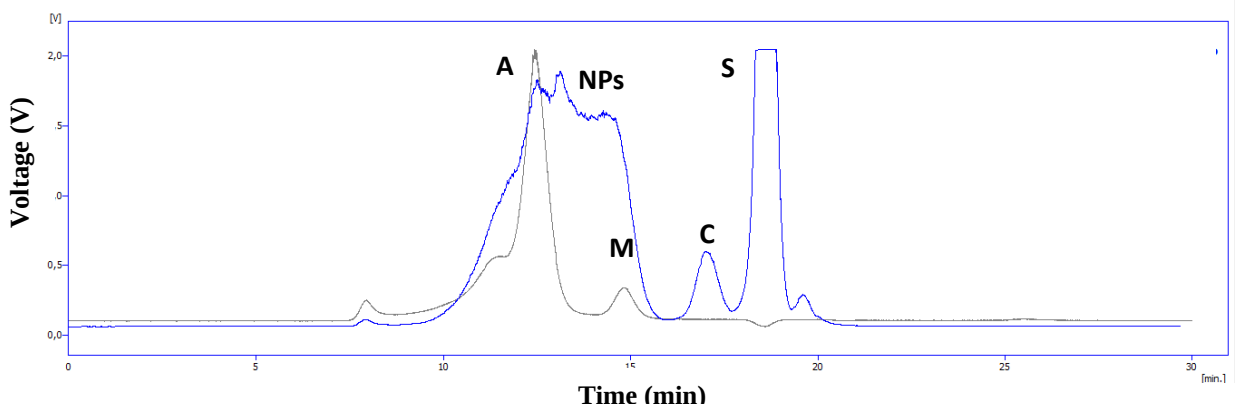

Figure 4. Chromatogram from GPC-HPLC analysis showing the UV (green) and ELSD (red) signals fromproteins and NPs in HS 1:10 respectively. A: albumin; M: myoglobin; NPs: nanoparticles: S: salts.; C: coating. Nanoparticle´s peak was coming out 0.63 minutes after the albumin peak.

E) XGp-Gd nanoparticles in HS (diluted 1:100)

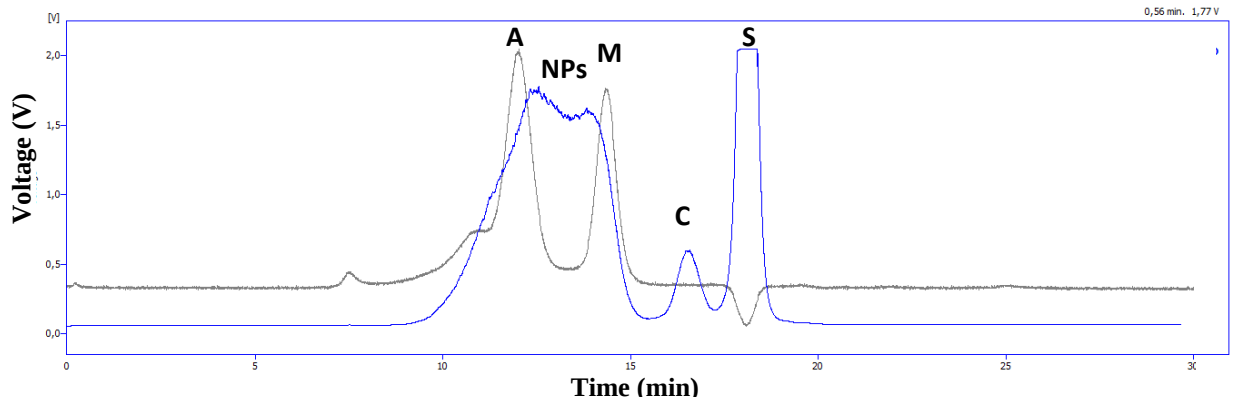

Figure 5. Chromatogram from GPC-HPLC analysis showing the UV (grey) and ELSD (blue) signals from proteins and NPs in HS 1:100 respectively. A: albumin; M: myoglobin; NPs: nanoparticles: S: salts; C: coating. Nanoparticle´s peak was coming out 0.51 minutes after the albumin peak.

F) IXGp-Gd nanoparticles in water (batch 2)

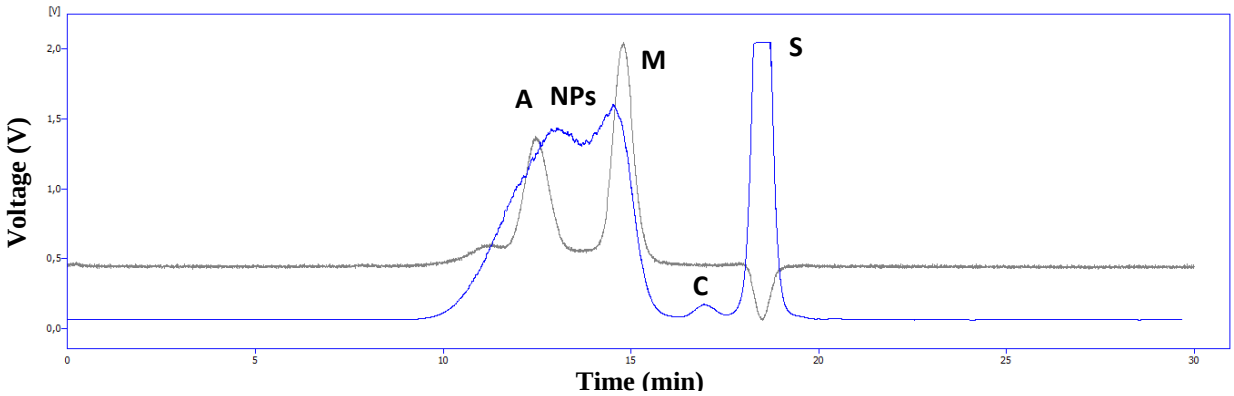

Figure 6. Chromatogram from GPC-HPLC analysis showing the UV (grey) and ELSD (blue) signals from proteins and NPs in water respectively. A: albumin; M: myoglobin; NPs: nanoparticles: S: salts; C: coating. Nanoparticle´s peak was coming out 1.0 minutes after the albumin peak.

G) IXGp-Gd nanoparticles in urine

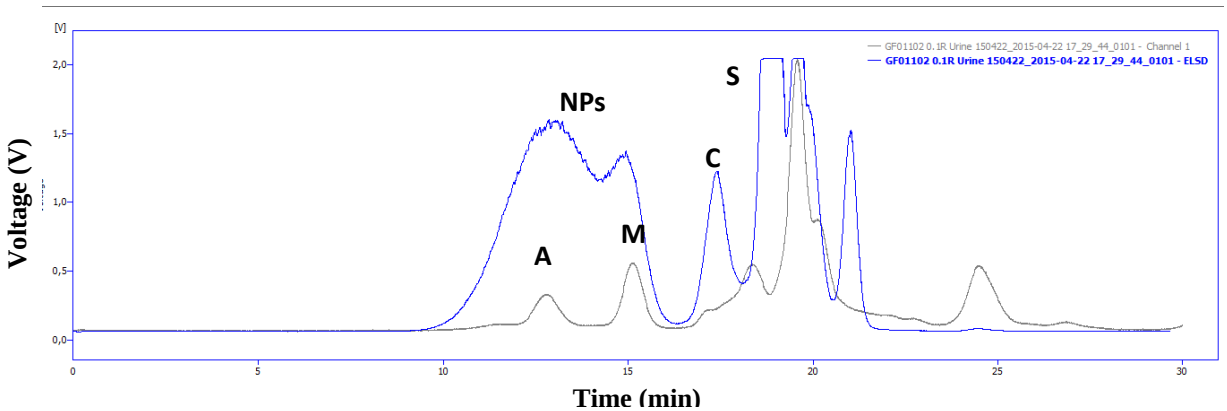

Figure 7. Chromatogram from GPC-HPLC analysis showing the UV (green) and ELSD (red) signals from proteins and NPs in urine respectively. A: A:albumin; M: myoglobin; NPs: nanoparticles: S: salts; C: coating. Nanoparticle´s peak v coming out 0.4 minutes after the albumin peak.

Appendix V

ELISA Standard curves in different biological matrices

Water Batch 1

Sample	[Si]uM	Abs 450 nm	Expected [PEG]uM	Measured [PEG]uM	Standard deviation
Std 1	0.55	0.34	0.13	0.01	-0.92
Std 2	1.09	0.16	0.26	0.34	0.29
Std 3	2.19	0.09	0.53	0.60	0.14
Std 4	4.37	0.03	1.06	1.09	0.03
Std 5	8.75	0.00	2.12	1.91	-0.10

Water Batch 2

Sample	[Si]uM	Abs 450 nm	Expected [PEG]uM	Measured [PEG]uM	Standard deviation
Std 1	0.20	1.09	0.05	0.01	-0.75
Std 2	0.66	0.71	0.16	0.14	-0.11
Std 3	1.25	0.37	0.30	0.35	0.14
Std 4	2.50	0.13	0.60	0.66	0.09
Std 5	4.00	0.06	0.97	0.93	-0.04

SBF

Sample	[Si]uM	Abs 450 nm	Expected [PEG]uM	Measured [PEG]uM	Standard deviation
Std 1	0.20	0.59	0.05	-0.23	-5.70
Std 2	0.66	0.26	0.16	0.13	-0.20
Std 3	1.25	0.15	0.30	0.35	0.16
Std 4	2.50	0.06	0.60	0.74	0.23
Std 5	4.00	0.03	0.97	1.01	0.04

HS

Sample	[Si]uM	Abs 450 nm	Expected [PEG]uM	Measured [PEG]uM	Standard deviation
Std 1	0.20	0.43	0.05	-0.09	-2.85
Std 2	0.66	0.18	0.16	0.27	0.70
Std 3	1.25	0.17	0.30	0.31	0.04
Std 4	2.50	0.08	0.60	0.63	0.04
Std 5	4.00	0.02	0.97	1.18	0.22

Urine

Sample	[Si]uM	Abs 450 nm	Expected [PEG]uM	Measured [PEG]uM	Standard deviation
Std 1	0.20	0.81	0.05	0.05	-0.07
Std 2	0.66	0.28	0.16	0.21	0.30
Std 3	1.25	0.25	0.30	0.24	-0.21
Std 4	2.50	0.13	0.60	0.64	0.05
Std 5	4.00	0.09	0.97	0.97	0.00

Appendix VI

ICP-OES accuracy: concentration determination of Si, P and Gd

Correction factor = Expected / Measured (ICP-OES)

Gd					
Sample	**Expected Gd (µM)**	**Matrix**	**ICP matrix (% HNO_3)**	**Gd measured (µM)**	**Correction factor**
1	298,96	Water	1%	285,73	1,05
2	99,65	Water	1%	106,21	0,94
3	9,97	Water	1%	9,50	1,05
4	1,00	Water	1%	0,56	1,77
5	298,96	HS	1%	321,35	0,93
6	99,65	HS	1%	109,37	0,91
7	9,97	HS	1%	10,12	0,98
8	1,00	HS	1%	0,64	1,55
9	298,96	HS	0.1%	224,39	1,33
10	99,65	HS	0.1%	69,29	1,44
11	9,97	HS	0.1%	7,55	1,32
12	1,00	HS	0.1%	0,58	1,73
13	298,96	Urine	1%	309,21	0,97
14	99,65	Urine	1%	108,67	0,92
15	9,97	Urine	1%	9,86	1,01
16	1,00	Urine	1%	0,62	1,61
17	298,96	SBF	1%	307,62	0,97
18	99,65	SBF	1%	109,21	0,91
19	9,97	SBF	1%	9,94	1,00
20	1,00	SBF	1%	0,57	1,74
21	Reference	Water	1%	6297,92	-
22	Reference	Water	1%	6280,83	-
23	Reference	Water	1%	6255,50	-

Si					
Sample	**Expected Si (µM)**	**Matrix**	**ICP matrix (% HNO_3)**	**Si measured (uM)**	**Correction factor**
1	5539,35	Water	1%	5847,70	0,95
2	1846,45	Water	1%	1952,33	0,95
3	184,64	Water	1%	202,34	0,91
4	18,46	Water	1%	16,95	1,09
5	5539,35	HS	1%	6678,92	0,83
6	1846,45	HS	1%	2274,18	0,81
7	184,64	HS	1%	229,26	0,81
8	18,46	HS	1%	18,70	0,99
9	5539,35	HS	0.1%	5136,40	1,08
10	1846,45	HS	0.1%	1681,56	1,10
11	184,64	HS	0.1%	171,07	1,08
12	18,46	HS	0.1%	13,44	1,37
13	5539,35	Urine	1%	5605,73	0,99
14	1846,45	Urine	1%	1899,83	0,97
15	184,64	Urine	1%	192,67	0,96
16	18,46	Urine	1%	18,53	1,00
17	5539,35	SBF	1%	5617,08	0,99
18	1846,45	SBF	1%	1921,96	0,96
19	184,64	SBF	1%	195,61	0,94
20	18,46	SBF	1%	16,88	1,09
21	Reference	Water	1%	116003,49	-
22	Reference	Water	1%	118251,50	-
23	Reference	Water	1%	114739,48	-

P					
Sample	**Expected P (µM)**	**Matrix**	**ICP matrix (% HNO_3)**	**p measured (uM)**	**Correction factor**
1	4240,37	Water	1%	4674,47	0,91
2	1413,46	Water	1%	1549,92	0,91
3	141,35	Water	1%	160,50	0,88
4	14,13	Water	1%	12,92	1,09
5	Reference	Water	1%	88728,94	-
6	Reference	Water	1%	90407,93	-
7	Reference	Water	1%	88018,39	-

Appendix VII

GPC-HPLC chromatograms of fractionated nanoparticles

A) Fractions 2-6 in water

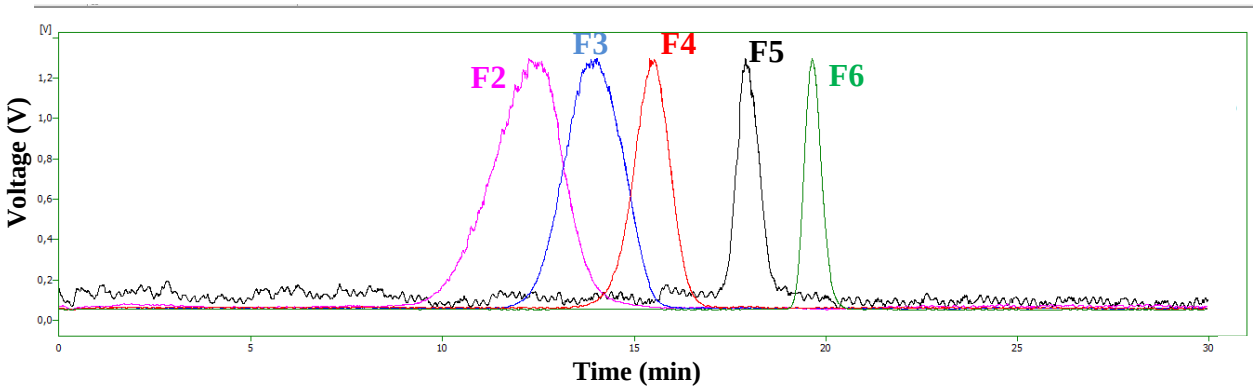

B) Fractions 2-6 in SBF

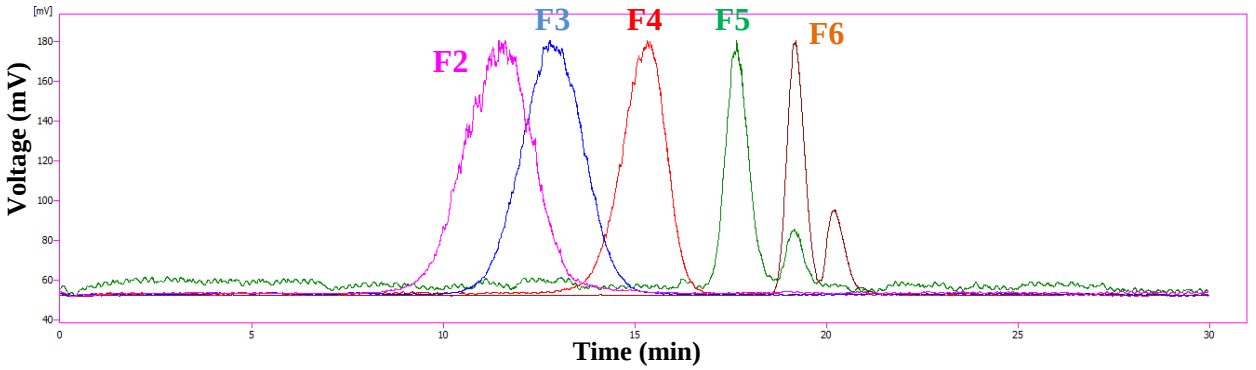

C) Fractions 1-6 in HS

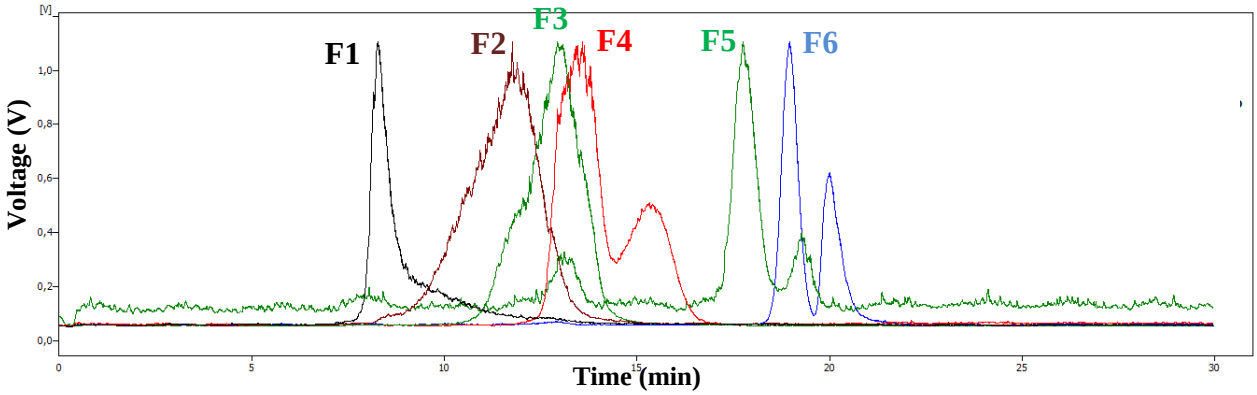

D) Fractions 2-6 in HS (1:10)

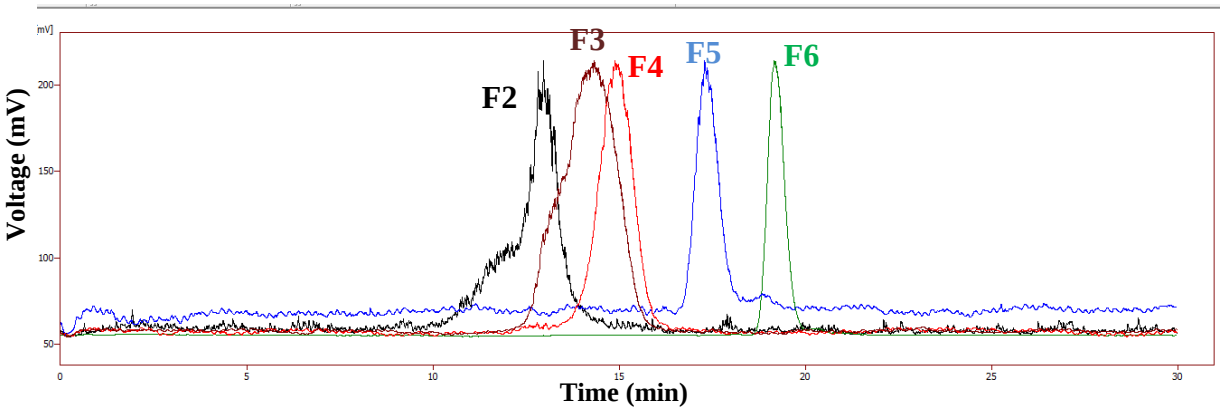

E) Fraction 2-6 in HS (1:100)

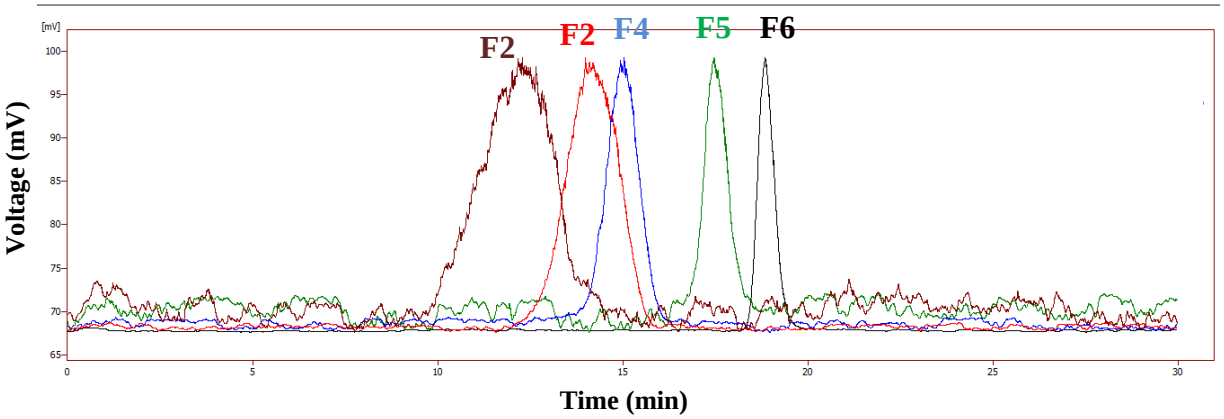

F) Fractions 2-6 in urine

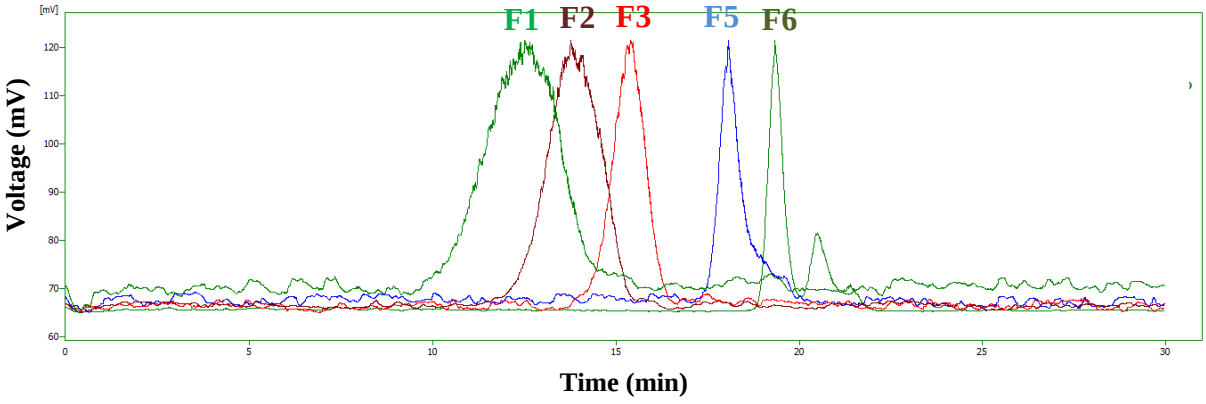

Appendix VIII

Protein and nanoparticle concentrations (µg/ml) in serum and urine fractions

A) Fractions in HS

Sample	[NPs] (µg /ml)	[Protein] (µg/ml)*	Ratio protein/NP
GF01058 0.1R	28494,26	50520,38	1,77
F1	17,00	192,22	11,31
F2	176,62	512,85	2,90
F3	482,90	1996,80	4,13
F4	353,53	592,43	1,68
F5	30,86	9,96	0,32
F6	3,48	2,26	0,65
F7	0,82	0,00	0,00
∑	1065,21	3306,52	-

*Obtained with Bradford assay (see 3.9.2 Material and Methods)

B) Fractions in HS 1:10

Sample	[NPs] (µg /ml)	[Protein] (µg/ml) *	Ratio protein/NP
GF01058 0.1R	8825,75	4726,53	0,54
F1	0,84	1,46	1,74
F2	146,55	83,90	0,57
F3	269,83	50,75	0,19
F4	119,64	6,45	0,05
F5	17,59	0,70	0,04
F6	2,43	1,46	0,60
F7	0,14	0,70	5,06
∑	557,01	145,43	-

*Obtained with Bradford assay (see 3.9.2 Material and Methods)

C) Fractions in HS 1:100

Sample	[NPs] (µg /ml)	[Protein] (µg/ml)*	Ratio protein/NP
GF01058 0.1R	8671,13	672,71	0,08
F1	0,28	1,46	5,31
F2	109,94	3,90	0,04
F3	256,92	7,32	0,03
F4	113,83	3,90	0,03
F5	18,63	0,70	0,04
F6	2,46	3,07	1,25
F7	0,06	1,46	23,38
∑	502,11	21,83	-

* Obtained with Bradford assay (see 3.9.2 Material and Methods)

D) Fractions in urine

Sample	[NPs] (µg /ml)	[Protein] (µg/ml) *	Ratio protein/NP
GF01058 0.1R	8209,53	18,12	0,00
F1	0,93	4,74	5,10
F2	137,25	3,07	0,02
F3	217,11	3,90	0,02
F4	107,16	3,07	0,03
F5	15,81	1,46	0,09
F6	2,03	0,70	0,34
F7	0,40	3,07	7,59
∑	480,70	20,03	-

* Obtained with Bradford assay (see 3.9.2 Material and Methods)

Appendix IX

Fractionation dates in the different matrices

Matrix	Date	Matrix	Date	Matrix	Date
Water 1º	2015-03-10	HS	2015-03-04	Urine	2015-03-17
Water 2º	2015-03-28	HS 1:10	2015-03-20	-	-
SBF	2015-03-02	HS 1:100	2015-03-23	-	-

POPULAR SCIENCE SUMMARY

Gema Fernández

Tracing nanoparticles in biological matrices

Cancer includes a heterogeneous group of diseases that arises due to an uncontrolled proliferation of cells which are able to invade normal tissues. Magnetic resonance imaging (MRI) has been widely used to detect cancer in its earliest stage. However, there is a need for new contrast agents (CAs) with higher sensitivity. Consequently, cancer nanotechnology has emerged as a new potential field which includes the design of material in a scale range from 1-100 nanometers with clinical use for cancer therapy and diagnosis.

Nanomaterials include a wide range of particles used as versatile molecular devices like vectors for drug delivery or CAs to enhance contrast images from tumor tissues. Spago Nanomedical AB in Lund is studying a potential nanomaterial-based contrast agent to be used in MRI. The main structure of the nanoparticle consists of a polymeric central core, which contains a metal ion inside, together with a coating attached to the surface (Figure 1). This coating is made of polyethylene glycol (PEG) chains which form a passive surface that reduces aggregation and undesired interactions in the body.

These particles can be delivered into the tumor tissue through passive targeting. This strategy can be used because during their growth, cancer cells create new but defective blood vessels. Thus, tumor vasculature has an enhanced permeability and lack of an efficient lymphatic drainage which gives rise to the so called enhanced permeability and retention (EPR) effect. This effect allows the nanoparticles to accumulate selectively in the tumor and remain there for a longer time compared to a normal tissue.

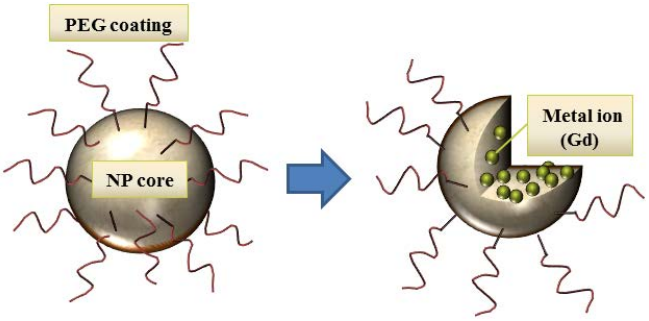

Figure 1. Nanoparticle structure consisting of a central core with a metal ion inside and a coating attached to the surface of the particle. NP: nanoparticle; PEG: polyethylene glycol; Gd: gadolinium.

Do nanoparticles look the same after being injected into the body?

In this project, a dummy particle mimicking a nanoparticle-based contrast agent was further investigated to set up a combined bioanalysis method to extract and characterize the nanomaterial from relevant biological matrices (e.g urine, serum). The final goal was to demonstrate that the identity of the particles (the main physicochemical properties) remain unaffected after being injected into the blood of animals during *in vivo* trials. Problems can arise if the content of the nanoparticles is released to the biological fluids or if particles aggregate and lodge somewhere in the body. The nanoparticles were isolated and separated by size using gel permeation chromatography (GPC). The resulting fractions were analyzed in terms of composition and coating using inductively coupled plasma optical emission spectroscopy (ICP-OES) and enzyme-linked immunosorbent assay (ELISA) respectively. The results proved the presence of nanomaterial in the biological matrices and showed a successful separation of the nanoparticles by size with high rate of recovery. Furthermore, it was possible to analyze the core and coating components of the extracted material in an accurate and efficient way. This study shows the importance of characterizing the nanomaterial and proves its identity before going into clinical trials.

Advisor: **Dr. Sania Bäckström**
Master´s Degree project in Molecular Biology, 45 credits, 2015
Department of Biology, Lund University